UMBC

DISSERTATION APPROVAL SHEET

Title of Dissertation: Nanostructures Encapsulating Antimalarial Drugs for Improved
Systemic Lupus Erythematosus Treatment

Name of Candidate: Marilyn Allen

Doctor of Philosophy, 2021

Graduate Program: Chemical and Biochemical Engineering

Dissertation and Abstract Approved:

Jennie Leach

Jennie Leach

Associate Professor

Chemical, Biochemical & Environmental Eng
7/26/2021 | 11:24:11 AM EDT

Gregory Szeto

Gregory Szeto

Assistant Investigator

Allen Institute for immunology
7/28/2021 | 11:22:08 AM EDT

NOTE: *The Approval Sheet with the original signature must accompany the thesis or dissertation. No terminal punctuation is to be used.

Curriculum Vitae

NAME: Marilyn E. Allen.

DEGREE AND DATE TO BE CONFERRED: Ph.D., 2021.

SECONDARY EDUCATION:
West Windsor-Plainsboro High School, Plainsboro, NJ, 2012.

COLLEGE INSTITUTIONS ATTENDED:
University of Maryland, Baltimore County (UMBC), Baltimore, MD
Doctor of Philosophy in Chemical and Biochemical Engineering, 2021.
Tufts University, Medford, MA
Bachelor of Science in Chemical and Biological Engineering, May 2016.

MAJOR: Chemical and Biochemical Engineering.

PROFESSIONAL PUBLICATIONS:
Allen, M.E., Golding, A., Rus, V., Karabin, N.B., Li, S., Lescott, C.J., Bobbala, S., Scott, E.A., and Szeto, G.L. *Targeted Delivery of Chloroquine to Plasmacytoid Dendritic Cells Enhances Inhibition of the Type I Interferon Response*. bioRxiv 2021[preprint server, manuscript submitted].

Allen, M.E., Rus, V., and Szeto, G.L. *Leveraging Heterogeneity in Systemic Lupus Erythematosus for New Therapies.* Trends Mol Med 2020.

PROFESSIONAL POSITIONS HELD:
- **University of Maryland School of Medicine**, Baltimore, MD, *Volunteer,* March 2020.
- **Association for Women in Science – Greater Baltimore Chapter**, Baltimore, MD, *VP Public Relations,* Feb. 2020 - June 2021.
- **The Annual Biomedical Research Conference for Minority Students**, Anaheim, CA, *Exhibitor and Poster Judge*, Nov. 13-16, 2019.
- **Lupus Foundation of America**, *Ambassador*, April 2019 - Present.
- **Annual STEM Event at the University of Maryland, Baltimore**, Baltimore, MD, *Volunteer*, 2018 - 2020.
- **UMBC BioCHEGS Graduate Student Organization**, Baltimore, MD, *Senator*, Sep. 2016 - May 2017; *President*, Sep. 2017 - May 2018.
- **Meyerhoff Advisory Board**, Baltimore, MD, *Member*, 2016 - 2019.
- **Higher Achievement Baltimore**, Baltimore, MD, *Mentor/Volunteer*, 2016.
- **American Association of Immunologists**, *Member*, Jan. 2019 - Present.
- **Graduate Women in Science**, *Member*, Jan. 2019 - June 2021.
- **Biomedical Engineering Society**, *Member*, May 2019 - Present.
- **The National Society of Black Engineers**, **Tufts University Chapter**, *President*, 2014 - 2016; *Membership Chair*, 2013 - 2014, **UMBC Chapter**, *Member*, 2012 - 2021.

ABSTRACT

Title of dissertation:	NANOSTRUCTURES ENCAPSULATING ANTIMALARIAL DRUGS FOR IMPROVED SYSTEMIC LUPUS ERYTHEMATOSUS TREATMENT
	Marilyn E. Allen, Doctor of Philosophy, 2021
Dissertation directed by:	Jennie Leach, Ph.D. Department of Chemical, Biochemical, Environmental Engineering

Systemic lupus erythematosus (SLE) causes damaging inflammation in multiple organs via the accumulation of immune complexes. These complexes activate plasmacytoid DCs (pDCs) via TLR7 and TLR9, contributing to disease pathogenesis by driving secretion of inflammatory type I IFNs. Antimalarial drugs, such as chloroquine (CQ), are TLR antagonists used to alleviate inflammation in SLE. However, they require 3 months of continuous use before achieving therapeutic efficacy and can accumulate in the retinal pigment epithelium with chronic use resulting in retinopathy. We hypothesized that poly(ethylene glycol)-b-poly(propylene sulfide) (PEG-b-PPS) filamentous nanostructures, filomicelles (FMs) could improve drug activity and reduce toxicity by directly delivering CQ to pDCs via passive, morphology-based targeting. Healthy human PBMCs were treated with soluble CQ or CQ-loaded FMs, stimulated with TLR agonists or SLE patient sera, and type I IFN secretion was quantified via multi-subtype IFN-α ELISA and MX1 gene expression using real-time RT-qPCR. Our results showed that 50 μg CQ/mg FM decreased *MX1* expression and IFN-α production after TLR activation with either synthetic nucleic acid ag-

onists or immune complex rich sera from SLE patients. Cellular uptake and biodistribution studies showed that FMs preferentially accumulate in human pDCs *in vitro* and in tissues frequently damaged in SLE patients (*i.e*., liver and kidneys) while sparing the eye *in vivo*. These results showed that nanostructure morphology enables drug delivery, and CQ-FMs may be equally effective and more targeted than soluble CQ at inhibiting SLE-relevant pathways.

NANOSTRUCTURES ENCAPSULATING ANTIMALARIAL DRUGS
FOR IMPROVED SYSTEMIC LUPUS ERYTHEMATOSUS
TREATMENT

by

Marilyn E. Allen

Dissertation submitted to the Faculty of the Graduate School of the
University of Maryland, Baltimore County, in partial fulfillment
of the requirements for the degree of
Doctor of Philosophy
2021

Advisory Committee:
Jennie Leach, Ph.D., Chair/Advisor
Gregory Szeto, Ph.D., Co-Advisor
Douglas Frey, Ph.D.
Amit Golding, M.D., Ph.D.
Evan Scott, Ph.D.
Violeta Rus, M.D., Ph.D.

Dedication

To my father and mother who have been there to celebrate, encourage, and champion me. I am forever grateful for their love, prayers, and support that have grounded me throughout this process.

To my grandmothers, Kathleen and Laura, who overcame many obstacles to grant me the opportunities I have today. Their commitment to education and life-long learning have empowered me during my academic journey.

Acknowledgments

I want to thank my mentors who have shaped my intellectual and professional development during the completion of this work.

Thank you to my thesis advisor, Greg Szeto, for trusting me to establish a new research area in his lab and, importantly, providing the guidance, training, and encouragement to make this project a success. I am very grateful for unique opportunities to grow as a researcher and train in his lab.

My committee members, Amit Golding, Douglas Frey, Evan Scott, Jennie Leach, and Violeta Rus, encouraged me to think critically about the research and provided invaluable expertise. They have proved to be wonderful mentors and collaborators during my graduate studies.

ment process was an invaluable experience because I was able to appreciate research from a new perspective.

I can hardly find the words to express my gratitude to my family. My parents, Marc and Liz, have been there for every milestone and challenge that accompanied me on my journey to this degree. Because of them, I was motivated and supported to finish. My brother, Marcus, having finished graduate school, served as a secondary mentor and advisor. He reminded me that life continues while in school and to take time to enjoy the process.

Table of Contents

Chapter 1:   Introduction and Literature Review

The first mention of lupus in medieval literature dates back to a 9th century man, Eraclius, from the city of Liège who was diagnosed with a disease called "the wolf" [1].The etymological origin of *lupus* is Latin for wolf, which is in reference to the way cutaneous rashes "eat at the flesh" [1]. Lupus falls within the expertise of rheumatologists, clinicians and researchers who are experts in musculoskeletal disease and systemic autoimmune conditions affecting the joints, muscles, and bones. There are four types of lupus: cutaneous, drug-induced, neonatal, and systemic lupus erythematosus (SLE). The Lupus Foundation of America estimates 1.5 million people in the United States are affected by a form of lupus. SLE is the most common form, representing 70% of people with lupus.

SLE is characterized as an autoimmune, immune-complex mediated disease that causes inflammation of multiple organs or organ systems. SLE is thought to be caused by a combination of genetic susceptibility and environmental exposures. It is the most heterogeneous autoimmune disease with a variety of clinical manifestations, organ involvement, disease severity, and laboratory abnormalities. The clinical presentation of SLE is varied, unpredictable, and includes transient, evolving symptoms that mimic other diseases, leading to its classification as one of medicine's "great imitators." This contributes to a delay in diagnosis estimated to be up to six years after presentation of initial symptoms [2] and difficulty in treatment. SLE can affect men and women across age, ethnic, and racial groups. However, there is a strong female bias, with women comprising up to 90% of patients [3, 3, 4]. Women of African, Asian, Hispanic/Latino, and Native American ancestry or ethnicity are

two to three times more likely to develop the disease than women of European ancestry. The disease predominately presents in women of childbearing age (15-44 years old) [5], which raises specific challenges regarding disease management during pregnancy.

The disease is characterized by the dysregulation of the innate and adaptive immune system (Fig. 1.1), leading to loss of tolerance to nuclear antigens. Antinuclear antibodies are generated that recognize a variety of antigens and are present in 95% of patients at diagnosis. Some autoantibodies precede diagnosis by years in patients that are asymptomatic, while others appear a few months before onset of clinical manifestations. The most common manifestations among SLE patients [6] are hematological [7]; musculoskeletal (i.e., arthritis); cutaneous rash; photosensitivity; constitutional symptoms (i.e., fever, fatigue, weight loss, oral or nasal ulcers); renal [8]; neuropsychiatric [9]; pleurisy [10]; pericarditis [11]; and Raynaud's phenomenon. Pathologically, deposition of circulating immune complexes comprised of endogenous nuclear antigen and autoantibodies leads to tissue and organ damage [12].

1.1   Standard of Care

Treatment of SLE aims to control disease activity, prevent organ damage, reduce morbidity, and improve patient survival and health-related quality of life. Current standard of care is dictated by type and severity of organ involvement. Antimalarial drugs, non-steroidal anti-inflammatory drugs, and low dose corticosteroids are used to treat constitutional symptoms and mild disease. Broad immunosuppression with methotrexate, azathioprine,
cyclophosphamide, cyclosporine, mycophenolate mofetil, leflunomide, and tacrolimus is reserved for patients with persistent manifestations and moderate-to-severe organ involvement. All immunosuppressive drugs are associated with significant toxicity and a wide
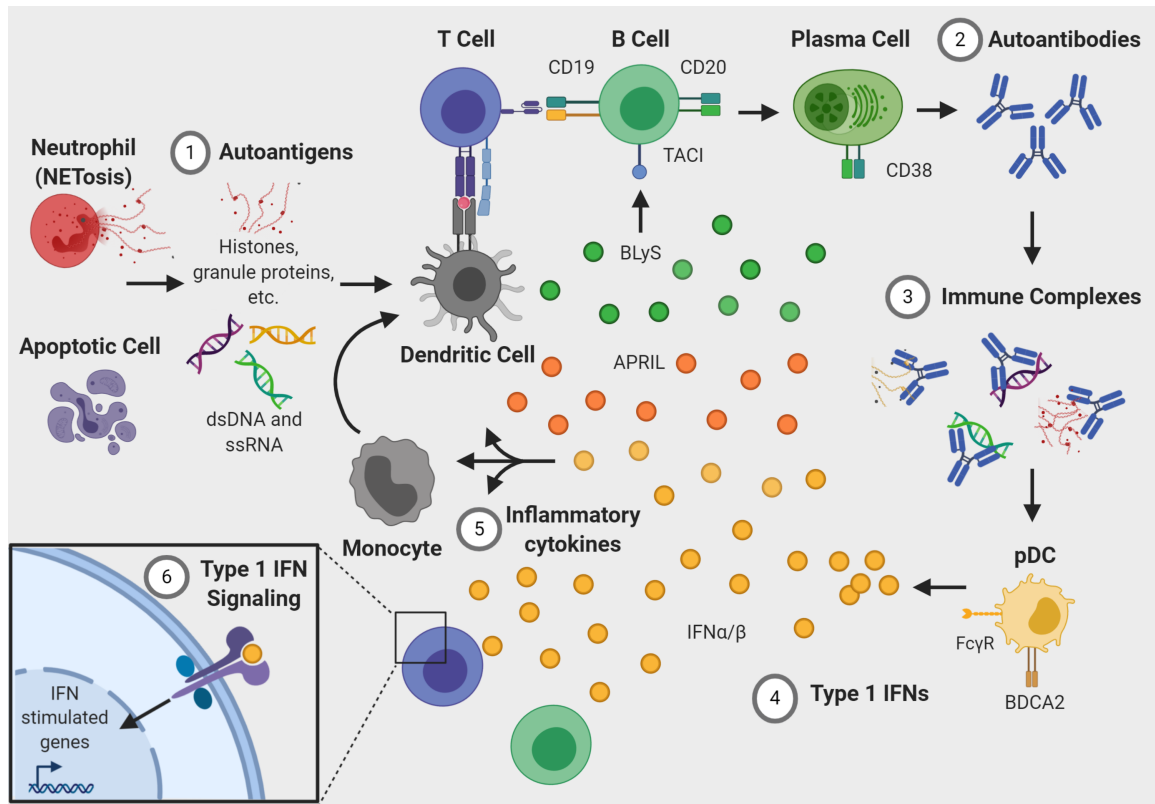
Figure 1.1: **SLE pathogenesis.** (1) Autoimmune responses are initiated by immune recognition of autoantigens derived from diverse sources, including apoptotic material from dead and dying cells and neutrophil extracellular trap debris. These autoantigens include double-stranded DNA (dsDNA), histones, small nuclear RNP (snRNP), Ro/SSA, and La/SSB. (2) Autoantigens are presented by dendritic cells to self-reactive CD4+ T cells, which provide help to B cells, resulting in cellular activation and the production of pathogenic autoantibodies by plasma cells. (3) Autoantibodies bind to circulating autoantigens to form immune complexes that engage Fc gamma receptors (FcγRs) on plasmacytoid dendritic cells (pDCs), leading to internalization via endocytosis.(4) Intracellular toll-like receptors (TLRs)-7 and -9 are activated by nucleic acids in immune complexes, resulting in type I interferon (IFN) production. (5) Immune complexes and chronic immune activation contribute to excessive production of proinflammatory cytokines. IFN-α is one major cytokine in this milieu, which promotes production of pro-B cell survival cytokines (e.g., APRIL, BLyS) via the innate immune cells to support B cell maturation. IFN-α can also contribute to pathogenic activation of T cells and differentiation of monocytes into dendritic cells. (6) Many cytokine receptors, including type I and II IFNs, transduce signals using the Janus kinase (JAK)/signal transducer and activator of transcription (STAT) pathway. Type I IFN receptors activate JAK/STAT to drive transcription of IFN-stimulated genes to promote inflammation. Immunological networks are shown with arrows. Abbreviations: APRIL, A proliferation-inducing ligand; BLyS, B lymphocyte stimulator; IFNAR, interferon alpha and beta receptor; TACI, transmembrane activator and calcium modulator and cyclophilin ligand interactor. Modified from Allen *et. al.*, (2020) [13].

3

range of morbidities. Early detection and aggressive medication regimens have substantially improved SLE survival outcomes from 50% in the 1960s to 90% in the 1990s [14]. Despite this progress, from 2000 to 2015, SLE was among the leading causes of death among young women aged 15-24 in the United States [15–17], and the physical burden of SLE has an economic impact of $20,000-$50,000 lost annually per patient from combined direct health care costs and lost work hours [18–20]. There is no known cure.

1.1.1 Management of Flares

Important aspects of clinical management are the treatment and prevention of disease flares. Variability in clinical trial design has resulted in different definitions of SLE flare with no universal consensus. An international meeting convened by the Lupus Foundation of America proposed defining an SLE flare as an episode associated with organ damage, significantly worse patient outcomes as evaluated by an assessor, and consideration of an increase in or modification of treatment [21]. SLE flares are intermittent and may occur without any clear warning. Flares can be symptomatic, with clinical manifestations, such as joint pain, skin rash, or oral ulcers, or silent and only detected through laboratory testing of hematologic and renal parameters. Triggers such as stress, infection, injury, hormones, drugs, and UV light may exacerbate inflammation and cause immune system hyperactivity [22]. Nonrenal disease flares are classified as mild, moderate, or severe [23]. Mild flares are managed by a combination of hydroxychloroquine, glucocorticoids, methotrexate, and azathioprine. Treatment for nonrenal severe flares adds mycophenolate mofetil and cyclophosphamide to drug regimens used for mild flares [23]. Hydroxychloroquine is a cornerstone treatment for all SLE patients due to multiple advantages, including cardioprotective effects [24], improved patient survival [24], reduction of disease flares and disease activity [25], and decreased thrombotic events [26]. Lifelong treatment continues

with hydroxychloroquine unless contraindicated due to retinal toxicity, a rare side effect for 10% of patients who develop retinopathy after 20 years of use [27, 28]. Moderate-to-severe flares resulting in kidney damage from lupus nephritis are treated based on the histological class of the renal biopsy. Lupus nephritis is a serious manifestation and one of the leading causes of morbidity and mortality, affecting approximately 50% of patients [29]. Glomerular lesions in immune complex-mediated lupus nephritis are classified according to the 2003 International Society of Nephrology/Renal Society nomenclature in six classes, from class I with mesangial involvement to class VI with advanced sclerosing lesions in >90% of glomeruli [30, 31]. Lupus nephritis patients with class III, IV, and V lesions receive antimalarial drugs along with immunosuppressive agents (i.e., mycophenolate acid derivatives, cyclophosphamide, or calcineurin inhibitors) and corticosteroids, but management should be individualized for each patient.

1.1.2 Management of SLE During Pregnancy

SLE predominantly impacts women during reproductive age. Pregnant women with SLE are at high risk for maternal and fetal morbidities. Management of high disease activity and prevention of flares prior to conception are imperative. With proper care, women can maintain a healthy pregnancy with symptom monitoring and regular examinations by a rheumatologist and a maternal–fetal obstetrics team. Sixty years ago, women with SLE were advised against pregnancy due to high fetal death rates and severe flares. Today, management of symptoms and pregnancy is possible, resulting in a decrease in pregnancy loss from 43% in the 1960s to 17% in the early 2000s [32]. Adverse outcomes include miscarriage, preterm birth, intrauterine growth retardation, pre-eclampsia, congenital heart block, and neonatal SLE [33]. Risk of preterm birth increases to approximately 60% of SLE pregnancies with increasing Systemic Lupus Erythematosus Disease Activity Index

5

(SLEDAI) disease activity [34]. Women with active lupus nephritis, renal insufficiency, pulmonary arterial hypertension, and antiphospholipid syndrome are also at increased risk for pregnancy complications [35]. As a result, laboratory screening of antiphospholipid antibodies, testing for anti-Ro antibodies that are associated with fetal congenital heart block and neonatal lupus, and monitoring for renal involvement are recommended.

Measurement of complement proteins, C3 and C4, as biomarkers for disease activity during SLE pregnancy is complicated by the fact that these proteins are generally elevated in normal pregnancies and, thus, less reliable as a marker of flares [36]. However, a study found that increased levels of Bb and sC5b-9 early in pregnancy were significantly associated with adverse outcomes in patients with SLE and/or antiphospholipid antibodies [37]. Medications that are generally acceptable during pregnancy and breastfeeding include hydroxychloroquine, azathioprine, cyclosporine, tacrolimus, steroids, and intravenous immunoglobulins [38]. Choice of drugs used during pregnancy and breastfeeding incorporates physician input, prevention of disease activity, reduction of harm to the fetus, and limited adverse side effects when compared to untreated disease. Adherence to hydroxychloroquine during pregnancy has multiple benefits, including a favorable risk-to-benefit ratio [39, 40], lower risk of pre-eclampsia [41], reduced disease activity, decreasing steroid doses, and limiting risk of neonatal cardiac manifestations [42]. Risk assessments of biologics, such as belimumab and rituximab, are limited and require more analysis. Future studies exploring the compatibility of novel therapies with pregnancy will be important for broadening treatment options in this patient group.

1.2   History, Use, and Mechanism of Action of Antimalarial Drugs for SLE Therapy

Antimalarial drugs, specifically hydroxychloroquine (proprietary name, Plaquenil) and chloroquine (proprietary name, Aralen), form the basis of pharmacotherapy for SLE. They have good safety profiles and are the cheapest and most commonly prescribed disease-modifying anti-rheumatic drugs for SLE patients [43, 44]. The first use of antimalarial drugs, quinine, was thought to be used in 1630 for the wife of a Peruvian Viceroy, the Countess of Chinchon, to successfully treat 'tertian fever' or malaria. The drug was derived from powdered cinchona bark, which is now known to supply over 30 active alkaloids with antipyretic, anti-inflammatory, antimalarial, myorelaxant, and antiarrhythmic properties [45]. In 1820, J.B. Caventou and P.J. Pelletier extracted oil from chinchona bark resulting in quinine. In 1894, J.S. Payne prescribed quinine to successfully treat what was described as features of a lupus rash [46]. However, it was during World War II where the efficacy of antimalarial drugs for rheumatic diseases was revealed. Soldiers prescribed quinacrine (proprietary name, Atabrine) as a malaria prophylactic saw symptomatic improvements of inflammatory arthritis and cutaneous lupus. This lead to critical research that defined the use of antimalarial drugs for autoimmune diseases. By the 1950s, chloroquine and hydroxychloroquine were introduced with better tolerability and efficacy than quinacrine [46], and the U.S. Food and Drug Administration (FDA) approved the use of hydroxychloroquine for lupus in 1955.

Hydroxychloroquine and chloroquine are weak bases belonging to a class of drugs called 4-aminoquinolines. Antimalarial drugs are administered as salts, such as hydroxychloroquine sulfate and chloroquine phosphate, to increase water solubility. Both drugs have characteristically long half-lives (40-60 days) due to their extensive volume of

distribution in the blood [47] and long mean residence times (approximately 1,300 h for hydroxychloroquine and 900 h for chloroquine) within aqueous cellular and intracellular compartments [48]. Antimalarial drugs also deposit in melanin rich areas such as the skin and the retinal pigmented epithelium [49]. Retinopathy, or damage to the retina, is the most severe complication association with treatment. Risk is increased for drug doses exceeding 5 mg/kg body weight per day; prolonged use (10-25 years); high cumulative dose (>600-1,000 g); and chronic kidney disease [50]. Ocular adverse reactions can be minimized by routine ophthalmologic examination and adhering to a recommended maximum dose of 5.0 mg/kg actual body weight per day [23]. A limitation of hydroxychloroquine and chloroquine treatment is the delayed onset of action. Patients require up to >3 months of continuous treatment before receiving any therapeutic benefits from antimalarial drugs [47]. Despite being well absorbed after oral administration (70-80 % bioavailiability), antimalarial drugs have prolonged half-lives (40-50 days), resulting in extended periods of time before adequate (96 %) steady state drug levels are achieved [47]. A related challenge of hydroxychloroquine treatment is non-adherence: in a cohort of 1,956 SLE patients older than 18 years old, only 58% of participants followed their hydroxychloroquine treatment regimens for at least 80% of the study [51]. Low blood concentrations of hydroxychloroquine are associated with increased risk of flares in SLE patients [52].

There are multiple mechanisms of action of antimalarial drugs (Fig. 1.2).

As weak bases, hydroxychloroquine and chloroquine accumulate in acidic lysosomes (lysosomotropism) and interfere with lysosomal activity and autophagy [54–56]. Antimalarial drugs increase the pH of endosomal compartments, impairing major histocompatibility complex class II-mediated autoantigen processing and presentation via the lysosomal pathway [53]. In addition to inhibition of lysosomal activity and autophagy, antimalarial drugs also inhibit Toll-like receptor (TLR) signalling pathways. Changes to pH mediated by hydroxychloroquine and chloroquine can interfere with endosomal TLR7 and
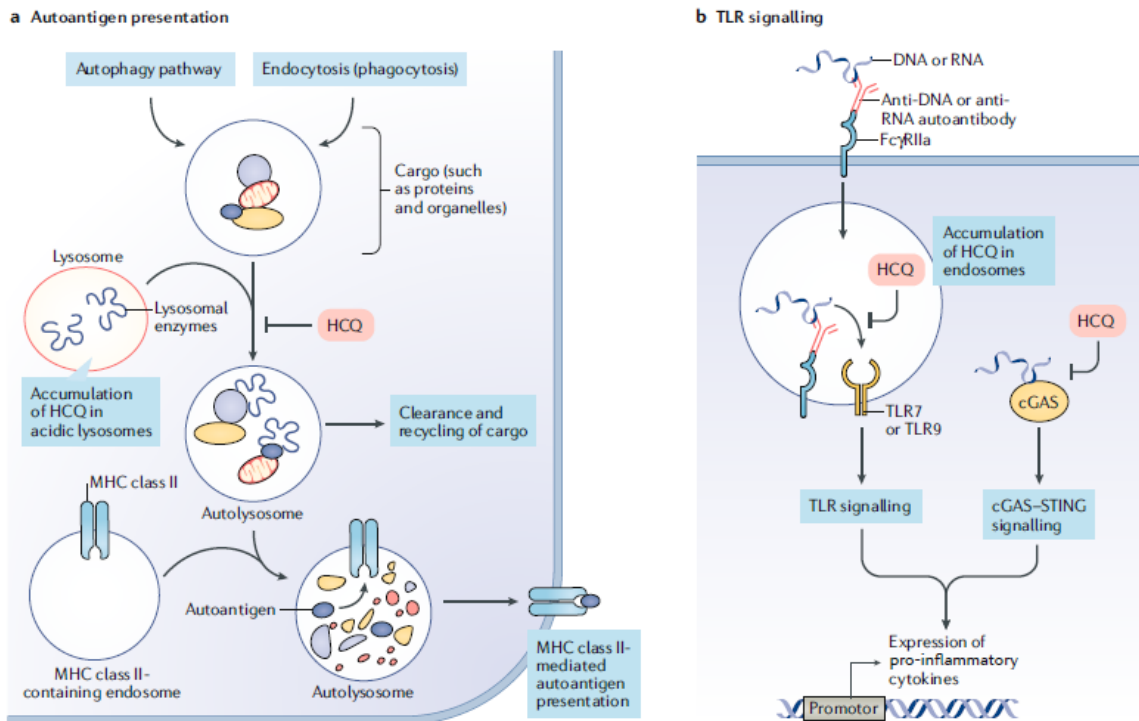
Figure 1.2: **Proposed mechanisms of action for hydroxychloroquine. a**) Hydroxychloroquine (HCQ) enters and accumulates in lysosomes along a pH gradient. In lysosomes, hydroxychloroquine increases the pH in autolysosomes, inhibiting lysosomal enzymes that degrade extracellular cargo acquired via endocytosis or phagocytosis and intracellular cargo through autophagy **b**) Hydroxychloroquine can also accumulate in endosomes and bind to the minor groove of double-stranded DNA. This drug can inhibit Toll-like receptor (TLR) signalling by altering the pH of endosomes (involved in TLR processing) and/or preventing TLR7 and TLR9 from binding their ligands (RNA and DNA, respectively). Hydroxychloroquine can also inhibit the activity of the nucleic acid sensor cyclic GMP-AMP (cGAMP) synthase (cGAS) by interfering with its binding to cytosolic DNA. By preventing TLR and cGAS-stimulator of interferon genes (STING) signalling, hydroxychloroquine can reduce the production of pathogenic pro-inflammatory cytokines, including type I interferons. Image from Schrezenmeier, E. and Dörner, T. (2020) [53].

TLR9 processing and subsequent activation [57]. These drugs also directly bind to nucleic acids (i.e., DNA or RNA) of immune complexes, preventing TLR7 and TLR9 activation by masking key binding epitopes [58–61]. Another proposed mechanism of action is inhibition of the nucleic acid sensor cyclic GMP-AMP (cGAMP) synthase (cGAS) via impaired ligand binding [62]. Preventing TLR and cGAS-stimulator of IFN genes (STING)

signalling leads to a reduction in pro-inflammatory cytokines, such as type I interferons [62]. In SLE patients, significant evidence indicates IFN-α is a central mediator of SLE [63, 64]. Among adult SLE patients, 50–75% have a high type I IFN signature [65]. IFN-α drives SLE by diverse mechanisms, including suppressing regulatory T cell development [66], activating autoreactive T cells [67], and supporting autoantibody production in B cells [68]. Plasmacytoid dendritic cells (pDCs) are professional IFN-producing cells found in <1% of blood, producing 1,000X more IFN-α than other immune cells [69]. Within the context of SLE, pDCs take up immune complexes via FcγRs into endosomes where they activate TLR7 and TLR9, triggering type I IFN production by transcription factors such as IFN regulatory factor (IRF)-7. *In vitro*, antimalarial drugs reduce IFN-α, tumor necrosis factor (TNF), IL-6, and CCL4 production in pDC and natural killer cell co-cultures stimulated with RNA-containing immune complexes [70, 71] and decrease IL-1, IL-6, TNF, and IFN-γ in mononuclear cells [72]. In SLE patients, hydroxychloroquine reduces serum IFN-α levels [73] and inhibits immune activation via downregulation of the co-stimulatory molecule CD154 on CD4+ T cells [74].

Antimalarial drugs have numerous benefits: affordable [44]; safe for pregnant women (Section 1.1.2); well-tolerated with adjunctive immunomodulatory treatment (Section 1.1.1); reduces risk of renal disease and probability of renal damage [75]; improves survival [24]; and decreased disease activity. However, these benefits may be eclipsed by some of the challenges of treatment: prolonged (>3 months) use required before achieving therapeutic efficacy [47]; inconsistent patient compliance [51]; and risk of retinopathy with chronic use [27, 28]. For my thesis (Fig. 1.3), I test the innovative concepts that: 1) antimalarial drugs loaded into nanostructures and delivered directly to pDCs will reduce the dose required for therapeutic efficacy, 2) drug delivery will focus biodistribution to organs with high disease activity, such as the kidneys, while simultaneously 3) decreasing the risk of side effects such as retinopathy by reducing drug accumulation in the eye.
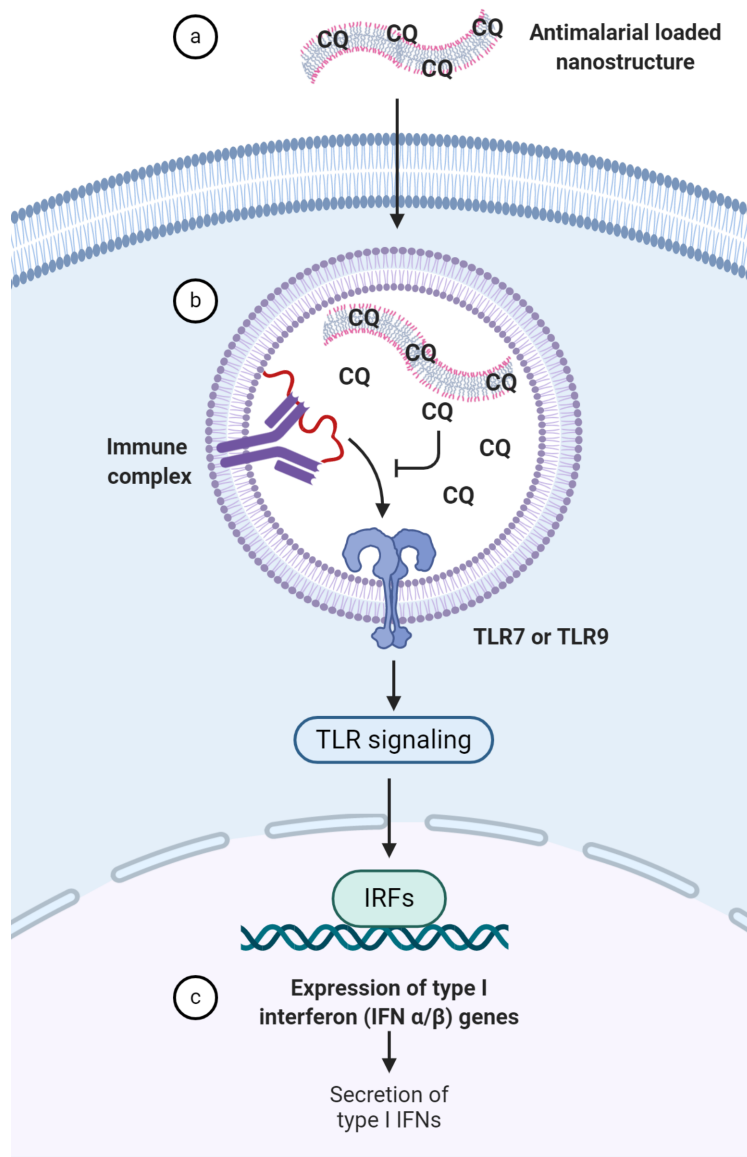
Figure 1.3: **Key figure. a**) Antimalarial drug loaded polymeric nanostructures traffic into endosomes where intracellular TLR7 and TLR9 are located. **b**) Controlled release of antimalarial drug, such as chloroquine (CQ), results in the inhibition of TLR7 and TLR9 activation by masking the binding epitope of nucleic acids contained on immune complexes. **c**) TLR inactivation and subsequent prevention of TLR signalling will prevent the production of pro-inflammatory cytokines, such as IFN-α, a major driver of SLE pathogenesis.

1.3 Nanostructures: Overview and Within the Context of Autoimmunity

The clinical benefit of drugs and novel vaccines is dependent upon their route of administration, which influences biodistribution, pharmacokinetics, absorption, metabolism, duration of therapeutic effect, clearance, and toxicity [76]. Efficacy may also be impacted by the controlled release of a drug at the therapeutic concentration and precise location needed to combat disease [77]. The inability of drugs to reach their designated target site results in only 1 in 9 new chemical entities receiving regulatory approval [78]. Even in ideal *in vivo* conditions, drugs may be degraded en route, be prohibited by endothelial structures (i.e., blood-brain barrier or blood-cerebrospinal fluid barrier), or result in undesirable side effects from accumulation in healthy tissue rather than disease sites. To address these limitations, drug delivery systems are engineered to selectively target and/or control release of drugs. These systems can improve pharmacokinetic and biodistribution profiles of drugs; compartmentalize drugs to tissue-, organ-, cell-, or subcellular-specific areas; biodegrade; minimize frequent dosing and maintain therapeutic drug concentration; deliver both hydrophobic and hydrophilic drugs; and other advantages [79]. With increasing prevalence of chronic disease, pharmaceutical advancements, and growth in biologics development, the drug delivery system industry is projected to reach USD $900 billion by 2025, according to Transparency Market Research. One type of drug delivery system is nanostructures.

Nanostructures are defined as materials on the scale of 1 to 100 nanometers (nm) in size in at least one direction (**Figure 1.4**).

As a reference, this page measures on average 100,000 nm thick. Nanostructures may be customized by their physicochemical features (*i.e.*, shape, size, hydrophobicity, and surface charge) and can take multiple forms: metallic, organic, inorganic, and polymeric [81]. They can also be used for varied applications: drug delivery, imaging, biosensing, and antimicrobial applications. As drug delivery platforms, nanostructures may passively
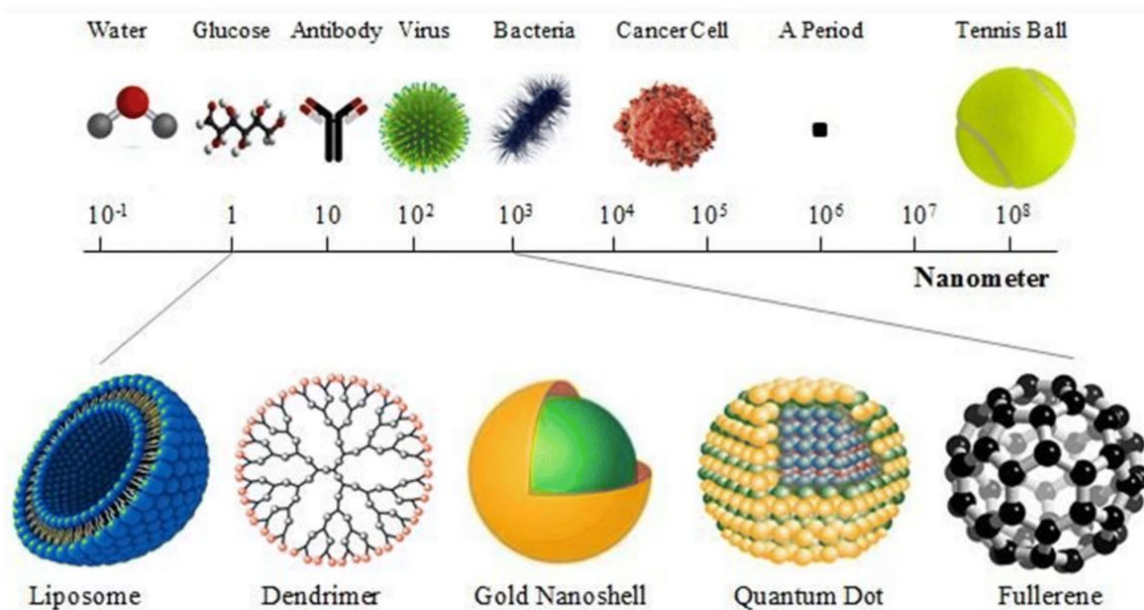
Figure 1.4: **Nanoscale.** Image from [80]

or actively deliver drugs to site-specific tissues and organs. Passive targeting relies on the nanostructures characteristics, not conjugation or ligands. For active targeting, nanostructure surfaces are decorated with moieties, such as antibodies and peptides, to anchor to receptors at the target site. When the nanostructures reach their desired location, there are a few mechanisms by which they can release their drugs, such as diffusion, solvent, chemical reactions, and stimuli-controlled release [79]. One of the major challenges with nanostructures is biological barriers that limit bioavailability and minimize therapeutic impact. Opsonization and sequestration by the mononuclear phagocyte system, adsorption of plasma proteins, nonspecific distribution, hemorheological limitations, cell membrane internalization, endosomal escape, and multidrug resistance all form hurdles to drug delivery systems [82]. These hurdles can be further complicated by route of administration, disease type, and disease severity. Innovative design principles are used to allow nanostructures to stealthily escape biological barriers. Some of these strategies include functionalizing nanostructures with poly(ethylene glycol)(PEG) or PEGylation [83], self-peptides (*e.g.*,

CD47 peptides) [84], or the coating of cell membranes from autologous leukocytes [85] or red blood cells [86]. Efforts to enhance nanostructure design has led to improved patient outcomes and expanded treatment options for a range of diseases, such as autoimmunity.

Nanotechnology, or the study and application of small materials, has grown since Richard Feynman introduced the concept in 1959 at the American Physical Society meeting at the California Institute of Technology. In 1995, the U.S. FDA approved liposomal doxorubicin (Doxil) for treatment of Kaposi's sarcoma [87]. In December 2020, the U.S. FDA issued an emergency use authorization for Moderna's mRNA-1273 and Pfizer-BioNTech's BNT162b2 vaccine against coronavirus disease 2019 caused by severe acute respiratory syndrome coronavirus 2 [88, 89]. Both vaccines utilize a lipid nanostructure formulation. Within the context of autoimmunity, PEG conjugates have been FDA-approved for the treatment of multiple sclerosis (IFN-β_{1a} drug Avonex) in 1996 [90] and rheumatoid arthritis in (Certolizumab pegol drug Cimzia) 2009 [91]. Currently, there is no approved drug delivery system, specifically nanostructures, for the treatment of SLE.

Preclinically, there are many emerging nanostructure strategies to tackle SLE. For example, an overarching problem in SLE pathogenesis is the formation and circulation of self-antigen and autoantibody containing immune complexes. Currently, plasmapheresis combined with intravenous cyclophosphamide, a potent alkylating agent that kills immune cells by inhibiting protein synthesis, is used to decrease pathogenic autoantibody titers [92, 93]. However, this treatment option does not lead to remission in severe end-organ damage. Another approach is the use of nucleic acid-scavenging dendrimers, synthetic polymers with repeated branching chains, to draw nucleic acid containing cell debris from apoptotic and dying cells. Previous work used a nucleic acid-scavenging dendrimers consisting of PAMAM-G3 as a high-affinity binding target to circulating nucleic acids in a spontaneous mouse models of SLE [94]. Although PAMAM-G3 reduced glomerulonephritis and circulating nucleic acids in mouse models, the high dose and toxicity of a high generation PA-

14

MAM dendrimer is a concern for *in vivo* studies and clinical translation. Another example is the use of nanostructures to target specific immune cells playing a role in SLE pathogenesis. IL-2 is a cytokine that supports T cell activation and proliferation, yet is decreased in SLE patients [95]. In lupus mouse models, a similar decrease in IL-2 reduces the number of regulatory CD4+ T cells (Tregs), leading to compromised immune tolerance [96, 97]. A Phase II clinical trial showed that SLE patients on standard treatment receiving low-dose IL-2 had expanded T_{regs} and natural killer cells and better remission rates compared with the placebo [98]. Horwitz and coworkers used anti-CD2/CD4 antibody coated poly(lactic-co-glycolic acid) (PLGA) nanostructures loaded with IL-2 and TGFβ to expand of CD4+ and CD8+ T_{reg} cells *in vivo* in lupus-prone mice, leading to suppression of anti-DNA antibodies and reduction of renal disease [99]. Previous studies by Look and colleagues encapsulated immunosuppressant mycophenolic acid, the prodrug form of mycophenolate mofetil used for SLE patients (Section 1.1), in spherical poly(ethylene) glycol nanogels coated with a lipid membrane. They found that these nanogels were more effectively internalized by a culture of CD11c+ bone marrow derived dendritic cells (BMDCs) *in vitro* than control polymer. Their nanogel platform also improved survival of lupus-prone NZB/W F1 mice and suppressed inflammatory cytokine production better than control polymer [100]. Nanostructures have also been used to issue low stability short interfering RNAs (siRNAs) *in vivo* without threat of degradation from nucleases. Shimizu and colleagues administered mitogen-activated protein kinase 1 (MAPK1) siRNA/nanostructure complexes to target glomeruli in the MRL/*lpr* lupus nephritis model [101]. Activation of p38 MAPK1 is thought to contribute to renal disease in MLR/*lpr* mice [102]. Targeted delivery of siRNAs, responsible for silencing the MAPK1 gene, to glomeruli via poly(ethylene glycol)-poly(L-lysine)-based nanostructures improved kidney function and reduced proteinuria [101].

1.4 Research Question

SLE therapies have made significant improvements over the last 10 years. In 2011, the monoclonal antibody belimumab inhibiting B lymphocyte stimulator (BLyS) was the first new FDA approval for SLE in >50 years. Preclinical studies show BLyS overexpression drives lupus-like disease in mice by providing key survival signals for autoreactive B cells and triggering proinflammatory T cells [103–105]. In two Phase III trials, belimumab reduced the numbers of plasma and B cells while significantly reducing SLE disease activity and severe flare risk [106]. Intravenous administered belimumab is indicated for adults and children with active, autoantibody positive SLE receiving standard treatment or adults with active lupus nephritis on other medications [107, 108]. In 2021, the U.S. FDA approved voclosporin in combination with a background immunosuppressive therapy regimen to treat adult patients with active lupus nephritis. This will be the second FDA approved therapy for lupus nephritis and the first oral treatment specifically for that manifestation. A Phase III trial AURORA (ClinicalTrials.gov Identifier: NCT03021499) of the calcineurin inhibitor voclosporin in patients with active lupus nephritis showed that treatment with voclosporin and standard of care doubled the proportion of complete kidney response compared with placebo and standard of care. This study also showed that voclosporin can be used with mycophenolate mofetil and low-dose corticosteroids for lupus nephritis treatment without increasing the rate of serious adverse events. Despite FDA approvals of belimumab and voclosporin, these therapies still require complementary, highly toxic immunosuppressive agents and corticosteroids to be effective. Even with other emerging SLE drug candidates, drug delivery and toxicity are persistent limitations.

Nanostructures may enhance drug delivery while mitigating adverse side effects and accumulation in off-target sites. For my thesis, I propose to directly target pDCs using antimalarial drug loaded cylindrical, filomicelle nanostructures without the use of a tar-

geting ligand, treating autoimmunity by suppressing TLR activation and subsequent type I IFN responses (Fig. 1.3). pDCs, the leading producer of IFN-α, is a major driver in early disease progression [63]. pDCs engulf nucleic acid-containing immune complexes via their FcγRIIa receptors and deliver immune complexes to their endosomal compartment. This leads to endosomal activation of TLR7 and TLR9 and recruitment of cytoplasmic pathway-dependent adaptor molecule, myeloid differentiation primary response 88. Downstream transcription factors such as interferon regulatory factors (IRF)-3 and IRF7 then initiate type I IFN expression. Specifically, no current approach uses passive, shape-based nanostructure targeting of antimalarials to pDCs to inhibit TLR activation. TLRs also have many potential for therapeutic targets because gene polymorphisms of TLRs lead to disease susceptibility [109], TLR ligands exacerbate disease [110, 111], and TLR inhibitors (i.e., antimalarial drugs) alleviate disease [112]. This approach will target SLE at a highly disease relevant site and pathway. By loading antimalarial drugs in nanostructures that target pDCs, I expect to increase the onset of active drug, limit toxicity, and decrease the antimalarial dose normally prescribed to lupus nephritis patients. My thesis will contribute to the field by 1) developing a novel drug delivery platform for SLE, 2) focusing nanostructure targeting to pDCs in SLE, 3) evaluating how morphology impacts immune cell targeting, and 4) determining how biodistribution of nanostructures informs drug biodistribution and toxicity.

Chapter 2: PEG-*b*-PPS Filomicelles Maintain Morphology Before and After Antimalarial Drug Loading

2.1   Introduction

The nanostructures we used to target pDCs are self-assembled poly(ethylene glycol)-b-poly(propylene sulfide) (PEG-*b*-PPS) block copolymers (**Figure 2.1**). PEG-*b*-PPS are non-immunogenic and non-inflammatory, exhibiting neither anti-PEG antibodies nor complement activation in both mice and non-human primates [113, 114]. While PEGylation is often used as a strategy to improve serum half-life and stability, PEGylated biopharmaceuticals have induced anti-PEG antibodies in patients, thereby reducing efficacy and leading to adverse side effects [115, 116]. Many PEGylated nanostructures are also known to activate the complement system, one of the first lines of defense in the innate immune system against invasive pathogens [117, 118]. The system consists of a series of serum and membrane-bound proteins that work to target pathogens via inflammation, phagocytosis, or cell membrane attack [119]. The tolerability and biocompatibility of PEG-*b*-PPS suggests the ability of these nanostructures to translate well from the bench to the clinic. The hydrophilic PEG fraction controls the morphology of the self-assembled nanostructures [120].The hydrophobic PPS block contributes to self-assembly, aggregate stability and retention of drug payload [121]. Upon oxidation, the hydrophobic PPS block coverts to hydrophilic poly(sulfoxide) or poly(sulfone), leading to nanostructure disassembly and release of drug payload [113]. These oxidation-sensitive nanostructures allow for release of

18

drug in the endolysosome of immune cells. This is important for inactivation of endosomal TLR7 and TLR9 by chloroquine, CQ, and resulting inhibition of the type I IFN response [53].

Figure 2.1: **Chemical structure of PEG-*b*-PPS nanostructures.**

Control nanostructures are poly(lactic-co-glycolic acid) (PLGA), an FDA approved polymer for drug delivery. For example, Lupron Depot containing a gonadotropin releasing hormone agonist, leuprolide acetate, in PLGA was approved for injection based delivery for the palliative treatment of advanced prostate cancer in 1989 [122]. More recently, Bydureon Bcise was approved in 2017 for PLGA encapsulated exenatide for treatment for type 2 diabetes [122]. As with PEG-*b*-PPS, PLGA is a highly biocompatible and biodegradable polymer. PLGA degrades by hydrolysis of its ester linkages into monomers lactic and glycolic acids, resulting in the release of drug payload. These monomers are typical byproducts of metabolic processes and are eliminated from the body as water and CO_2. Both PEG-*b*-PPS and PLGA nanostructures were loaded with hydrophobic CQ and characterized for size, morphology, and physicochemical properties.

2.2 Methodology

2.2.1 Materials

Chloroquine, 95% purity was purchased from Ark Pharm (Arlington Heights, IL, USA). Acid-terminated, 50:50 lactide/glycolide molar ratio, molecular weight (MW) 7,000-17,000 poly(D, L-lactide-co-glycolide) (PLGA); MW 25,000, 88% hydrolyzed polyvinyl alcohol (PVA); poly(ethylene glycol) methyl ether MW 2000; and organic solvents were purchased from Sigma Aldrich (St. Louis, MO, USA). Propylene sulfide was acquired from TCI Chemicals. Micro Float-A-Lyzer Dialysis Device, biotech grade cellulose ester, 8-10 kDa molecular weight cut off (MWCO) was purchased from Repligen (Waltham, MA, USA).

2.2.2 Nanostructure Formulation

Block copolymer PEG-*b*-PPS was synthesized as previously described [123]. PEG-*b*-PPS filamentous worm-like micelles, or filomicelles (FMs) were loaded with the hydrophobic antimalarial drug, CQ, via thin-film hydration. This is a method of loading and assembling nanostructures by drying polymer and drug co-dissolved in an organic solvent to a thin film and rehydrating to form small, uniform nanostructures [124]. Thin film hydration is preferred due to its straightforward protocol and minimal exposure of drugs to organic solvents, preventing alterations of drug activity. Some disadvantages include low encapsulation, heterogeneous nanostructure sizes, and small batches. An alternative strategy is flash nanoprecipitation, a technique that boasts scalability, reproducibility, and high loading of drug in nanostructures [114]. For flash nanoprecipitation, the organic phase consisting of hydrophobic drug and an amphiphilic block copolymer is impinged upon an aqueous solution under turbulent conditions using rapid multi-stream mixers [125]. The supersaturated solution precipitates and results in stabilized drug loaded monodisperse nanostructures.

The procedure requires a four stream multi inlet vortex mixer, a two stream confined impingement jet mixer, or other microfluidic mixer systems. Thin film hydration was chosen because it was simple and required no additional equipment. Briefly, 5-10 mg of PEG_{45}-b-PPS_{44} polymer was co-dissolved with equal mass CQ in 200 μL chloroform in a 5 mL sterile, clear, LPS-free glass vial. The solvent was evaporated at room temperature (RT) for 3-5 h, resulting in a thin film. The thin film was rehydrated at a total polymer concentration of 5-15 mg/mL with 1X phosphate-buffered saline (PBS) at pH 7.4 under gentle agitation overnight. CQ loaded nanostructures were purified from free CQ by 10K MWCO polyethersulfone membrane spin columns (VWR; Radnor, PA, USA) at 10,000 xg for 1-2 minutes and equilibrated with PBS solution.

FDA approved biodegradable and biocompatible PLGA polymer served as a control untargeted nanostructure. Spherical PLGA nanostructures were fabricated by oil-in-water emulsion/solvent evaporation technique [126]. Briefly, 5-10 mg PLGA and equal mass CQ was dissolved in 500 μL chloroform. The organic phase was emulsified in 2 mL of 0.5% PVA in 1X PBS solution using a probe sonicator at 50% amplification for 2 minutes on ice. The emulsion was added dropwise to 10 mL of 5% PVA in 1X PBS solution at RT. The continuous phase was homogenized at 6,800 x rpm with the T 25 digital ULTRA-TURRAX (IKA; Wilmington, NC, USA) and left to stir overnight at 600 x rpm at RT until the organic solvent was evaporated and nanostructures were hardened. CQ-loaded spherical PLGA nanostructures were purified from free drug by centrifugation for 5 minutes at 14,000 x g and washed three times with diH_2O. There are many different top-down approaches to PLGA nanostructure synthesis, such as emulsion evaporation, emulsion diffusion, solvent displacement and salting out. In a top-down method, nanostructures are formed from preformed polymer. Physicochemical properties of the nanostructures can be controlled for by choice of organic solvent (*i.e.*, increase hydrophobic interactions between polymer and drug, stabilize suspensions by controlling nanostructure dispersion state) or initial polymer

to drug concentration (*i.e.*, encapsulation efficiency and size). The emulsion-evaporation technique for encapsulated nanostructures was chosen due to its efficiency; easy implementation and scale-up; low fluctuations of polymer concentration; narrow size variability of nanostructures; low energy consumption due to minimal use of high energy equipment; and the ability to load both hydrophilic and hydrophobic active compounds [127].

2.2.3   Nanostructure Characterization

The size, morphology and physicochemical properties of each nanostructure batch were analyzed using small-angle X-ray scattering (SAXS), transmission electron microscopy (TEM), and dynamic light scattering (DLS) with zeta potential. SAXS is an analytical method used to determine averaged particle sizes or shapes. The advantage of SAXS is that size distributions can be determined over multiple nanostructures versus a select hundreds or thousands of nanostructures analyzed in traditional electron microscopy. SAXS was used to quantify the aspect ratio and variable length of the filamentous PEG-*b*-PPS nanostructures. SAXS was performed at the University of Maryland, College Park X-Ray Crystallographic Center using the Xenocs Xeuss SAXS/WAXS/GISAXS small-angle system with 8 keV (wavelength = 1.5 A) collimated X-rays. Samples were measured at 2.5 m from the CCD detector and analyzed within the 0.004-0.2 A^{-1} q-range calibrated by diffraction patterns of silver behenate. SAXS analysis was performed using IgorPro (WaveMetrics, Inc.; Portland, OR, USA) for 2D to 1D reduction and normalization of acquired sample scattering from buffer scattering. Model fitting was completed using SASVIEW 4.X based on the flexible cylinder model with the following parameters: 2 μm cylinder length, 150 nm persistence length, and 8 nm PPS core radius [128]. A limitation of SAXS is that analysis methods assume a constant shape, such as cylinder, and homogeneity over a given sample. Direct visualization of nanostructures using microscopy helps elucidates

irregularities or variations in shape [129].

To complement SAXS analysis, the FEI Morgagni 268 100 kV TEM equipped with a Gatan Orius CCD camera was used to compare morphology and appearance of blank and CQ-loaded nanostructures. TEM is a high resolution and high magnification technique that utilizes the transmission of an electron beam to image a sample. This method provides higher resolution than light-imaging techniques and is preferred for determining the size, size distribution, and morphology of nanostructures. For TEM processing, 10 µL of 12 mg/mL unloaded or loaded nanostructures were added to FCF200-Cu-TB coated grids for 3 minutes. Excess sample was removed with Whatman paper. 10 µL of autoclaved MegaPure water was added to the grids and then immediately removed with Whatman paper. 10 µL of 2% uranyl acetate was added to the grids for 2 minutes, followed by removal of excess stain. The grids were immediately processed after negative staining.

DLS is a technique that measures size and size distribution of nanostructures and other particulate dispersed or dissolved in a liquid. As the name implies, DLS measures the Brownian motion of nanostructures and the associated intensity of light scattering over time [130]. The speed intensity of fluctuations is dependent upon the size of the nanostructure. Smaller nanostructures diffuse more quickly than larger nanostructures. The hydrodynamic size of nanostructures is measured from the translational diffusion coefficient by using the Stokes-Einstein equation. The size of the nanostructure is the diameter of a sphere. For non-spherical particulates, such as rod-shaped nanostructures, a new rotational motion must be established to assume for differences in light scattering [131]. Zeta potential is the electric charge of a nanostructure's surface. Charge is an important nanostructure characteristic because it is a major determinant of serum protein absorption and cellular internalization by the mononuclear phagocyte system, mainly tissue resident macrophages [82]. Both size, size distribution, and zeta potential were measured at 1 mg/mL of nanostructures in 1X PBS solution (pH 7.4) using the Malvern Zetasizer Nano ZS.

Loading capacity, total loaded drug per mass of nanostructure, and encapsulation efficiency, percentage of initial drug mass successfully entrapped in the nanostructures, were measured by dissolving a known mass of loaded nanostructures in dimethyl sulfoxide (DMSO) followed by UV/Vis spectrophotometry analysis using the Mettler Toledo UV5 Nano. Drug loading per mass of nanostructure was determined by developing a standard curve of chloroquine in diluted in DMSO using the characteristic wavelength corresponding to maximum absorption of chloroquine at approximately 334 nm [49]. Drug release kinetics provides important information on the behavior and performance of nanostructures before time-consuming and expensive *in vivo* experiments. Release mechanisms and kinetics can be measured using a range of methods including sample and separation, dialysis membrane, and continuous flow. Dialysis membrane is the most widely used method due to its simple and straightforward set-up [132]. The basic principle is the drug loaded nanostructures are loaded into a dialysis membrane with a sufficiently high membrane molecular weight cut-off that would allow the drug to rapidly diffuse into the outer release medium. Diffusion is driven by the volume ratio of the inner compartment containing the drug loaded nanostructures and the outer compartment containing the release medium. A limitation of the dialysis membrane method is that it assumes that the drug release from the nanostructure is equal to the diffusion of the drug across the membrane from the inner compartment to the outer compartment [132]. Drug release kinetics were measured by placing drug-loaded nanostructures into microdialysis devices in 1X PBS solution with 1% bovine serum albumin (BSA) at 37 °C (physiological temperature), 5% CO_2. Samples were analyzed by UV/Vis spectrophotometry, as above, after 0, 2, 4, 6, and 24 h.

2.2.4   Statistics

All statistical analyses were performed using GraphPad Prism 9 software (GraphPad Software, San Diego, CA). A minimum of three independent replicates were conducted for nanostructure characterization experiments. Paired t-tests was used to test for statistical significance.

2.3   Results and Discussion

FMs and control spherical PLGA nanostructures were synthesized by thin-film hydration and emulsion/solvent evaporation, respectively. Nanostructure morphology was verified via SAXS. As expected, SAXS analysis of FMs best fit the scattering profile to a flexible cylinder model (**Supplemental Figure A.1**). The aspect ratio was calculated, and drug loading had no significant effect when comparing unloaded ($X^2 = 0.008$) versus CQ-loaded ($X^2 = 0.0012$) FMs (**Figure 2.2a**).

Key limitations of SAXS analysis methods are the assumptions of constant shape and homogeneity in a given sample. Direct visualization by TEM was used to complement SAXS and reveal potential variations in morphology [129]. Representative images showed that the morphology of unloaded and CQ-loaded FMs were consistent with micron length and 50 nm cross-sectional diameter (**Figure 2.2b**). DLS determined control spherical PLGA nanostructures had an average hydrodynamic diameter of 662.5 nm and 0.272 polydispersity index (PDI) for blank nanostructures compared to 562.6 nm and 0.221 PDI for CQ-loaded nanostructures. The PDI is a measure of particle diameter distribution, which ranges from 0 (perfectly uniform sample) to 1 (highly heterogeneous sample).

Surface charge is an important nanostructure characteristic because it is a major determinant of serum protein adsorption and cellular internalization by the mononuclear phago-
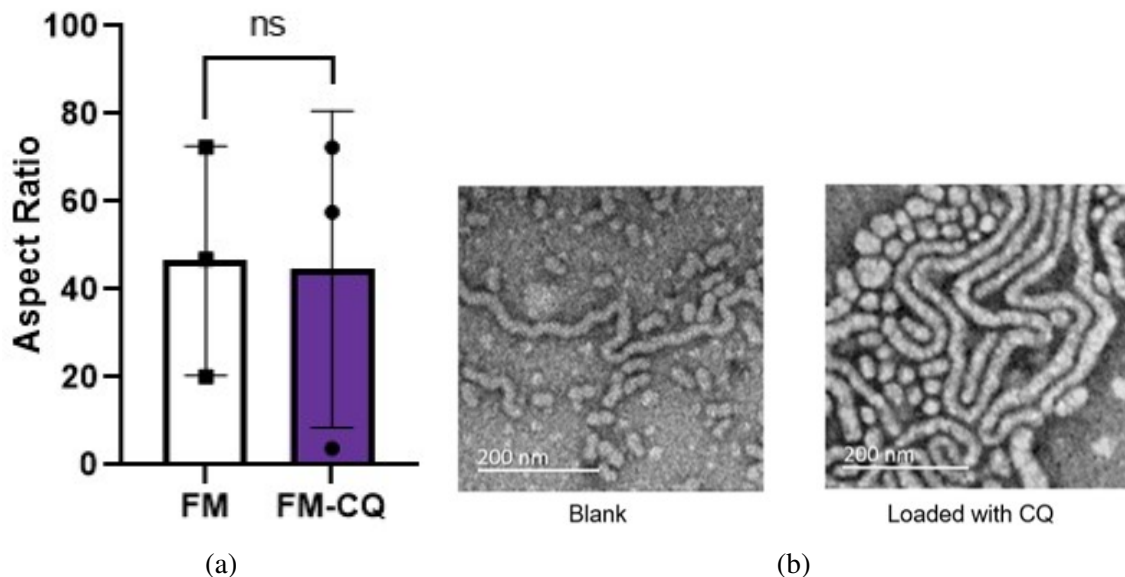
Figure 2.2: **CQ loading did not alter morphology of nanostructures.** **a**) Aspect ratio (width/height) of blank FMs ($n = 3$) and CQ-loaded FMs (FM-CQ) ($n = 3$). Length and diameter were measured by SAXS using the flexible cylinder model and the following parameters: 2 μm cylinder length, 150 nm persistence length, and 8 nm PPS core radius. Paired t-test for statistical analysis. **b**) Representative images from FEI Morgagni M268 100 kV TEM showed blank (left) and CQ-loaded (right) FMs at 12 mg/mL in 1X PBS. Samples were stained with 2% uranyl acetate.

cyte system, which consists mainly of tissue-resident macrophages [82]. Nanostructure surface charge also plays an important role in stability, where greater repulsion between nanostructures reduces aggregation [127]. The zeta potential of blank and loaded nanostructures was determined to be negative (**Figure 2.3**). Neutral or anionic nanostructures are less likely to adsorb serum proteins, be sequestered by tissue-resident macrophages, and have short serum half-lives in comparison to cationic nanostructures [133, 134]. These data confirmed that the physical (morphology, size) and biochemical (charge) properties of nanostructures were not affected by drug loading.

Next, we characterized the loading and release properties of CQ. Loading capacity and encapsulation efficiency were determined by dissolving CQ-loaded nanostructures in DMSO and quantifying CQ by UV/Vis spectrophotometry (**Supplemental Figure A.2**).
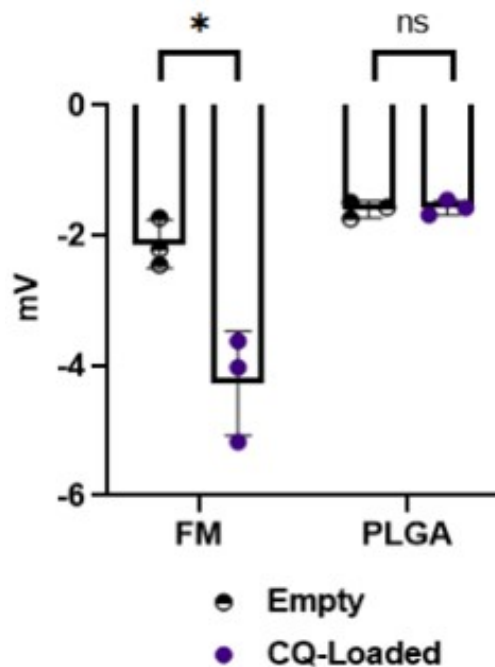
Figure 2.3: **Blank and CQ-loaded nanostructures are anionic.** Zeta potential ($n = 3$) of CQ loaded and blank (left) FMs or (right) PLGA. Data were shown as means with error bars representing standard deviation. Paired t-test was used for statistical analysis. Statistical significance: $*p < 0.05$. All samples were measured in 1X PBS solution (pH 7.4) at 1 mg/mL.

The average loading capacity was 49.96 ± 5.529 μg CQ per mg particle (mean ± standard deviation) for FMs (**Figure 2.4**) and 12.07 ± 2.255 μg CQ per mg particle for spherical PLGA nanostructures (**Figure 2.4**). The encapsulation efficiency for CQ was 50% for FMs and 0.6% for spherical PLGA nanostructures (**Figure 2.4**). In **Supplemental Figure A.3**, we also showed the versatility of drug loading in FMs by encapsulating other hydrophobic payload important in SLE treatment (**Section 1.1**), such as azathioprine and methylprednisolone, using the thin film hydration method. Overall, FMs demonstrated a high CQ loading capacity and maintained morphology before and after drug encapsulation (**Figure 2.2**). In comparison, PLGA had a considerably lower CQ loading capacity and encapsulation efficiency profiles (**Figure 2.4**). We optimized the PLGA formulation (**Section 2.2**) to improve drug retention by troubleshooting the interactions between polymer, drug,

and solvent. This included exploring different drug:polymer ratios; organic solvents; homogenizer and agitation speeds; and surfactant (*i.e.*, PVA) concentrations. Despite these modifications, CQ loading in PLGA maximized at the current formulation protocol.
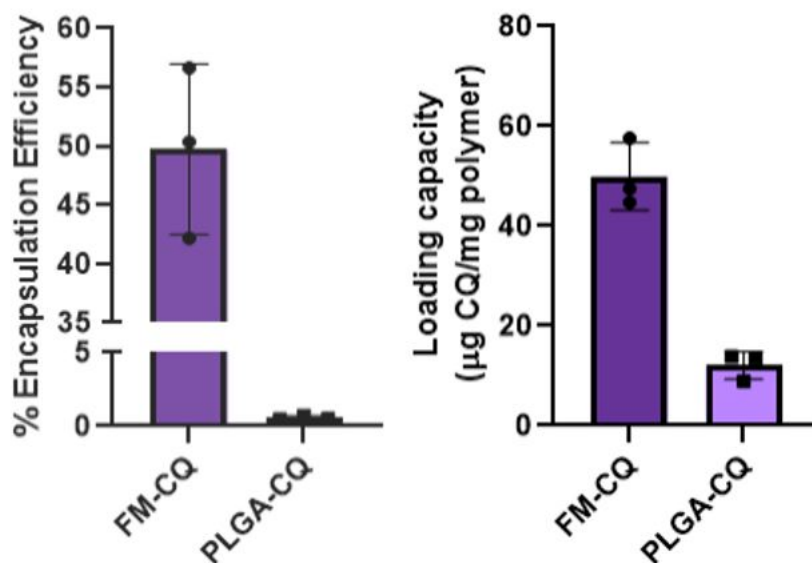

Figure 2.4: **CQ load into FM and PLGA nanostructures.** Loading capacity (*n* = 3) and encapsulation efficiency (*n* = 3) of CQ-loaded (left) FMs or (right) spherical PLGA nanostructures. All samples were measured in 1X PBS solution, pH 7.4 at 1 mg/mL. Data show mean and error bars represent standard deviation.

An ideal drug delivery system will release drug at a specific site and rate appropriate for the disease model and therapeutic intent. Controlled release of drug delivery systems consists of two parts: 1) diffusion of the drug from the polymeric matrix and 2) degradation of the polymer, liberating the encapsulated drug from the polymer matrix. For kinetic release studies, FMs were incubated *in vitro* for up to 24 h, and a characteristic burst release was observed followed by a plateau at approximately 50% release of encapsulated CQ (**Figure 2.5**). As expected, there is an initial burst release followed by a slow or controlled release from the polymeric matrix. Overall, these results demonstrated that CQ efficiently loaded into FMs and enabled controlled release.
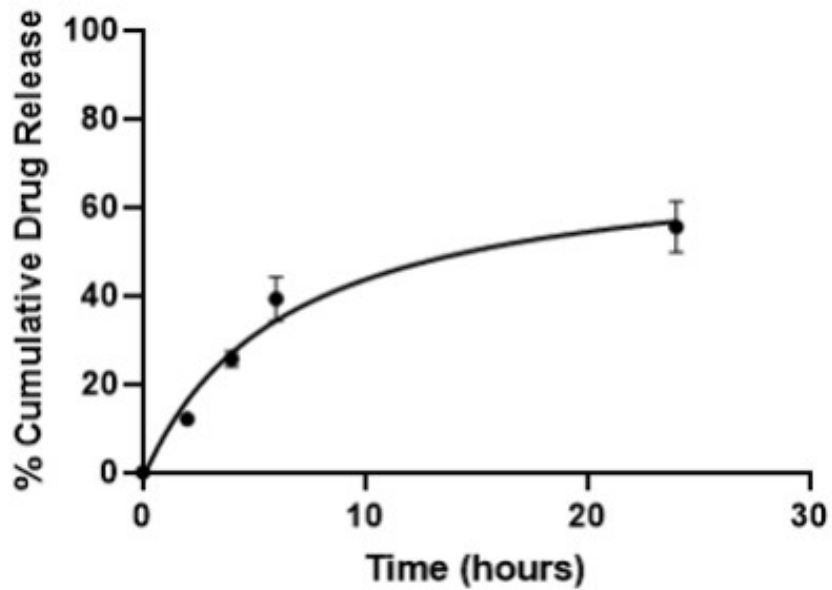
Figure 2.5: **CQ drug release profile from FMs.** CQ-loaded FMs ($n = 3$) were placed in 10K MWCO dialysis tubing in 1X PBS buffer plus 1% BSA for 0, 2, 4, 6, and 24 h at 37 °C, 5% CO_2. Each time point shows the average percentage cumulative drug release; error bars represent standard deviation.

Chapter 3:   Filomicelle Nanostructures Preferentially Associate with pDCs *In Vitro* and Spare the Eye *In Vivo*

3.1   Introduction

Blood circulation times [135], biodistribution, cell interactions, and clearance by recognition of the mononuclear phagocyte system [136] are impacted by nanostructure physiochemical properties and morphology (**Section 2.3**). In this work, we use morphology-based targeting of two nanostructure formulations, filamentous PEG-*b*-PPS and spherical PLGA, to deliver CQ to immune cells driving disease in SLE patients. The hydrophilic PEG fraction (f) of the total block copolymer molecular weight informs the geometry of the nanostructures, where $f > 45\%$ results in spherical micelles, $f <$ in filamentous micelles, and $45\% > f > 25\%$ in spherical polymersomes [121]. Morphology drastically alters cellular biodistributions. Spherical (*i.e.*, micelle or polymersomes) or cylindrical (*i.e.*, filomicelle) PEG-*b*-PPS are biodegradable with high specificity to blood-resident phagocytes, liver macrophages and tissue-resident dendritic cells [121]. In particular, FMs accumulate in 95% of splenic pDCs after the subcutaneous injection [137].

Passive targeting of PEG-*b*-PPS nanostructures avoids the use of cell-specific ligands to effectively target pDCs. Active targeting involves the addition of cell-specific ligands. While active targeting boasts numerous advantages, such as facilitated internalization, improved localization, and selective targeting, there are limitations. A few disadvantages of active targeting include: 1) immunogenicity of target ligand, resulting in increased clear-

ance, 2) receptor-mediated endocytosis, and 3) difficulties in scale-up and formulation optimization. For SLE therapeutics, active targeting of pDCs through antibodies is being investigated to blunt type I IFN production. Human pDCs express the cell surface receptor blood DC antigen 2 (BDCA2 or CD303) [138]. BIIB059 is a humanized IgG1 monoclonal antibody that crosslinks BDCA2 [139, 140], leading to inhibition of TLR7 and TLR9-induced IFN-α/β by both BDCA2 and FcγRIIa receptor internalization [138] and signaling that shares many components with the B cell receptor [139, 140]. In the Phase II LILAC trial and a small Phase I trial, BIIB059 ameliorated cutaneous lupus symptoms, reduced pDC skin infiltration, and normalized type I IFN responses, including *MxA* gene expression, showing benefit in both cutaneous lupus erythematosus patients and SLE patients with active joint or skin manifestations [141]. The trial design measured skin disease activity while monitoring IFN responses in whole blood and skin. The primary type I IFN producers, pDCs, preferentially accumulate in active skin lesions as well as kidneys of SLE patients [142, 143]. Larger studies are needed to determine efficacy and may also evaluate the potential for BIIB059 to ameliorate other pDC-driven organ manifestations, such as lupus nephritis. Overall, BIIB059 was well tolerated. The main reported side effect was elevated risk of infection due to dampening of pDC-mediated antiviral responses initiated by dose-dependent internalization of BDCA-2. Prolonged (112 days) BDCA-2 internalization occurred at high doses (20 mg/kg) of BIIB059 [141]. It remains unknown how prolonged BDCA-2 internalization reduces surface BDCA-2, whether receptor internalization limits the effects of subsequent BIIB059 doses, and how this shifts thinking on long-term dosing regimens. Currently, no approach uses passive, morphology-based nanostructure targeting of antimalarial drugs to pDCs to inhibit TLR activation and subsequent type I IFN production.

3.2 Methodology

3.2.1 Nanostructure *In Vitro* Distribution

FMs were loaded with the lipophilic fluorescent tracer, Vybrant DiD cell-labeling solution (Thermo Fisher; Waltham, MA, USA), via thin-film hydration method (as decribed in **Section 2.2**). In a 5 mL sterile, clear, LPS-free glass vial, 2.5 μL Vybrant DiD cell-labeling solution and 5-10 mg of PEG-*b*-PPS was co-dissolved in 150 μL dichloromethane. The solvent was evaporated at RT for 3-5 h and then resuspended at a total polymer concentration of 5-15 mg/mL with 1X PBS at pH 7.4 under gentle agitation overnight. Dye-loaded nanostructures were purified from free dye by dialysis or 10K MWCO polyethersulfone membrane spin columns (VWR; Radnor, PA, USA) at 10,000 xg for 1-2 minutes and equilibrated with PBS solution. Lipophilic dye loaded nanostructures at 200 μg/mL were incubated at 37°C, 5% CO_2 in 1 million fresh human peripheral blood mononuclear cells (PBMCs) from healthy donors (New York Blood Center; New York, NY) for up to 48 h in RPMI 1640 medium with GlutaMAX plus 10% fetal bovine serum (FBS), 1% sodium pyruvate, 1% nonessential amino acids (NEAA), 1% penicillin-streptomycin solution (penstrep), and 20 ng/mL recombinant human IL-3 (BioLegend; San Diego, CA, USA) to determine cellular distribution. PBMCs were stained with a viability dye and fluorescent antibodies to distinguish cellular subsets including CD19+ B cells (clone HIB19; Brilliant Violet 421), CD3+ T cells (clone OKT3; APC/Cy7), and CD123+ pDCs (clone 6H6; PE).

3.2.2 Nanostructure *In Vivo* Distribution

C57BL/6 is the most widely used inbred strain for general laboratory purpose. Female C57BL/6 mice, 6-8 weeks old, (Jackson Laboratory; Bar Harbor, ME USA) were injected intravenously by retro-orbital sinus with 150 μL free DiD (50 μg/mL in 1X PBS

solution) or DiD loaded FMs (7.5 μg of loaded DiD in each sample in 150 μL PBS). After intravenous injection, nanostructures are typically distributed in the blood, liver and spleen [144]. In the blood, nanostructures are sequestered by cells of the mononuclear phagocytic system such as dendritic cells, monocytes and resident macrophages in the spleen, liver and lymph nodes [82, 145]. The internalization of nanostructures by these cells is driven by opsonization, a process where the immune system targets a foreign particle for clearance via phagocytosis. This is facilitated by serum proteins (*i.e.*, albumin, apolipoproteins, complement components and immunoglobulin) coating the nanostructure when it enters the bloodstream [146, 147]. After protein adsorption, nanostructures are recognized by Fc receptors or complement receptors, which are important for serum protein recognition. This initiates a signaling pathway that regulates the actin cytoskeleton in phagocytes. The phagocytes then produce membrane protrusions that encapsulate the nanostructure and internalize it within the cell as an early endosome, late endosome, lysosome, and phagolysosome [148].

At 1- and 24-h post-injection, the eyes, kidneys, liver, and spleen were collected, mechanically dissociated, and digested with 0.1% collagenase, type 4 in Hanks' Balanced Salt Solution (Worthington; Lakewood, NJ, USA) followed by red blood cell lysis with ammonium-chloride-potassium lysing buffer (Lonza; Basel, Switzerland). Cells were filtered through a 70 μm nylon, DNase/RNase free, non-pyrogenic cell strainer (VWR; Radnor, PA, USA) and washed with 1X PBS. Single cell suspensions of each tissue at 250,000 cells per 200 μL in 1X DPBS were read on a BioTek Cytation 5 plate reader at the absorbance maximum of DiD (*i.e.*, 644 nm). The total mass of DiD per tissue was quantified by interpolation of sample measurements onto a standard curve of known concentrations of DiD in 1X DPBS using the characteristic maximum absorbance. Cell suspensions were stained for viability and phenotypic, anti-mouse cell surface markers, CD11b (clone: M1/70, FITC), CD11c (clone: N418, PE), CD3 (clone: 17A3, Brilliant Violet 605TM), and CD19 (clone: 6D5, PerCP/Cy5.5). Stained cells were then run on a flow cytometer and

analyzed for uptake of DiD loaded nanostructures.

3.2.3   Flow Cytometry

Flow cytometry is a laser-based method for multiparameter analysis of a single-cell suspension from cell culture or tissue samples. Flow cytometry analysis can determine the cell size and granularity; expression of cell surface and intracellular molecules; distinct cell types in a heterogeneous cell population; viability status; and purity of isolated sub-populations. Fluorescent labeled antibodies and dyes are curated in panels specific to the specifications of the flow cytometer used (*i.e.*, lasers and filters). These antibodies and dyes stain cells and detect cell-specific characteristics. The resulting fluorescence intensity or dye signal is then analyzed. The multicolor panels for the human and mouse experiments are described above. The flow cytometry staining protocol is described below:

Either Human TruStain FcX or TruStain FcX PLUS (BioLegend; San Diego, CA, USA) was used to block nonspecific binding of human or mouse Fc receptors, respectively, prior to immunostaining. For human cells, 5 μL of Human TruStain FcXTM was added per million cells in 100 μL staining volume of PBS plus 1% BSA. Cells were incubated for 5 minutes at RT. For mouse cells, 0.25 μg of TruStain FcX PLUS was added per million cells in a volume of 100 μL PBS plus 1% BSA for 5 minutes at RT. After blocking, cells were stained at 1:100 dilution with conjugated fluorescent antibodies (**Table 3.1**) in PBS plus 1% BSA for 15-20 minutes in the dark and on ice. Cells were washed with PBS. To discriminate between live and dead cells, Zombie Aqua Fixable Viability dye was used. This amine-reactive fluorescent dye binds to cytoplasmic proteins exposed by permeable dying cells, producing a high signal that can be detected and used to differentiate dead from live cells. Amine dyes are preferred over DNA-dyes (*i.e.*, 7-AAD and propidium iodide)

that bind to exposed DNA from compromised, dying cells because they can be used where cell fixation is required and they boast a wide range of excitation and emission spectra for diverse multi-color flow cytometry panel setups. Zombie Aqua Fixable Viability dye, diluted 1:1000 in PBS, was added to cells for 15-30 minutes at RT and in the dark. Cells were washed, resuspended in PBS plus 1% BSA, and immediately analyzed on a flow cytometer. A BD LSR II with 405, 488, 561, and 640 nm excitation laser lines or Beckman Coulter CyAn ADP consisting of 405, 488, and 635 nm excitation laser lines was used for flow cytometry analysis of fluorescently labeled cells. Data were analyzed using FlowJo LLC software v10.7 (BD). The gating strategies are available in the supplementary figures.

Table 3.1: Flow Cytometry Antibodies

Antibody	Clone	Catalog Number
Brilliant Violet 421 anti-human CD19	HIB19	302233
APC/Cy7 anti-human CD3	OKT3	317341
PE anti-human CD123	6H6	306005
PerCP/Cy5.5 anti-human CD4	RPA-T4	300529
APC/Cy7 anti-human CD1c	L161	331519
FITC anti-mouse/human CD11b	M1/70	101205
PE anti-mouse CD11c	N418	117307
Brilliant Violet 605 anti-mouse CD3	17A3	100237
PerCP/Cy5.5 anti-mouse CD19	6D5	115533

3.2.4   Study Approval

The animal study was reviewed and approved by UMBC Institutional Animal Care and Use Committee (OLAW Animal Welfare Assurance D16-00462).

3.2.5   Statistics

All statistical analyses were performed using GraphPad Prism 9 software (GraphPad Software, San Diego, CA). A minimum of three independent replicates were conducted for

human PBMCs experiments. For *in vivo* biodistribution experiments, 3-4 mice were used. Unpaired t-tests and ANOVA were used to test for statistical significance. P-values were adjusted for multiple comparisons by Tukey's or Šídák's test, and adjusted p-values <0.05 were considered significant.

3.3   Results and Discussion

Nanostructure size and shape are known to significantly alter their delivery and biodistribution in vitro and in vivo [82]. We evaluated whether FMs could address two key design needs: 1) targeting and preferential accumulation in pDCs in vitro and 2) biodistribution favoring major target organs in SLE while avoiding off-target effects in the eye *in vivo*. FMs were loaded with the lipophilic fluorescent dye DiD for tracking and added to cultures of human PBMCs *in vitro*. Flow cytometry was used to determine cellular targeting and association after 6, 24, and 48 h. pDCs represent an average of 0.29% of all cells in healthy human PBMCs but accumulated more FMs than B and T cells after 48 h (**Figure 3.1a**).

DiD+ cells were quantified, and their median fluorescent intensity calculated to estimate both the fraction of cells taking up nanostructures as well as the amount of nanostructures internalized per cell. pDCs were consistently associated with nanostructures compared to more abundant cells (12.6% DiD+ of T cells) and total live cells (98.08% of PBMCs) (**Figure 3.1a**). The intensity of DiD in pDCs was also highest among all analyzed cell types (average MFI of 25.73 after 48 h), suggesting FMs accumulated mainly in pDCs (**Figure 3.1b** and representative gating strategy shown in **Supplemental Figure A.4**). Together, these results demonstrated the highly targeted accumulation of FMs in pDCs despite their relatively low abundance.

The biodistribution of nanostructures is strongly influenced by parameters such as size, morphology, dose, and administration route. Typically, accumulation in blood filtration
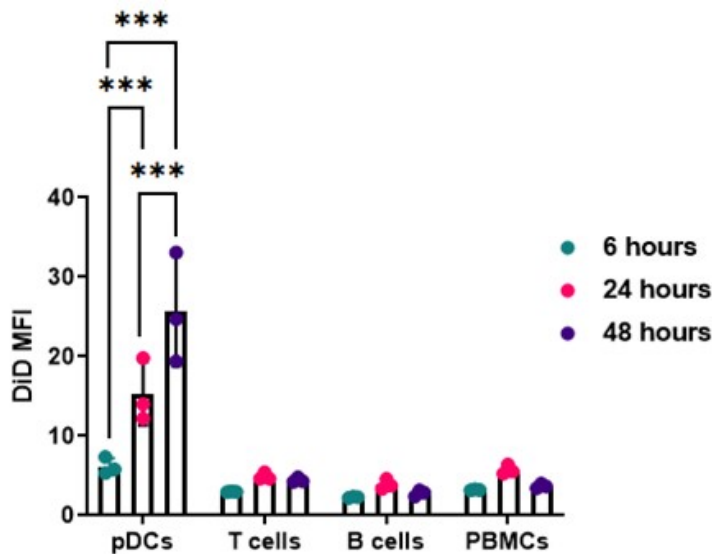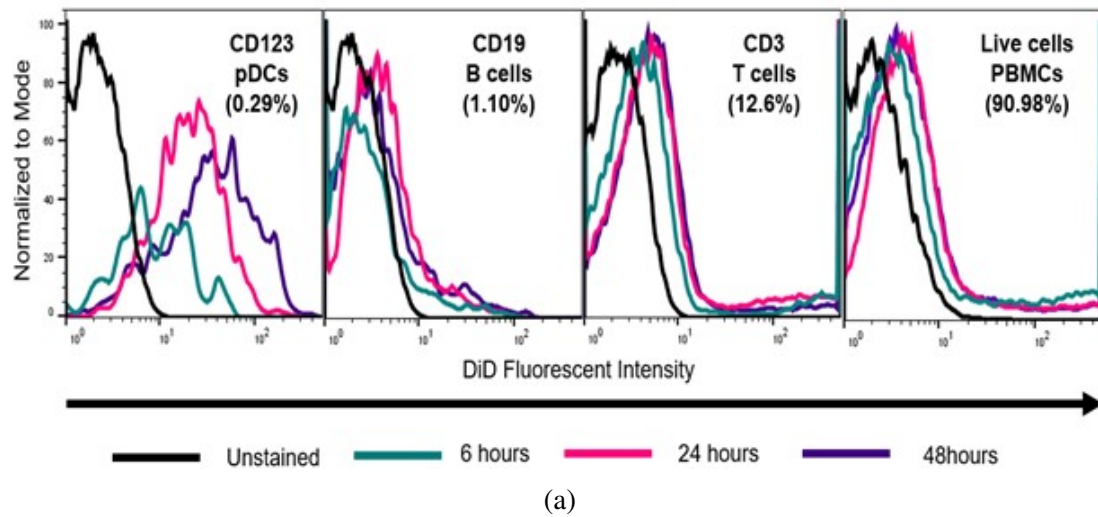
Figure 3.1: **DiD-loaded FMs preferentially accumulated in pDCs in vitro.** FMs were loaded with DiD fluorescent tracer dye. Fresh human PBMCs were cultured with 200 μg/mL DiD-loaded FMs for 6, 24 and 48 h in supplemented RPMI 1640 plus GlutaMAX medium with 10% FBS and 20 ng/mL IL-3 at 37°C and 5% CO_2 ($n = 3$ independent donors). (A) Representative histograms and (B) median fluorescent intensity of DiD from (A). Bars represent mean ($n = 3$) with standard deviation. Statistical analysis: Tukey's multiple comparison two-way ANOVA and $p < 0.05$ was considered significant: ***$p < 0.001$. Gating strategies are described in **Supplemental Figure A.4**.

organs (*e.g.*, kidney, liver, spleen) is undesirable for drug delivery because nanostructures

are filtered from circulation by discontinuous or fenestrated endothelia or sequestered by
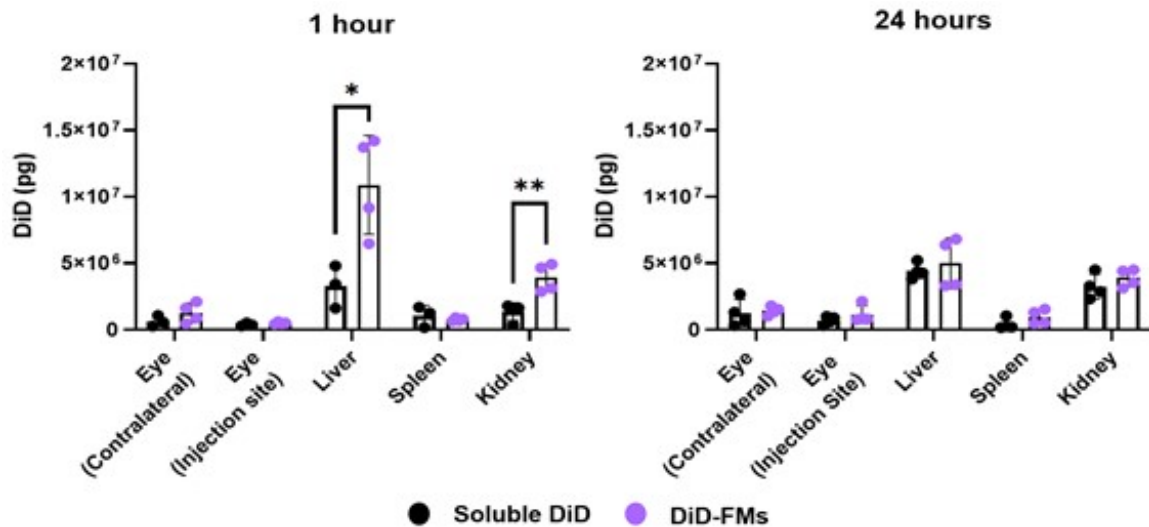
Figure 3.2a: **Organ- and cellular-level biodistribution of DiD-loaded FMs in C57BL/6 Mice.**

the mononuclear phagocyte system [82, 145]. In SLE, these are critical sites of disease activity for targeting drug delivery. Biodistribution of DiD-loaded FMs was analyzed after intravenous injection in C57BL/6 mice. FMs accumulated in the kidneys and liver 1-h post-injection and dye signal was cleared by the body after 24 h with minimal accumulation in the eye (**Figure 3.2a**). Yi and colleagues have also shown that FMs have minimal accumulation in the heart and lungs [121]. The decreased accumulation of FMs in the eye suggests the potential to reduce antimalarial retinopathy by minimizing off-target drug accumulation, potentially eliminating a primary toxicity of soluble CQ.

Within each organ, we analyzed the percentage of immune cells that were DiD+ to determine FM uptake (**Figure 3.2b**). We observed a significant increase in splenic CD19+ B cells associated with DiD-loaded FMs after 24 h. CD11c+ dendritic cells and CD11b+ myeloid cells also showed increased DiD signal between 1- and 24-h post-injection in the liver and spleen, consistent with their passive endocytic function. This may also be partially driven by the high aspect ratio and minimal curvature regions of FMs (normalized curvature, $\Omega > 45°$), which can induce faster internalization by phagocytosis compared to
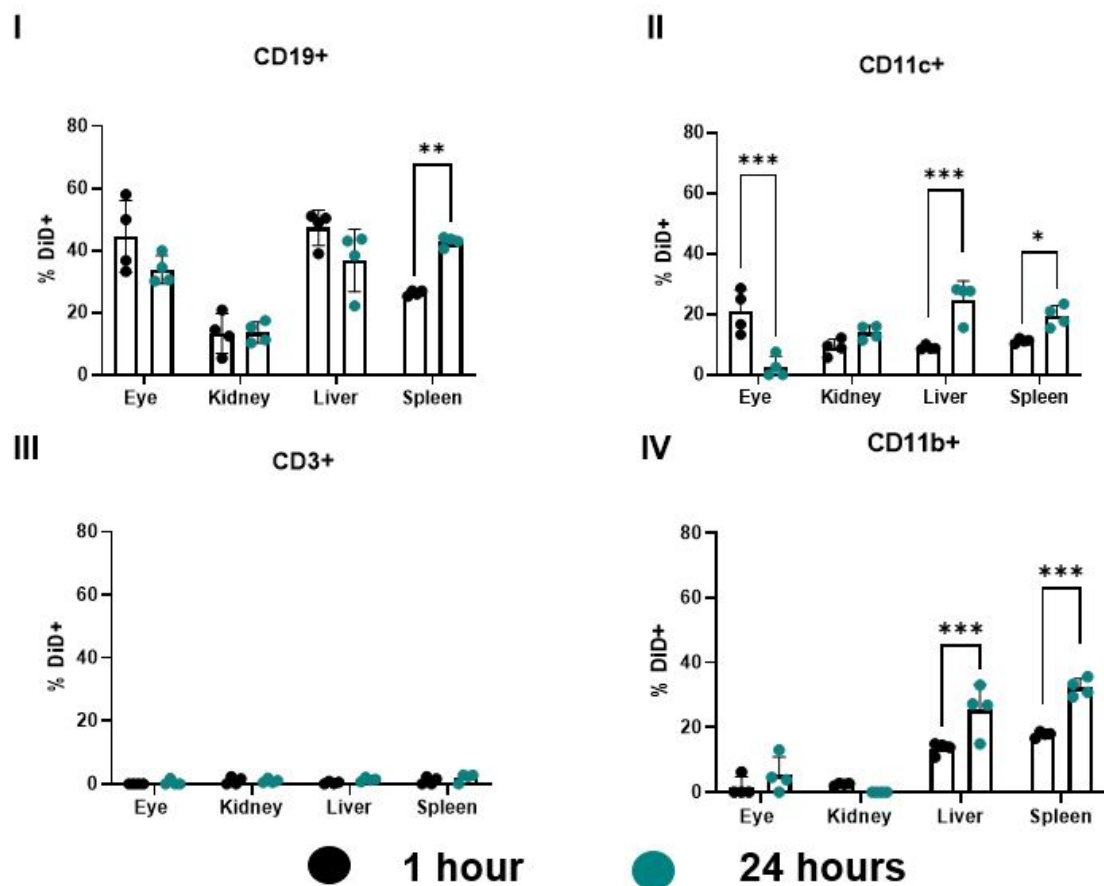
Figure 3.2b: **Organ- and cellular-level biodistribution of DiD-loaded FMs in C57BL/6 Mice, continued.** DiD-loaded FM were synthesized as described and administered by intravenous injection into the retro-orbital sinus. Mice were sacrificed at 1 h or 24 h post-injection and organs were mechanically dissociated and digested by collagenase, type 4. **Figure 3.2a**) The absorbance at 644 nm of 250,000 single cell suspensions from C57BL/6 mice (n = 3-4) at each organ was calculated against a standard curve of DiD in 1X DPBS. Graphs compare tissue distribution of DiD-loaded FMs or soluble FMs at both 50 μg/mL. Statistical analysis completed by unpaired t tests. Statistical significance: *p 0.05 and **p < 0.01. **Figure 3.2b**) Single-cell suspensions were stained and analyzed by flow cytometry. Immune cells from both eyes were pooled, stained, and analyzed by flow cytometry. Graphs compare cellular uptake of DiD-loaded FMs at different time points. Each cell type was mutually exclusive to other cell markers. Particle uptake was analyzed in the following cells: (I) CD19+ B cells, (II) CD11c+ dendritic cells, (III) CD3+ T cells, and (IV) CD11b+ myeloid cells. Statistical analysis was completed by two-way ANOVA with Šídák's multiple comparison test. Statistical significance: *p < 0.05, **p < 0.01, and ***p < 0.001.

spherical nanostructures ($\Omega < 45°$) [149]. The increased cellular signal from 1 h to 24 h may be the result of cells in the mononuclear phagocyte system facilitating the clearance of FMs from circulation and at those organ sites. These results demonstrated favorable drug delivery properties at the tissue and cellular level to address key disadvantages of a soluble free drug, including avoiding the eye and targeting drugs into immunopathogenic cell types and tissue sites of disease activity.

Chapter 4:   Chloroquine-Loaded Nanostructures Decrease *MX1* Gene Expression in Human Cells Stimulated with TLR Agonists *In Vitro*

4.1   Introduction

IFNs are a large protein family important in antiviral immunity [150]. There are three distinct families. Type I IFN is the largest family and encodes for 13 IFN-α subtypes in humans, IFN-β, and single isoform, poorly defined genes (IFN-ω, IFN-ε, IFNδ, IFNτ, IFN-$\varkappa$, and IFN-ζ) [151]. IFNs are induced by viruses, bacteria, and microbial agents leading to recognition by pattern recognition receptors in the cytosol and endosomes in mainly macrophages, dendritic cells, and epithelial cells [152]. pDCs are the leading producers of type I IFN [69]. In SLE patients, IFN-α is triggered by nucleoproteins, nucleic acid cellular debris, and other endogeneous self-antigen found in immune complexes. Pro-inflammatory IFN-α is upregulated in 50-75% of adult SLE patients [65] can promote suppression of regulatory T cells [66], B cell differentiation to plasma cells, and the production of autoantibodies from those plasma cells [68], resulting in a positive feedback loop driving autoimmunity. High type I IFN activity is also associated with distinct SLE features, such as severe nephritis and arthritis [153]. Attenuating this pro-inflammatory type I IFN response is key to treating SLE. Multiple strategies are under development to inhibit type I IFNs, with the majority focused on antibodies that neutralize IFN-α [154], block its recep-

tor [155], or induce endogenous IFN-α antibodies [156].

SLE patients overexpress numerous interferon-stimulated genes (ISGs) [157, 158]. In particular, myxovirus resistance 1 (MX1) is a highly potent ISG [159] tightly regulated by type I and type III interferons [160]. Different viruses induce specific transcriptional programmes of ISGs, where MX1 plays an important role in influenze virus infection[151]. MX1 is one of the most frequently tested ISGs in SLE patients [161] and is elevated in the peripheral blood of this patient population versus healthy controls [158]. To test the efficacy of our CQ-loaded nanostructures, we quantify the gene expression of *MX1* after activation by TLR agonists or positive anti-dsDNA antibody SLE sera.

4.2 Methodology

4.2.1 *In Vitro* Activity of CQ-Loaded Nanostructures

Fresh, healthy human PBMCs were isolated from buffy coats obtained from the New York Blood Center via Ficoll-Paque PLUS density gradient separation [162]. Density gradient centrifugation is ubiquitously used to isolate PBMCs due to its simplicity and resulting viable and intact cell populations. For this process, buffy coat was diluted 1:1 in 1X Hank's balanced salt solution (HBSS) plus 2 mM of anticoagulant ethylenediaminetetraacetic acid (EDTA) and then layered on top of Ficoll-Paque PLUS. After centrifugation at 400 x g and RT for 30 min, with maximum acceleration and no deceleration rates, the buffy coat was separated in layers by density. From top to bottom, the layers represented: platelet and plasma; PBMCs; Ficoll and granulocytes; and red blood cells. PBMCs consist of lymphocytes (T, B, and natural killer cells), monocytes, and granulocytes (neutrophils, basophils, and eosinophils). Flow cytometry (staining protocol found in **Section 3.2.3**) was used to establish viability and cell distribution of each human PBMC donor using the following fluorophore-conjugated anti-human antibodies: CD4+ T cells (clone RPA-

T4; PerCP-Cy5.5), CD19+ B cells (clone HIB19; Brilliant Violet 421TM), CD123+ pDCs (clone 6H6; PE), and CD1c+ mDCs (clone L161; APC/Cy7).

FMs and PLGA nanostructures were loaded with CQ via thin film hydration or emulsion synthesis, respectively as in **Section 2.2.2**. One million PBMCs in 250 μL total volume of RPMI 1640 with GlutaMAX medium plus 10% FBS, 1% sodium pyruvate, 1% NEAA, and 1% pen-strep were treated with soluble CQ, empty nanostructures, or CQ-loaded nanostructures for 1 h at 3.91 μM and then stimulated with purified TLR agonists: 5 μg/mL ssRNA40/LyoVec (TLR7/8 agonist) [163] or 5 μM CpG-A ODN2216 (TLR9 agonist) [164], or 30% v/v sera from an SLE patient with moderately active disease and positive anti-dsDNA titers for 4, 6, and 24 h, respectively. ssRNA40 is a species-dependent TLR7/8 agonist, where human cells have a bias towards TLR8 and mouse cells bias towards TLR7, [165] and a U-rich single-stranded RNA derived from the HIV-1 long terminal repeat. ss-RNA40 induces the production of TNF-α and IFN-α in PBMCs [165, 166]. To enhance cellular uptake and prevent degradation, ssRNA was complexed with the cationic lipid Ly-oVec. Imidazoquinoline amine base analogs, such as resiquimod and imiquimod, were not used as TLR7/8 agonists because antimalarial drugs mechanism of action requires binding to nucleic acids for subsequent endosomal TLR inactivation (**Section 1.2**). CpG ODN or bacterial DNA is a TLR9 agonist and short synthetic single-stranded DNA molecule containing unmethylated CpG dinucleotides. There are three classes of CpG ODNs - Class A (Type D), Class B (Type K) and Class C - with different structural characteristics and that elicit diverse immune responses. The structure of Class A CpG ODNs results in increased endosomal uptake, leading to the maturation of pDCs and production of more IFN-α than stimulation followed by Class B or Class C CpG ODNs [164]. Anti-dsDNA autoantibodies from SLE sera contribute to end-organ injuries, such as the kidneys [167], and endogenous nucleic acid antigen serve as TLR9 ligands.

4.2.2 RT-qPCR

Following incubation at 37 °C, 5% CO_2, cells were spun down at 500 xg for 1 minute at RT. Total RNA was isolated from PBMCs using the Quick-RNA Miniprep Plus Kit (ZymoResearch; Irvine, CA, USA), amplified, and analyzed by TaqMan probe detection real-time reverse transcription-quantitative PCR (RT-qPCR). TaqMan Assays are used in RT-qPCR applications for sensitive, specific detection and quantification of nucleic acid targets. Briefly, RNA is transcribed into double-stranded complementary DNA (cDNA). High temperatures denature cDNA and low temperatures allow TaqMan probes, consisting of a fluorescent dye on the 5' end and a non-fluorescent quencher on the 3' end, to anneal downstream of primers on the single-stranded cDNA target sequence. *Taq* DNA polymerase extends the target sequence and cleaves the TaqMan probe, releasing the fluorescent dye from the quencher moiety. The fluorescent intensity is directly proportional to the amount of amplicon synthesized. In comparison to other methods, such as SYBR Green–based detection, TaqMan probe detection is preferred because it is highly specific and reproducible, requires no post-PCR processing, and allows for detection of two distinct sequences in one reaction tube. Nanostructure efficacy was determined by analyzing the downstream IFN-stimulated gene *MX1*, which is upregulated in the peripheral blood of SLE patients versus healthy patients [158] and highly expressed in kidneys of lupus nephritis patients before treatment [168]. Expression levels were normalized to β-actin control.

All real-time RT-qPCR reagents were purchased from ThermoFisher. The TaqMan probes included: Human MX1, FAM-MGB (assay id: Hs00895608_m1) and Human ACTB VIC-MGB PL (assay id: Hs01060665_g1). TaqPath 1-Step Multiplex Master Mix (No ROX) was used for all one-step multiplex real-time RT-qPCRs. Reactions were run on the CFX96 Touch Real-Time PCR Detection System using the following thermal cycle conditions: UNG incubation (1 cycle, 25°C, 2 minutes), reverse transcription (1 cycle, 53°C, 10

minutes), polymerase activation (1 cycle, 95°C, 2 minutes), and amplification (45 cycles at 95°C for 15 seconds and 60°C for 1 minute). The $2^{-\Delta\Delta CT}$ (Livak) Method was used for relative gene expression analysis. The Livak Method is for relative gene expression analysis that assumes the target and reference gene are amplified with efficiencies at 100% and within 5% of each other. The Livak ($2^{-\Delta\Delta CT}$) method is calculated as followed:

$$\Delta C_{T(test)} = C_{T(target,\ test)} - C_{T(ref,\ test)} \tag{4.1}$$

$$\Delta C_{T(calibrator)} = C_{T(target,\ calibrator)} - C_{T(ref,\ calibrator)} \tag{4.2}$$

$$\Delta\Delta C_T = \Delta C_{T(test)} - C_{T(calibrator)} \tag{4.3}$$

$$2^{-\Delta\Delta CT} = Normalized\ expression\ ratio \tag{4.4}$$

4.2.3   ELISA

MX1 is one of many genes related to type I IFN response. As a result, quantification of IFN-α production in tissue culture supernatant complemented RT-qPCR data. Cell-free supernatants were collected and stored at -80°C until testing for IFN-α production using the Human IFN Alpha All Subtype ELISA Kit (PBL Science; Piscataway, NJ, USA). Multi-subtype IFN-α ELISA was used because IFN belongs to a multi-gene family consisting of 13 different IFN-α subtypes and IFN-β in humans and 14 different IFN-α in mice [169].

4.2.4   Cell Isolation

Purified pDCs were isolated via the EasySep Human Plasmacytoid DC Enrichment Kit (STEMCELL Technologies; Vancouver, Canada). Isolation occurs via negative selection, a process that labels unwanted cells with antibodies for depletion using dextran-coated magnetic particles and a magnet. Soluble or CQ-loaded nanostructures at 3.91 µM total drug were cultured with 100,000 pDCs in RPMI 1640 with GlutaMAX plus 10% FBS, 1% sodium pyruvate, 1% NEAA, 1% pen-strep, and 20 ng/mL recombinant human IL-3. Cells and cell-free supernatants were isolated from stimulated pDC cultures and tested by real-time RT-qPCR and human IFN-α all subtype ELISA, respectively (as above). Depletion of pDCs by negative selection was used to confirm that reduction in type I IFN response was pDC dependent.

4.2.5   Study Approval

This study involved human subjects. Approval for this study was obtained from the University of Maryland School of Medicine Institutional Review Board (IRB) as well as the Baltimore VA Research Office of Human Research Protection. There is no identifiable medical information in this manuscript. All patient identifiers have been removed. Per our IRB-approved protocol, all participants signed informed consent. All identifiable information has been removed from the reported data.

4.2.6   Statistics

All statistical analyses were performed using GraphPad Prism 9 software (GraphPad Software, San Diego, CA). A minimum of three independent experimental replicates were conducted for human PBMCs. Paired or unpaired t-tests and ANOVA were used to test

for statistical significance. P-values were adjusted for multiple comparisons by Tukey's or Dunnett's test, and adjusted p-values <0.05 were considered significant.

4.3 Results and Discussion

A major goal for targeted delivery and controlled release is to potentiate drug activity. We compared the efficacy of CQ-loaded nanostructures to soluble CQ in two *in vitro* culture systems: human PBMCs stimulated with 1) TLR agonists or 2) sera from SLE patients with active disease. Previous studies show that 100 μM CQ maximally decreases pro-inflammatory cytokine secretion, including TNF-α, IL-6, and IL-1β [170, 171], and particularly, IFN- in human PBMCs after *in vitro* TLR stimulation [172]. We quantified the expression of *MX1*, an interferon-stimulated gene that is upregulated in SLE patients compared to healthy controls [158]. Healthy human PBMCs were stimulated with either ssRNA40/LyoVec (TLR7/8 agonist) or CpG ODN 2216 Class-A (TLR9 agonist) and left untreated or pretreated with soluble drug or drug-loaded nanostructures at 3.91 μM CQ. Soluble CQ and CQ-loaded nanostructures had comparable efficacy suppressing TLR7/8-mediated *MX1* gene expression in PBMCs (**Figure 4.1**). In contrast, CQ-loaded FMs were significantly more suppressive of TLR9-mediated *MX1* expression in PBMCs, approximately 2.6-fold more inhibitory than soluble drug (**Figure 4.2**). Nanostructures alone, only soluble CQ, or blank nanostructures cultured with soluble CQ did not stimulate *MX1* gene expression in healthy human PBMCs (**Supplemental Figure A.5**).

pDCs are well-known as the primary producers of type I IFN among immune cells in PBMCs, but they are notoriously low in abundance. We tested the contribution of pDCs to TLR-driven type I IFN by isolating purified human CD123+ pDCs, stimulating them with TLR agonists, and treating them with either soluble CQ or CQ-loaded nanostructures (**Figure 4.3** and **Figure 4.4**).
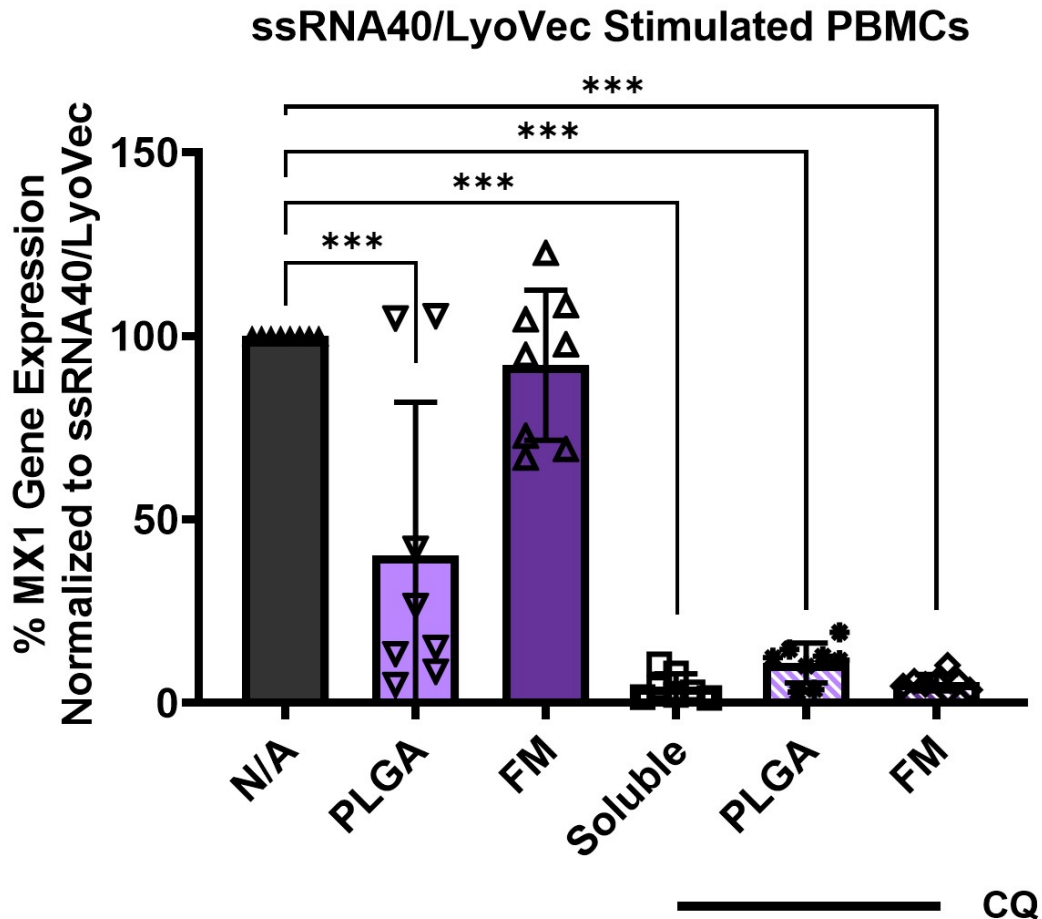
ssRNA40/LyoVec Stimulated PBMCs

Figure 4.1: **CQ-loaded nanostructures decreased MX1 expression like soluble drug after TLR7/8 activation.** Healthy human PBMCs were isolated, treated with 3.91 μM soluble or encapsulated CQ or equal mass blank nanostructures for 1 h, and then activated for 4 h with 5 μg/mL ssRNA40/LyoVec. Total RNA was isolated and *MX1* expression quantified using TaqMan RT-qPCR normalized to β-actin expression. All samples were normalized to TLR agonists alone. Data are means and standard deviation for *n* = 8 independent donors. Statistical significance was evaluated by one-way ANOVA with Dunnett's multiple comparisons test, ***p-adjusted < 0.001. Abbreviation: CL, control.
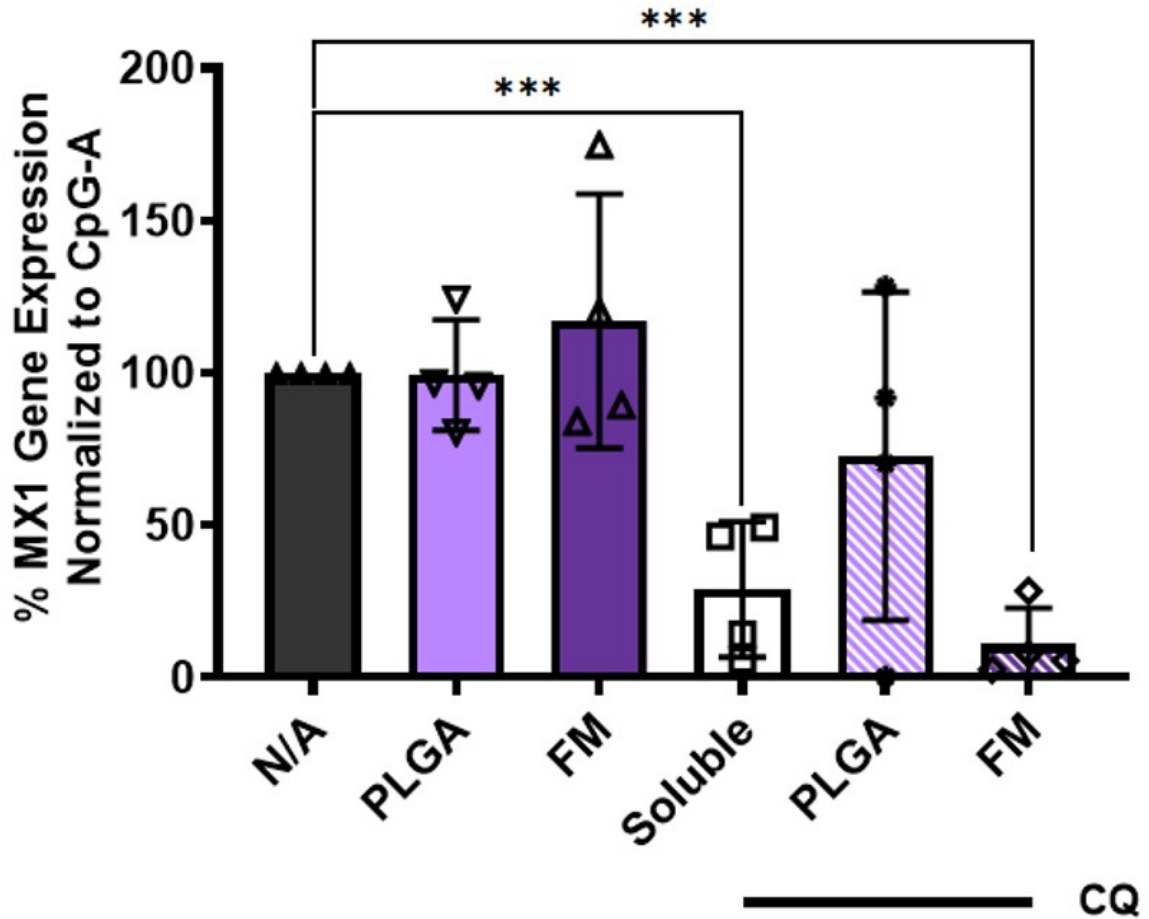
Figure 4.2: **CQ-loaded FMs decreased *%MX1* expression greater than CQ-loaded PLGA after TLR9 stimulation.** Healthy human PBMCs were isolated, treated with 3.91 μM soluble or encapsulated CQ or equal mass blank nanostructures for 1 h, and then activated for 4 h with 5 μM CpG A 2216 for 6 h. Total RNA was isolated and *MX1* expression quantified using TaqMan RT-qPCR normalized to β-actin expression. All samples were normalized to TLR agonists alone. Data are means and standard deviation for *n* = 4 independent donors. Statistical significance was evaluated by one-way ANOVA with Dunnett's multiple comparisons test, ***p-adjusted 0.001. Abbreviation: CL, control.
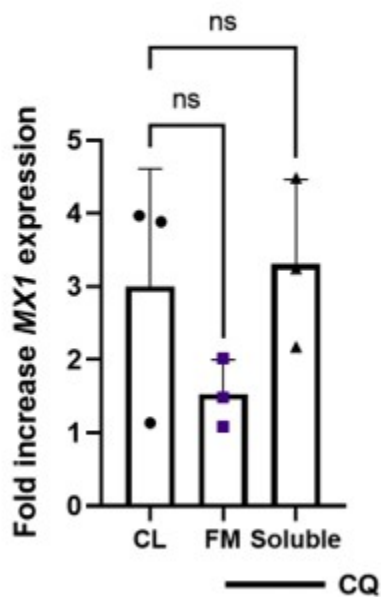
Figure 4.3: **pDCs did not substantially activate IFN response to TLR7/8 stimulation by ssRNA40/LyoVec.** PBMCs were processed by magnetic bead negative selection to purify pDCs. Isolated human CD123+ pDCs at 100,000 cells per condition ($n = 3$ independent donors) were pre-treated with soluble or CQ loaded FMs at 3.91 µM for 1 h and then stimulated with 5 µg/mL ssRNA40/LyoVec for 4 h. Total RNA was isolated to analyze *MX1* expression using TaqMan assays with β-actin control. Statistical analysis: one-way ANOVA with Dunnett's multiple comparisons test. Abbreviation: CL, control.
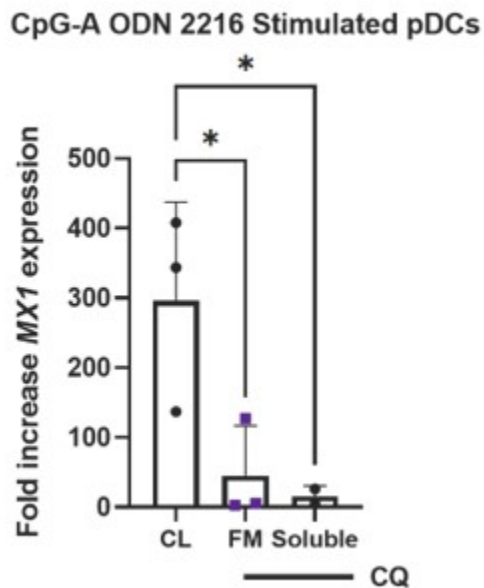
CpG-A ODN 2216 Stimulated pDCs

Figure 4.4: **CQ-loaded nanostructures decreased MX1 similar to soluble drug in isolated pDCs stimulated with TLR9 agonist.** PBMCs were processed by magnetic bead negative selection to purify pDCs. Isolated human CD123+ pDCs at 100,000 cells per condition ($n = 3$ independent donors) were pre-treated with soluble or CQ loaded FMs at 3.91μM for 1 h and then stimulated with 5 μM CpG-A for 6 h. Total RNA was isolated to analyze *MX1* expression using TaqMan assays with β-actin control. Statistical analysis: one-way ANOVA with Dunnett's multiple comparisons test where *p < 0.05. Abbreviation: CL, control.

Purified pDCs showed no significant *MX1* upregulation after activation by TLR7/8 ag-onist ssRNA40/LyoVec (**Figure 4.3**). This suggested the responding PBMC cell type to TLR7/8 stimulation was not pDCs in our experiments. The TLR7/8 agonist, ssRNA40, is introduced to PBMCs via a transfection agent, in this case, LyoVec. We hypothesize that suboptimal RNA delivery to cells may have impacted induction of type I IFN and IFN-stimulated genes, such as *MX1*. Future studies should explore other transfection agents and optimize ssRNA40 to transfection agent ratios for improved delivery and enhanced type I IFN expression. Unlike TLR7/8 stimulation, TLR9 stimulation of pDCs resulted in robust *MX1* upregulation, which could be strongly inhibited by both soluble CQ and CQ-loaded FMs. TLR9 stimulation with CpG-A ODN 2216 robustly stimulated type I IFN in purified pDCs, upregulating *MX1* expression 300X over unstimulated controls after 6 h (**Figure 4.4**). Soluble CQ and CQ-loaded FMs significantly decreased *MX1* (95% and 85% inhi-bition, respectively). Overall, these results demonstrated that soluble CQ and CQ-loaded nanostructures can efficiently suppress TLR7/8 and TLR9-stimulated type I IFN responses in PBMCs, and that pDCs were a primary target in TLR9 stimulation while a different PBMC cell type drove TLR7/8 responses.

Purified TLR agonists are strong stimulators of PBMCs but differ substantially from physiologic agonists. Circulating immune complexes in SLE are unique structures com-posed of autoantibodies and endogenous antigens, such as anti-dsDNA antibodies and self-DNA, and these are hypothesized to be a major driver of endosomal TLR activation and type I IFN pathogenesis in SLE. Anti-dsDNA autoantibodies are found in approximately 80% of patients with lupus nephritis [173], and are associated with TLR9 activation [174], and high IFN-α activity [175]. SLE serum has been previously shown to stimulate pDCs and produce IFN- [61]. CQ also has been shown to decrease IFN- production after pDC activation by SLE serum [58]. We used SLE patient sera as a more physiologic stimulator of PBMCs and proof-of-principle for clinical utility. Healthy PBMCs were isolated and

co-cultured with 30% v/v SLE sera for 24 h *in vitro*. We used a 75% lower dose of soluble CQ than reported in literature to inhibit SLE serum [58].

Soluble CQ did not significantly decrease type I IFN response stimulated by SLE sera (**Figure 4.5**). In contrast, pretreatment with equivalent dose of CQ-loaded FMs significantly decreased *MX1* expression induced by SLE sera by approximately 75% compared to no inhibition by either soluble drug or CQ-loaded spherical PLGA nanostructures (**Figure 4.5**). We also analyzed secretion of IFN-α with a multi-subtype ELISA that quantifies all 12 known IFN-α family proteins in humans [169]. As expected, based on *MX1* expression, IFN-α production was significantly decreased by CQ-loaded nanostructures, while soluble CQ had no effect (**Figure 4.6**). Both FMs and spherical PLGA nanostructures significantly inhibited IFN-α secretion, suggesting *MX1* is induced by more than IFN-α in our experimental system. Nonetheless, we note the modest induction and IFN secretion induced by anti-dsDNA positive SLE sera in our experiments. This may be due to inactive SLE sera induction at the time of measurement or variability in baseline type I IFN expression of healthy human PBMCs used for sera stimulation as a result of sex [176] or age [177] differences. Future studies should extend incubation time of SLE sera induction to allow more time for the activation of the PBMCs and to increase accumulated IFN secreted into the culture media for detection. Additionally, noting the demographics of donor PBMCs may aid in understanding differences in type I IFN responses between donor samples. Overall, these data showed that CQ-loaded nanostructures significantly decreased IFN-α production compared to soluble CQ in response to immune complexes from SLE patient sera. This suggests that CQ-loaded FMs may have utility as a novel drug formulation for treating SLE.
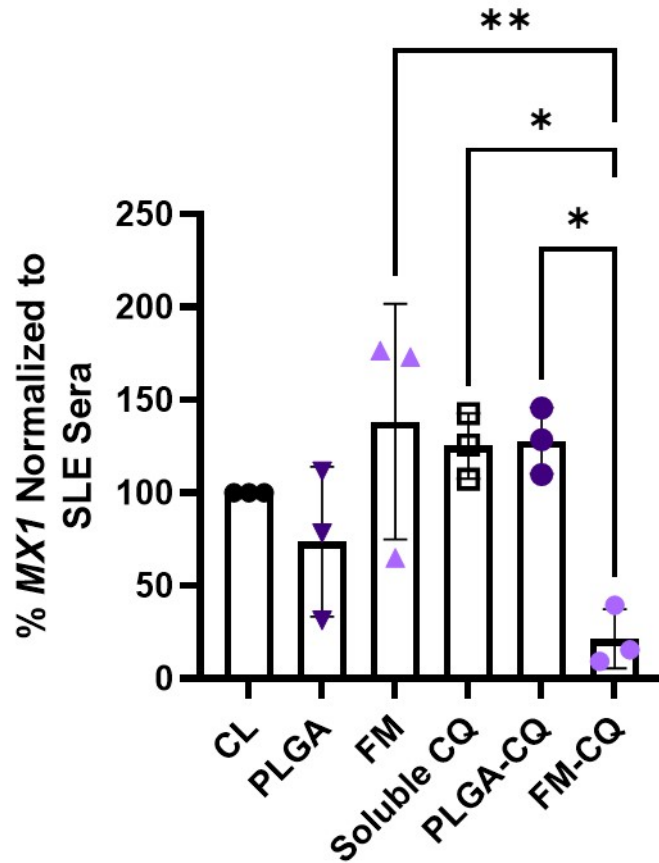
Figure 4.5: **CQ-loaded nanostructures decrease *MX1* in sera from SLE patients.** Healthy human PBMCs were treated with soluble or CQ-loaded nanostructures at 3.91 µM or equal mass blank nanostructures for 1 h, then stimulated with 30% v/v SLE patient sera for 24 h. Total RNA was isolated and *MX1* expression quantified using TaqMan RT-qPCR normalized to β-actin expression. Samples were normalized to SLE sera alone. Data are means and standard deviation for $n = 3$ healthy independent PBMC donors. Statistical significance was evaluated by one-way ANOVA with Tukey's multiple comparisons test, such that, *$p < 0.05$, **$p < 0.01$, and ***$p < 0.001$. Abbreviation: CL, control.
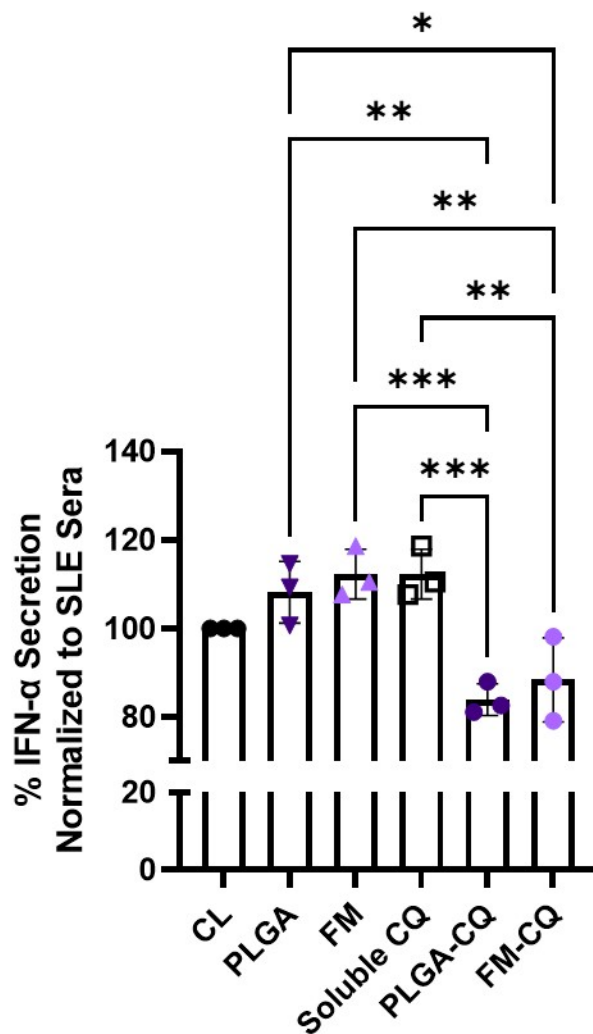
Figure 4.6: **CQ-loaded nanostructures decrease IFN-α secretion in sera from SLE patients.**. Healthy human PBMCs were treated with soluble or CQ-loaded nanostructures at 3.91 μM or equal mass blank nanostructures for 1 h, then stimulated with 30% v/v SLE patient sera for 24 h. Supernatants from cell culture were collected for multi-subtype IFN-α ELISA. All samples were normalized to SLE sera alone. Data are means and standard deviation for $n = 3$ healthy independent PBMC donors. Statistical significance was evaluated by one-way ANOVA with Tukey's multiple comparisons test, such that, *$p < 0.05$, **$p < 0.01$, and ***$p < 0.001$. Abbreviation: CL, control.

Chapter 5: Insignificant Changes in Type I IFN Expression in SLE Prone Pristane-Induced Mice Treated with Chloroquine-Loaded Nanostructures

5.1 Introduction

SLE is considered to be caused by environmental triggers and genetic susceptibility. For instance, occupational exposure of trichloroethylene (TCE), a degreasing solvent, has been identified as a possible risk factor for lupus where high levels of TCE are found in drinking water [178–180]. One of the most widely used environmental mouse model is the pristane-induced model [181]. Tetramethylpentadecane (TMPD) or commonly pristane is a naturally occurring hydrocarbon oil found in plants and at high levels in planktivorous sharks [182]. It works by stimulating IFN-α and IFN-β production in Ly6C^{hi} immature monocytes leading to local inflammatory response at the site of injection, the peritoneal cavity, and subsequent IgG autoantibody production and proinflammatory cytokine production [183]. pDCs can then augment type I IFN signature after autoantibodies and immune complexes develop. Pristane-induced SLE model is mouse strain dependent [184] and female biased where high type I IFN signature, immune complex-mediated nephritis, and autoantibody levels are prevalent in female Balb/c mice [183, 185]. Alternatively, NZB/WF1 has been used since the 1960s for autoimmune diseases and is considered the oldest and most commonly used model for SLE [186]. This model is female biased and

displays glomerulonephritis, splenomegaly, anti-nuclear antibodies and SLE relevant genes [186, 187]. NZB/WF1 mimics the disease progression of SLE patients and has a weak type I IFN signature [188].

One of the drawbacks of mouse models of SLE is the long disease incubation time (approximately >3 months) before active disease. Researchers have accelerated disease progression in the NZB/WF1 model by intravenously injecting adenoviruses expressing IFN-α or TLR agonists [189, 190]. Impact of IFN-α is dose dependent and displays less renal inflammatory cell infiltration and long lived plasma cells than the conventional spontaneous model [191]. The advantages of the accelerated model is decreased time to high disease activity (2 weeks post-injection versus 28 weeks in the genetic model) [192–195] and signs of proteinuria [189]. The adenovirus IFN-α5 accelerated NZB/W model is also a T-cell dependent model with characteristics such as: increased B cell TLR7 expression, T cells expressing IL-21, and increased serum levels of IL-6, BAFF, and TNF-α [195, 196]. Another alternative is the use of resiquimod, a TLR7/8 agonist, or imiquimod, a TLR7 agonist, applied to the ears of Balb/c mice for lupus-like autoimmunity. Imiquimod applied 3X weekly results in *IFNA1* and *MX1* gene upregulation in disease organs and glomerulonephritis with immune complex deposits (*i.e.* anti-dsDNA and anti-Sm) in 4 weeks compared to months in other models [197].

The pristane-induced, TLR-induced, and NZB/WF1 models have a known IFN signature; however, there are many other mouse models of SLE with absent or unknown IFN signatures that are frequently used in studies. For example, the chronic graft-versus-host disease (cGVHD) model is another experimentally induced mouse model that utilizes the transfer of DBA/2J splenocytes into an unirradiated healthy adult (C57BL/6 × DBA/2)F1 (B6D2F1) recipient to yield lupus-like loss of B cell tolerance, glomerulonephritis, and an overproduction of autoantibodies [198]. Because GVHD models are dependent upon activation and expansion of donor T cells, these models are typically used in studies for defin-

ing the role of T cell alloreactivity/autoreactivity in driving B cell autoantibody production and tissue damage. The advantages of the cGVHD are reduced inter-individual variability, ease of use, and shorter time to disease activity in comparison to most SLE mouse models. Another widely used mouse model for preclinical efficacy studies includes the spontaneous MRL/*lpr* mice. This model recapitulates many clinical features of human SLE primarily autoantibody production, dermatitis, and immune-complex mediated glomerulonephritis, which are worsened by IFNAR deficiency [199]. Disease activity in MRL/*lpr* mice is late-onset and found in both male and female mice [200]. This model is used to evaluate the role of TLRs in SLE and the development of extrafollicular autoreactive B cells. In this work, we used the pristane-induced model to test the efficacy of CQ-loaded nanostructures *in vivo* by measuring type I IFN response and other SLE-like manifestations. The pristane-induced model was chosen because it has the highest detectable type I IFN response across both genetic and environmental-induced models and clinical presentations similar to SLE patients [188].

5.2 Methodology

5.2.1 Materials

2,6,10,14-Tetramethylpentadecane (TMPD or pristane), 95% purity was purchased from ACROS Organics (Fair Lawn, NJ, USA). Calf thymus DNA (dsDNA) was purchased from Sigma (St. Louis, MO, USA). 1-Step Ultra 3,3,5,5-Tetramethylbenzidine (TMB)-ELISA Substrate Solution was purchased from Thermo Fisher (Waltham, MA, USA). Biotin-conjugated goat-anti-mouse IgG and horseradish peroxidase (HRP)–labeled streptavidin were obtained from BioLegend (San Diego, CA, USA).

5.2.2 Induction of Autoimmunity in Mice

Female Balb/c mice, 6-8 weeks old, were injected intraperitoneally one time with 0.5 mL pristane [181, 183].

5.2.3 Characterization of Manifestations in Lupus-Prone Mice

ELISA for Autoantibody Levels

Mice were evaluated for serum autoantibody levels. Pristane-induced mice primarily produce IgG autoantibodies to dsDNA (40% frequency in Balb/c mice) [183]. The frequency of anti-dsDNA autoantibodies in SLE patients (70-90%) versus healthy subjects (<0.5%) makes it one of the diagnostics for SLE [201]. Disease progression of pristane-induced mice was evaluated by ELISA for serum autoantibody levels (enzyme index ¿ 100%). Enzyme index (%) is defined as [202]: (OD_{450} of samples/ (Mean OD_{450} of control mice + 3 x standard deviation)) x 100. Mice are considered positive for lupus with an enzyme index >100% [202].

To determine enzyme index, ELISA plates were coated with 100 μL of 5 μg/mL calf thymus DNA and incubated overnight at 4 °C with shaking at 500 rpm with a 0.3 cm circular orbit. All subsequent shaking steps were performed similarly. The plates were then blocked with 200 μL blocking buffer (PBS plus 2% BSA) for 1-2 h at RT with shaking. Murine serum was diluted at 1:2000, 1:200 or 1:400 in 100 μL PBS plus 2% BSA and added to the plates for 2-3 h at RT with shaking. The plates were incubated with 100 μL of biotin-conjugated goat-anti-mouse IgG diluted 1:1000 with PBS plus 2% BSA for 1 h at RT with shaking. Afterwards, 100 μL of HRP–labeled streptavidin diluted 1:1000 with PBS plus 2% BSA was added to the plates and incubated for 0.5 h at RT with shaking. Between all of the above steps, the plates were washed 3X with at least 300 μL PBS plus 0.05% Tween-20.

100 μL TMB liquid substrate was incubated for 15-30 minutes at RT in the dark or until the desired color develops (*i.e.*, wells turn blue). With no wash step in between, the reaction was terminated by adding 100 μL 2M H_2SO_4 to each well. Positive results transitioned from blue to yellow. The plates were immediately read at an absorbance of 450 nm and 570 nm using the BioTek Cytation 5 plate reader. The absorbance was normalized by subtracting the absorbance at 570 nm from the absorbance at 450 nm.

Serum Creatinine

Creatinine levels were calculated using the Cayman Chemical (Ann Arbor, MI, USA) Creatinine (serum) Colorimetric Assay Kit. The kinetic assay relies on the Jaffe' reaction where a yellow/orange color results from the interaction between metabolite and alkaline picrate [203, 204]. The reaction is then read at an absorbance between 490-500 nm and the resulting color development is directly proportional to creatinine concentration. The kidneys maintain the clearance of creatinine from the blood and elevated serum levels are used as an indicator for renal function, suggesting a reduction in glomeruli filtration capacity [205].

Type I IFN Response in Mice

Total RNA was isolated from whole blood and peritoneal exudate cells using the Quick-RNA Miniprep Plus Kit (ZymoResearch; Irvine, CA, USA), amplified, and analyzed by TaqMan probe detection RT-qPCR. All real-time RT-qPCR reagents were purchased from ThermoFisher. The TaqMan probes included: Mouse MX1, FAM-MGB (assay id: Mm00487796_m1), Mouse ACTB VIC-MGB PL (assay id: Mm00607939_s1), and Mouse IRF7, FAM-MGB (assay id: Mm00516793_g1). TaqPath 1-Step Multiplex Master Mix (No ROX) was used for all one-step multiplex real-time RT-qPCRs. Experi-

mental setup and analysis was perform as described in **Section 4.2.2**.

5.2.4 *In Vivo* Activity of CQ-Loaded Nanostructures

FM and PLGA nanostructures were loaded with CQ, as previously described (**Section 2.2.2**). Three days after pristane induction, CQ-loaded nanostructures and dose-matched soluble drug were injected intravenously by retro-orbital sinus with 4.3, 34.4, or 172 µg CQ per kg body weight at 150 µL total volume in PBS. Untreated mice received 150 µL PBS. Blank FMs and PLGA were injected at equal total polymer concentrations to CQ-loaded counterparts at 150 µL total volume in PBS. The doses were determined by a dose conversion between human and mouse [206], using the reference 5 mg HCQ per kg body weight as the standard dose for SLE patients [23]. Mice received two doses separated by a week. Two weeks after the initial dose, peripheral blood and peritoneal exudate cells were collected for *MX1* and *IRF7* gene expression analysis using RT-qPCR. We chose two weeks for endpoint measurements because type I IFN production is establish starting at that time point [207].

5.2.5 Study Approval

The animal study was reviewed and approved by UMBC Institutional Animal Care and Use Committee (OLAW Animal Welfare Assurance D16-00462).

5.2.6 Statistics

All statistical analyses were performed using GraphPad Prism 9 software (GraphPad Software, San Diego, CA). A minimum of three mice per group or condition were used for *in vivo* experiments. Two-way ANOVA were used to test for statistical significance. P-values were adjusted for multiple comparisons by Tukey's test, and adjusted p-values

<0.05 were considered significant.

5.3   Results and Discussion

To determine a dosing strategy for *in vivo* experiments, we tested CQ-loaded FMs at different concentrations: 4.3, 34.4, or 172 µg CQ per kg body weight which correlated to 5, 40, and 200 mg total polymer per kg body weight, respectively. To our knowledge, this was the first use of nanostructures encapsulating CQ for treatment of lupus-prone mice. As a result, the objective of this study was to determine the optimum dose for use in larger *in vivo* experiments. The doses were chosen below and above the animal equivalent dose of HCQ, which is 61.5 mg CQ per kg body weight. The advantages of drug delivery systems include targeted delivery, minimized drug degradation, limited toxicity, and reduced dose frequency. As a result, using nanostructures has the potential to decrease the effective drug dose required to inhibit TLR activation and subsequent type I IFN in pristane-induced mice in comparison to soluble drug.

In testing the *in vivo* dosing strategy, we evaluated the associated toxicity of the nanostructures as measured by body and liver weight. One of the mechanisms of nanostructure removal is filtration by organs, such as the liver and kidneys. The resulting accumulation of nanostructures at these sites of filtration may lead to organ damage and inflammation. Our results showed that CQ-loaded FMs do not impact mouse body or liver weight (**Figure 5.1**), indicating no signs of organ-level or systemic associated toxicity. These results also complement our *in vivo* organ-level biodistribution data that shows that although DiD-loaded FMs associate in the liver, the dye signal is diminished after 24 h (**Figure 3.2**).

Another feature of human and pristane-induced mouse SLE presentation is immune complexes composed of autoantibodies and endogenous antigens. Approximately 50-90% of Balb/c mice develop anti-dsDNA autoantibodies 5-6 months after induction [181, 185].

As expected, mice used for our experiment did not produce autoantibodies against dsDNA two weeks after pristane induction, as indicated by an enzyme index $< 100\%$ (**Figure 5.2**). Impaired renal function by immune-complex mediated glomerulonephritis was not observed in pristane-induced mice at this time point, as determined by serum creatinine measurements (**Figure 5.3**). Glomerulonephritis is generally expected after immune complex formation (approximately >4 months post-induction) and deposition in the kidneys. Our 2 week time point was too early to evaluate serum creatinine, an indicator of renal function.

The efficacy of CQ-loaded FMs was evaluated by quantification of *MX1* in the blood and peritoneal exudate cells. This was used to measure inflammation and type I IFN induction. We tested *MX1* because it is elevated in ectopic lymphoid tissue of pristane-induced mice and *IRF7* because induction of IFN-α in this mouse model relies on the TLR7-MyD88-IRF7 pathway [183]. In both cases, mice treated with CQ-loaded FMs showed no significant difference from untreated mice (**Figure 5.4**). In the peritoneal exudate cells, *MX1* gene expression appeared to stabilize at 5 and 40 mg/kg doses. For future *in vivo* experiments, we chose 5 mg polymer/kg (equivalent to 4.3 µg CQ/kg) for the potential to impact type I IFN response using approximately 14,000X less than the animal equivalent dose of HCQ (61.5 mg CQ/kg).

In a larger *in vivo* experiment exploring the efficacy of CQ-loaded FMs versus soluble CQ, no formulation inhibited type I IFN response during treatment. Peritoneal exudate cells demonstrated wide variations in gene expression (**Figure 5.5**). However, *IRF7* gene expression stabilized in the peripheral blood. The results demonstrated (**Figure 5.6**) that pristane-induced Balb/c mice significantly induced *IRF7* in comparison to healthy, female Balb/c control mice. This experiment ended at two weeks of soluble CQ or CQ-loaded nanostructure treatment, when type I IFN response is known to be elevated in pristane-induced mice [183]. Future studies should explore extending treatment longer. In this
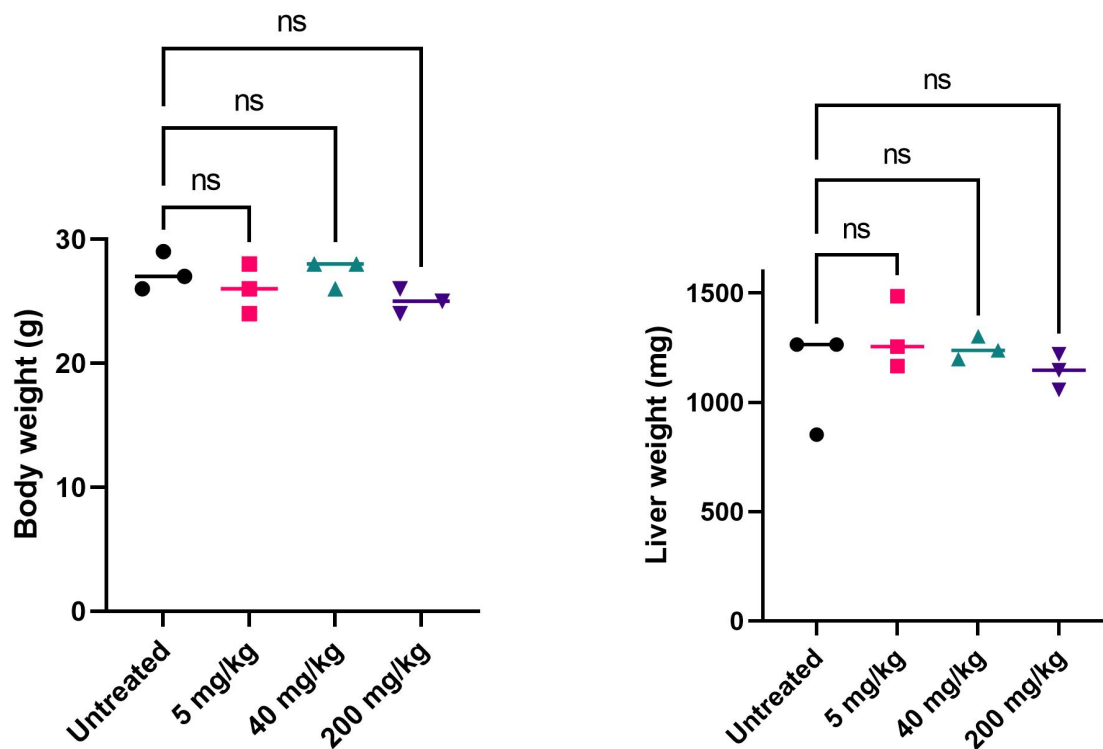
Figure 5.1: **CQ-FMs did not impact body or liver weight after treatment.** Female Balb/c mice ($n = 3$), 6-8 weeks old, were given an intraperitoneal injection of 0.5 mL pristane. Three days after induction, mice received 150 μL weekly intravenous injections of 5, 40, and 200 mg total polymer per kg of CQ-loaded FMs in PBS. Untreated mice received PBS. After two weeks of treatment, mice and their livers were weighed. Data show individual mice and medians. Statistical analysis: Tukey's multiple comparison two-way ANOVA.
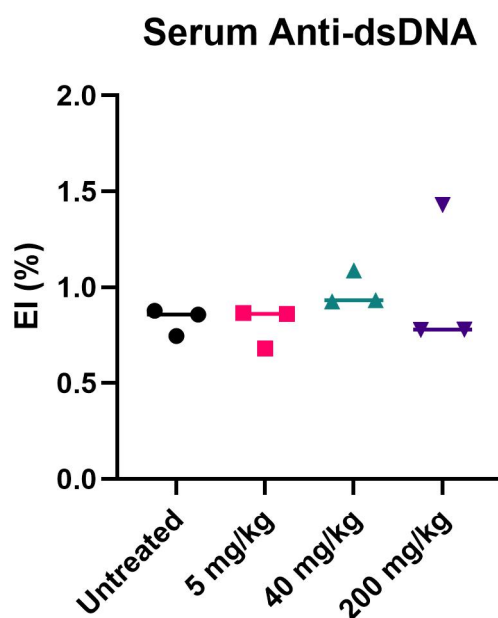
Figure 5.2: **Pristane-induced mice did not produce anti-dsDNA autoantibodies two weeks post-induction.** Female Balb/c mice ($n = 3$), 6-8 weeks old, were given an intraperitoneal injection of 0.5 mL pristane. Mice were treated with 5, 40, and 200 mg total polymer per kg of CQ-loaded FMs in PBS. Serum was collected at 2 weeks and autoantibodies quantified by ELISA. Data show individual mice and medians.
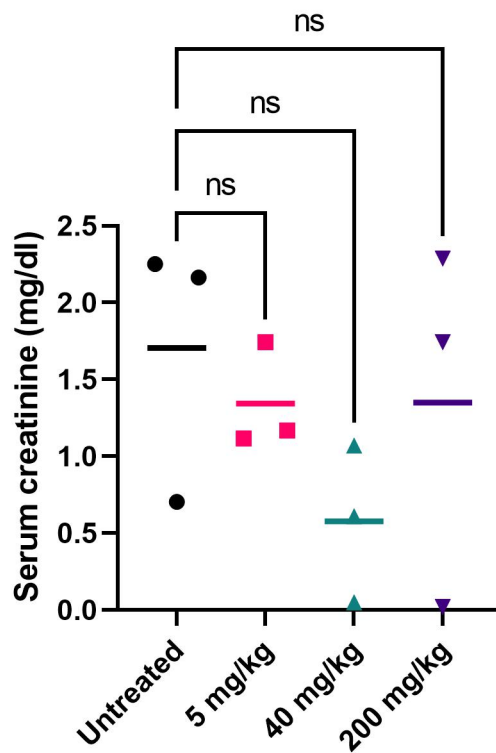
Figure 5.3: **No elevated serum creatinine levels in pristane-induced mice.** Female Balb/c pristane-induced mice ($n = 3$) were untreated with PBS or treated with 5, 40, and 200 mg total polymer per kg of CQ-loaded FMs in PBS. Serum was collected at 2 weeks post-induction and creatinine levels were quantified by the Jaffe' reaction. Data show individual mice and medians. Statistical analysis: Tukey's multiple comparison two-way ANOVA.
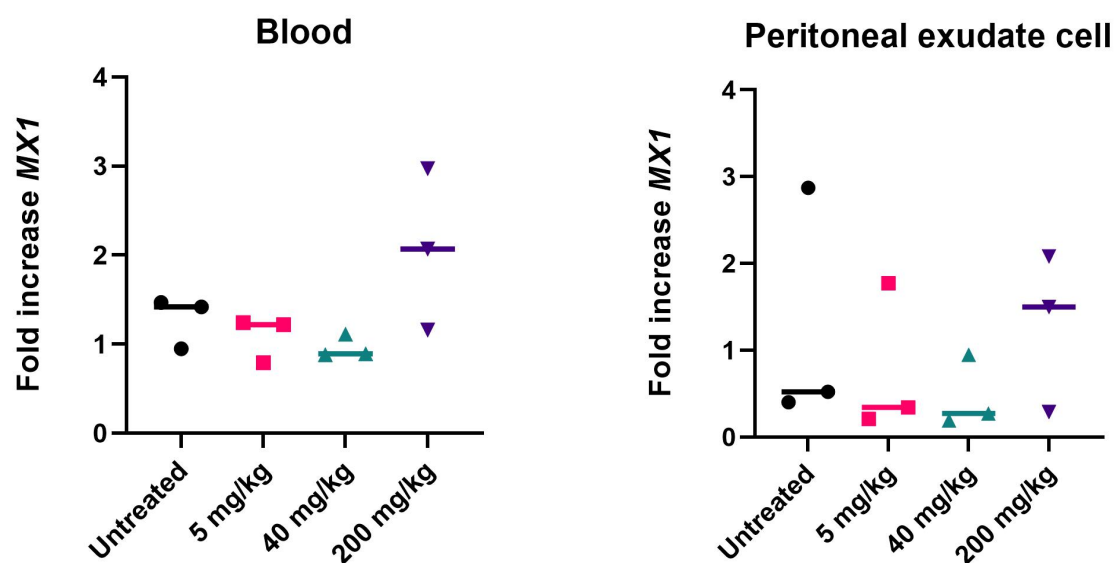
Figure 5.4: **CQ-loaded FMs had no impact on blood or peritoneal exudate cell *MX1* expression.** Pristane-induced BALB/c mice ($n = 3$) were untreated with PBS or treated with 5, 40, and 200 mg total polymer per kg of CQ-loaded FMs in PBS. Total RNA was isolated from blood or peritoneal exudate cells and *MX1* expression quantified using TaqMan real-time RT-qPCR normalized to β-actin expression. Data show individual mice and medians. Statistical analysis: Tukey's multiple comparison two-way ANOVA.

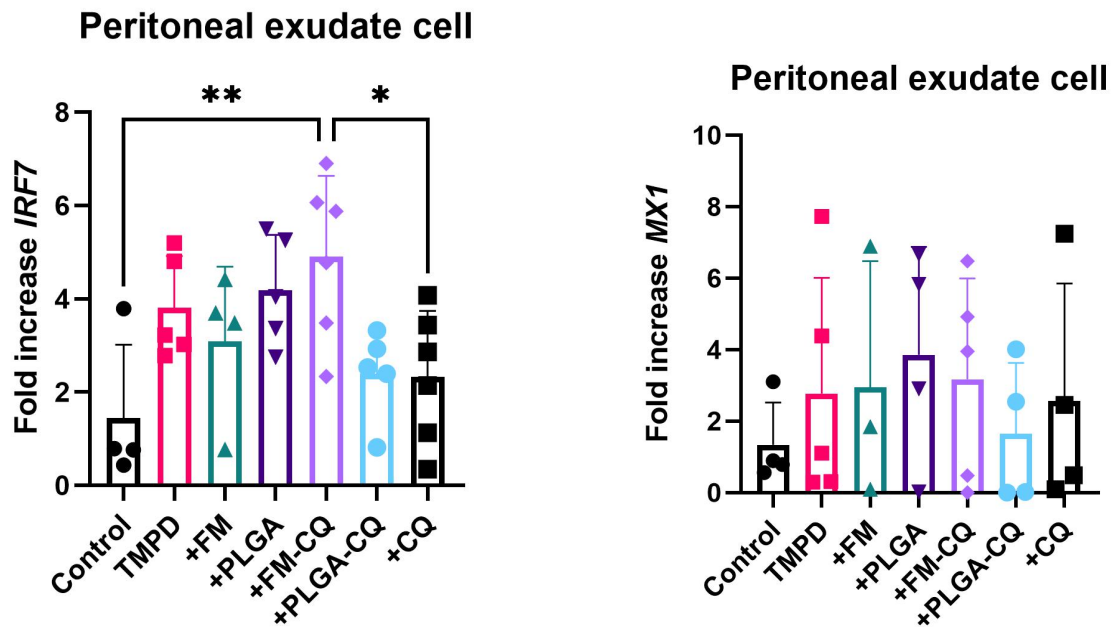Figure 5.5: **Soluble CQ and CQ-loaded FMs did not decrease ISGs in peritoneal exudate cells.** Pristane-induced BALB/c mice (n = 4-6) were untreated with PBS or treated with 5 mg total polymer per kg (equal to 4.3 µg CQ/kg) of soluble drug or CQ-loaded FMs in PBS. Equal weight unloaded nanostructures were injected in pristane-induced mice as controls. Controls are Balb/c mice and TMPD are untreated pristane-induced mice. Total RNA was isolated from peritoneal exudate cells and *IRF7* or *MX1* expression quantified using TaqMan real-time RT-qPCR normalized to β-actin expression. Data show mean and standard deviation. Statistical analysis: Tukey's multiple comparison two-way ANOVA, where p <0.05 was considered significant: *p < 0.05 and **p < 0.01.

lupus-prone model, type I IFN precedes anti-dsDNA or anti-nRNP or Sm autoantibody production. Based on the preferential association of FMs in pDCs (**Figure 3.1a** and **Figure 3.1b**) and the proposed mechanism of action of CQ as a TLR antagonist (**Section 1.2**), the development of nucleic acid-containing immune complexes may be a requirement for pDCs to augment type I IFN signature and for subsequent inhibition of TLR activation in pDCs by CQ-loaded nanostructures.
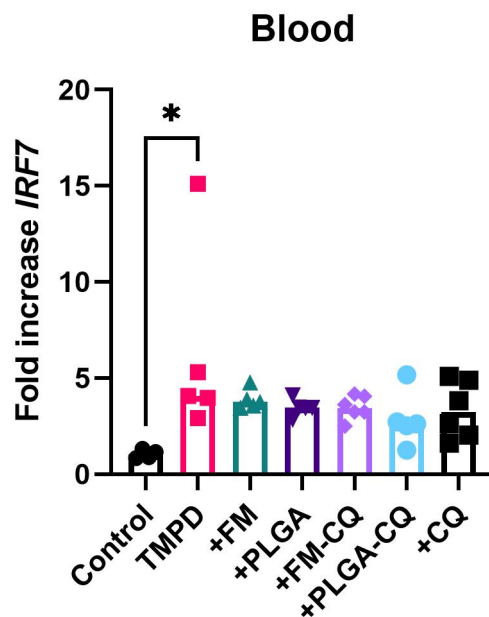
Figure 5.6: **Soluble CQ and CQ-loaded FMs did not decrease *IRF7* in the blood.** Pristane-induced BALB/c mice (*n* = 4-6) were untreated with PBS or treated with 5 mg total polymer per kg (equal to 4.3 µg CQ/kg) of soluble drug or CQ-loaded FMs in PBS. Equal weight unloaded nanostructures were injected in pristane-induced mice as controls. Controls are Balb/c mice and TMPD are untreated pristane-induced mice. Total RNA was isolated from blood and *IRF7* expression quantified using TaqMan real-time RT-qPCR normalized to β-actin expression. Data show mean and standard deviation. Statistical analysis: Tukey's multiple comparison two-way ANOVA, where p <0.05 was considered significant: *p < 0.05.

Chapter 6: Conclusions and Future Directions

The past decade has seen the first new drug approvals for SLE by the U.S. FDA in over 50 years. In 2011, the monoclonal antibody belimumab blocking B lymphocyte stimulator was approved for SLE and approved for lupus nephritis in 2020. In 2021, voclosporin, a calcineurin inhibitor, in combination with background immunosuppressive therapy, was approved for adult patients with active lupus nephritis. Voclosporin was the second FDA-approved therapy for lupus nephritis and the first oral treatment specifically for that manifestation [208]. Despite FDA approvals of belimumab and voclosporin, these therapies were studied in combination with a background of immunosuppressive agents and corticosteroids to achieve efficacy, and drug delivery and toxicity remain persistent limitations for these and other SLE treatments. Nanostructures can enhance drug delivery while mitigating adverse side effects by reducing accumulation in off-target cells and tissues. We demonstrated that targeting pDCs using antimalarial-loaded FMs could enhance suppression of TLR activation and subsequent type I IFN responses (**Figure 1.3**). To our knowledge, this is the first use of passive, morphology-based nanostructure targeting of pDCs to enhance TLR inhibition, and extends prior work demonstrating accumulation in pDCs [137]. TLR inhibition has great potential as a therapeutic strategy since gene polymorphisms of TLRs lead to disease susceptibility [109], TLR ligands contained in NETs or resulting from apoptotic cell death exacerbate disease [110, 111], and TLR inhibitors (*i.e.*, antimalarial drugs) alleviate disease [112]. Our approach targets SLE in disease-relevant sites and cells to inhibit key inflammatory pathways.

Our results showed that FMs accumulate in pDCs (**Figure 3.1a** and **Figure 3.1b**), professional IFN-α producing cells that represent <1% of cells in the blood but produce 1,000X more IFN-α than any other immune cell [69]. Concentrating drug delivery to pDCs may potentiate TLR antagonists, such as CQ, by increasing drug accumulation in the endosomal space to block TLR signaling more efficiently and downstream type I IFN responses. Additionally, passive targeting, which leverages physicochemical nanostructure properties (**Figure 2.2, 2.3, 2.4, 2.5**) and disease biology, presents an opportunity for FMs to accumulate at tissue sites of SLE-driven inflammatory damage like the kidneys (**Figure 3.2** and **Figure 3.2**). Targeting SLE-relevant organs (*e.g.*, kidneys and liver) can concentrate drug delivery to tissues where both immune complexes and pDCs are found during active disease, while limiting off-target effects. pDCs are important in lupus nephritis because they express high levels of IL-18R which allows the relocation of dendritic cells within the glomeruli by IL-18 stimulation. These dendritic cells then activate resident T cells, resulting in promotion of renal damage [142, 209]. FMs also escape accumulation in the eye (**Figure 3.2**) due to the size and morphology of the nanostructures and their impermeability of the blood-retinal barrier [210, 211]. This may reduce the risk of antimalarial-mediated retinopathy with chronic use of CQ [28] and long-term toxicity associated with the current CQ formulation. We hypothesize that the filamentous morphology (**Figure 2.2**) and phagocytosis of FMs facilitates internalization by pDCs [135, 149, 212], and thus, its unique morphology advances nanostructure drug delivery. Future studies should evaluate the molecular mechanisms and kinetics of FM uptake into endosomes and degradation by pH-mediated oxidation. A proposed method to discriminate between nanostructure internalization versus cell surface adherence is confocal microscopy or imaging flow cytometry. Trypan blue can be added to some the flow cytometry samples to quench the surface-bound fluorescence. Compartmental stains (*i.e.*, EEA1 for early endosomes, LAMP2 for late endosomes and Lysotracker for lysosomes) and chemical inhibitors (*i.e.*, chlorpromazine and

genistein to inhibit clathrin and caveolin-mediated endocytosis) can be used to track nanostructure internalization in endosomes and lysosomes.

We used synthetic oligonucleotide agonists ssRNA40 and CpG-A ODN 2216 to trigger TLR7/8 and TLR9, respectively, because human pDCs selectively express endosomal TLR7 and TLR9 to sense pathogenic and endogenous nucleic acids [213]. Although ssRNA40 is known to produce high levels of IFN-α in pDCs [163] and induce *MX1* gene expression in PBMCs [214], CQ-loaded FMs were not significantly different from soluble drug or spherical PLGA control (**Figure 4.1** and **Figure 4.3**). Since isolated pDCs did not show an *MX1* response to ssRNA40, we hypothesize that monocytes and other myeloid cells may be additional mediators of IFN-α production after TLR7/8 activation by ssRNA40 [165]. However, both soluble CQ and CQ-loaded FMs did suppress TLR9-mediated *MX1* in both PBMCs and isolated pDCs at the same CQ concentration (**Figure 4.2** and **Figure 4.4**). This represents a major advantage in that the total body exposure and off-target tissue accumulation of CQ is diminished with the delivery of antimalarial drug in nanostructures.

Many emerging drug delivery strategies have been tested preclinically against SLE. Previous studies have used mycophenolic acid [100, 215], cyclosporine A [216], azathioprine [217], and the prodrug of dexamethasone [218] in drug delivery platforms to target SLE relevant pathways, ameliorate glomerulonephritis in lupus-prone mice, and decrease proinflammatory cytokines. Our work builds upon existing studies by using a novel drug delivery approach to target pDCs without needing a targeting moiety for delivery of an FDA-approved drug, CQ, for SLE treatment. We chose antimalarial drugs because they are the mainstay first line, long-term SLE treatment regardless of renal involvement or disease severity [23]. By loading CQ in FMs, we decreased the *in vitro* concentration of CQ required to inhibit *MX1*, which is upregulated in SLE patients [158] (**Figure ??**). We showed that CQ-loaded FMs decreased *MX1* gene expression equivalent to soluble CQ in human PBMCs stimulated with purified TLR agonists (**Figure 4.1** and **Figure 4.2**). In human

PBMCs stimulated with anti-dsDNA positive SLE sera, soluble CQ did not inhibit *MX1* gene expression (**Figure 4.5**) or IFN-α secretion (**Figure 4.6**). We propose that SLE sera is less sensitive to CQ inhibition than synthetic oligonucleotide TLR agonists, as shown in previous studies [58], and concentration of CQ in the endosomal space may be more important for treatment in this scenario. Compared to previous studies, we used 75% less CQ loaded in FMs and showed a significant decrease in *MX1* gene expression (**Figure 4.5**) and IFN-α production (**Figure 4.6**), demonstrating the dose-sparing and dose-enhancement of CQ in FMs versus soluble CQ.

Future studies extending efficacy experiments of CQ loaded nanostructures in lupus-prone mouse models can better define the frequency of treatment as well as determine bioavailability of different routes of administration (**Figure 5.5** and **Figure 5.6**). A preclinical model with a strong type I IFN signature and clinical manifestations similar to SLE patients, such as the pristane-induced or NZB/W model [183, 188], will be important in demonstrating the efficacy of this treatment option *in vivo*. Our approach has therapeutic implications because CQ-loaded FMs may provide a more targeted inhibition of immune-complex-mediated inflammation in SLE, potentially sparing steroid or immunosuppressive treatment. This would result in both lower steroid toxicity as well as lower risk of infection, a serious threat to SLE patient health [219, 220].

Other strategies under development for type I IFN inhibition include: antibodies that neutralize IFN-α [154], block its receptor [155], or induce endogenous IFN-α antibodies [156]. Anifrolumab is a monoclonal antibody that blocks the type I IFN receptor subunit 1 (IFNAR1). A phase III clinical trials balanced anifrolumab efficacy with risk of infection. In the Phase III TULIP-2 trial, adults with moderate-to-severe SLE received monthly 300 mg anifrolumab or placebo intravenous infusions. The anifrolumab arm successfully reached the primary endpoint of improvement in the BICLA score [221]. These results came after the highly anticipated Phase III TULIP-1 clinical trial failed its primary end-

point [222]. The key difference between TULIP-1 and TULIP-2 was the disease activity measure used as primary endpoint: TULIP-1 used SRI-4 while TULIP-2 used BICLA. SRI-4 requires complete improvement in one severely affected organ or of multiple moderate manifestations. BICLA has increased sensitivity as it allows partial improvement but retains stringency as it requires improvement in all active domains [223]. Statistically significant benefits of anifrolumab reached in the TULIP-2 clinical trial include a reduction in corticosteroid use and clinically meaningful reductions in disease activity [221]. A significant potential side effect of antibodies against IFNAR1 is increased infection risk, with anifrolumab-treated patients reporting more than twice the frequency of herpes zoster (7.2%) and upper respiratory infections (21.7%) compared with placebo [221]. IFN-α kinoid (IFN-K) is a fusion of inactivated IFN-α to a carrier protein that generates endogenous polyclonal antibodies to block IFN. IFN-K received FDA fast-track designation in 2016. A subsequent Phase IIb trial showed promising results, including induction of neutralizing antibodies against IFN-α2b, decreased IFN signature, improved fatigue, and reduced corticosteroid dose [156]. However, IFN-K did not meet its primary endpoint. Long-term follow-up for this trial was terminated early due to pending financial reorganization of the sponsor, leaving the status of Phase III trials uncertain.

pDC inhibition is also being investigated to blunt type I IFN production. Human pDCs express the cell surface receptor blood DC antigen 2 (BDCA2 or CD303) [138]. BIIB059 is a humanized IgG1 monoclonal antibody that crosslinks BDCA2 [139, 140], leading to inhibition of TLR7/9-induced IFNα/β by both BDCA2 and FcγRIIa receptor internalization [138] and signaling that shares many components with the B cell receptor [139, 140]. In the Phase II LILAC trial and a small Phase I trial, BIIB059 ameliorated cutaneous lupus symptoms, reduced pDC skin infiltration, and normalized type I IFN responses, including *MxA* gene expression, showing benefit in both cutaneous lupus erythematosus patients and SLE patients with active joint or skin manifestations [141]. The trial design measured skin

disease activity while monitoring IFN responses in whole blood and skin. The primary type I IFN producers, pDCs, preferentially accumulate in active skin lesions as well as kidneys of SLE patients [142, 143]. Overall, BIIB059 was well tolerated. The main reported side effect was elevated risk of infection due to dampening of pDC-mediated antiviral responses initiated by dose-dependent internalization of BDCA-2. As of June 2021, the sponsor of BIIB059, Biogen, Inc., announced its first patient dosed in the phase III clinical trial, TOPAZ-1, to evaluate the clinical efficacy and assess the safety of BIIB059. In comparison to other treatment options, antimalarial-loaded nanostructures do not pose a risk of infection, providing an alternative to strategies that dampen antiviral immune responses.

To enhance the therapeutic potential of CQ drug delivery, future work should include investigating other nanostructure morphologies that can target other IFN-producing cell types such as myeloid cells and B cells. The PEG-*b*-PPS platform is ideal for these studies because by changing the hydrophilic weight fractions of the polymer, they can be self-assembled easily to form diverse morphologies such as spherical (*i.e.*, micelles and polymersomes) [121] and cubic (*i.e.*, bicontinuous cubic nanospheres) [224] nanostructures with distinct cellular biodistribution profiles [225]. Overall, this study illustrates the therapeutic potential of drug delivery of CQ for targeting SLE-relevant pathways, immune cells, and organ sites.

Appendix A: Supplemental Data
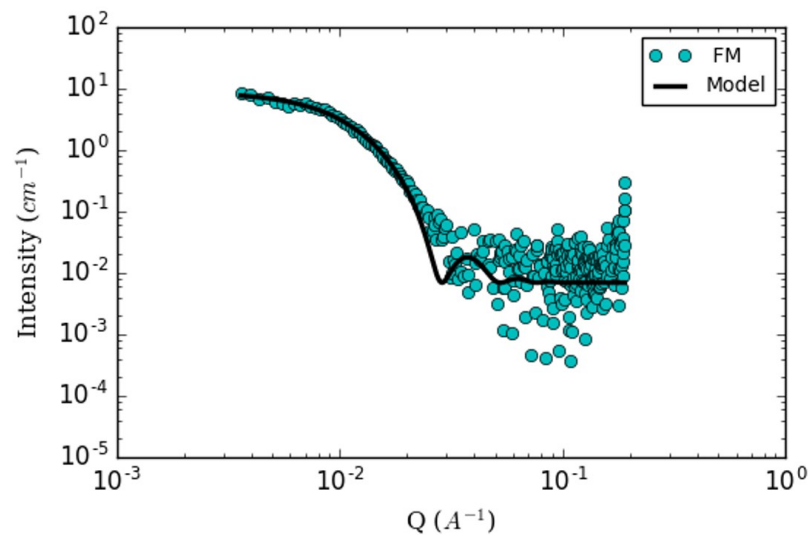
(a) Unloaded.
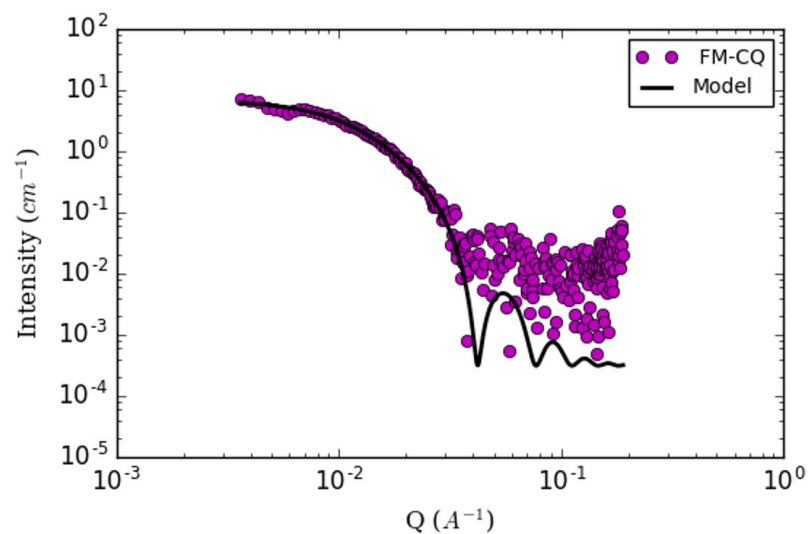
(b) Chloroquine Loaded.

Figure A.1: **SAXS model fit for blank and CQ-loaded FMs.** Unloaded ($X^2 = 0.008$) and CQ-loaded FM ($X^2 = 0.0012$) characteristics were determined by fitting the scattering profiles with a flexible cylindrical model using SASVIEW 4.X. Model analysis used the following parameters: 2 μm cylinder length, 150 nm persistence length, and 8 nm PPS core radius. Each sample was measured at 5 mg/mL in 1X PBS solution. Polydisperse and polymorphous samples were normalized to 1X PBS solution, pH 7.4. Solid lines represent the flexible cylinder fitting model and circles represent raw data.

Chloroquine in DMSO
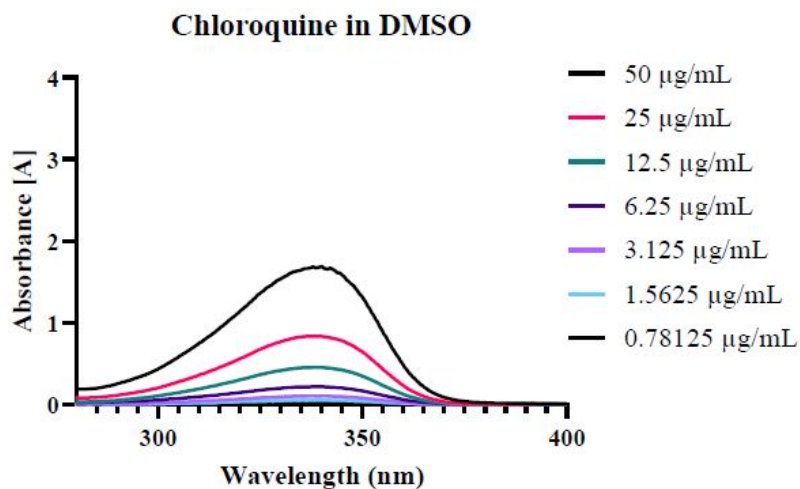
(a) Absorbance of Chloroquine in DMSO.
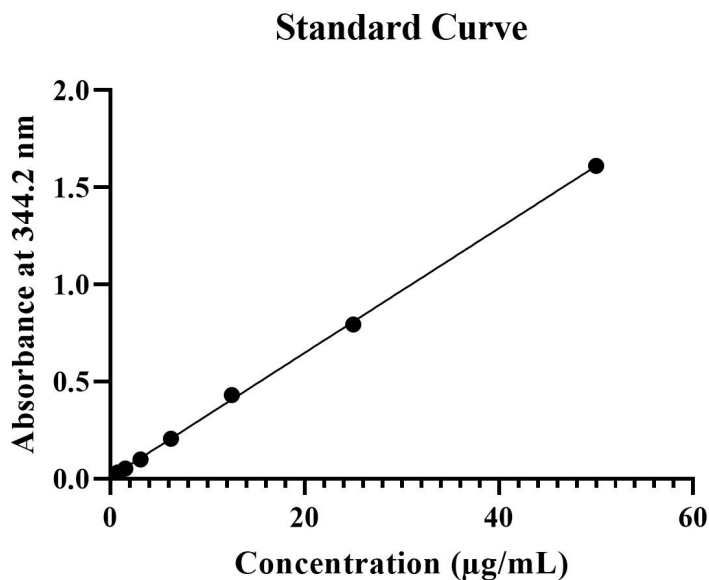
Standard Curve

(b) Standard Curve.

Figure A.2: **Standard curve of CQ in DMSO.** The standard curve was generated by serial dilutions of chloroquine in DMSO near the expected concentration of loaded chloroquine in nanostructures. $y = 0.03207x - 0.1392$, where y is the absorbance at 344.2 nm and x is the concentration of chloroquine in µg/mL ($R^2 = 0.9996$).

Azathioprine Loaded FMs
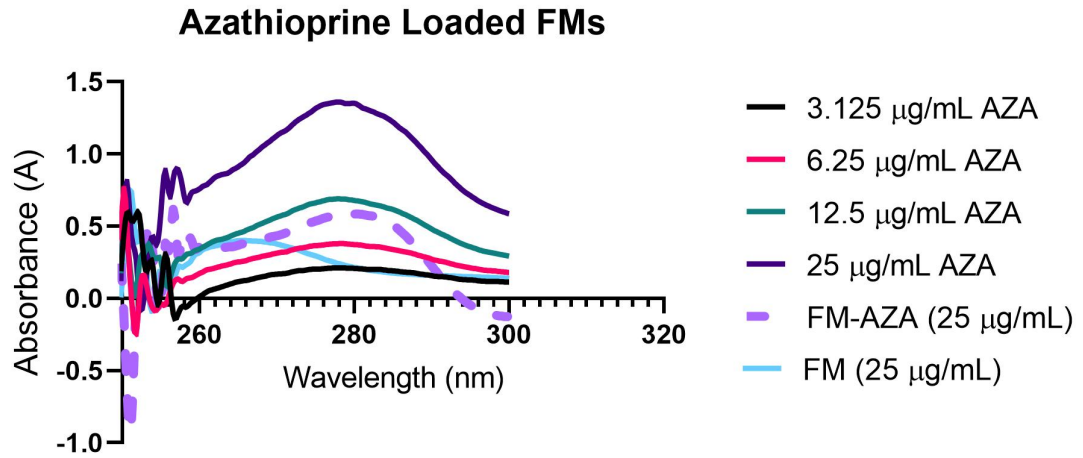
Figure A.3a: **Azathioprine or methylprednisolone load into FMs.**

Standard Curve of Azathioprine in DMSO
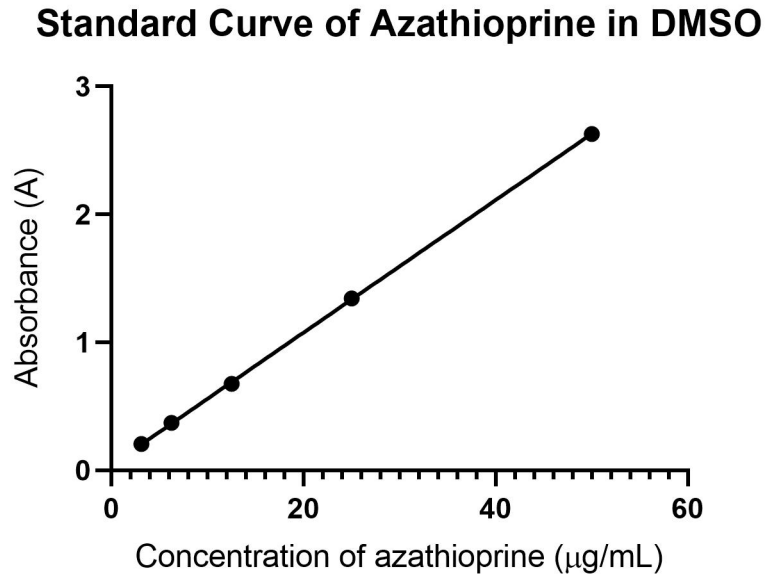
Figure A.3b: **Azathioprine or methylprednisolone load into FMs, continued.**

Methylprednisolone Loaded FMs
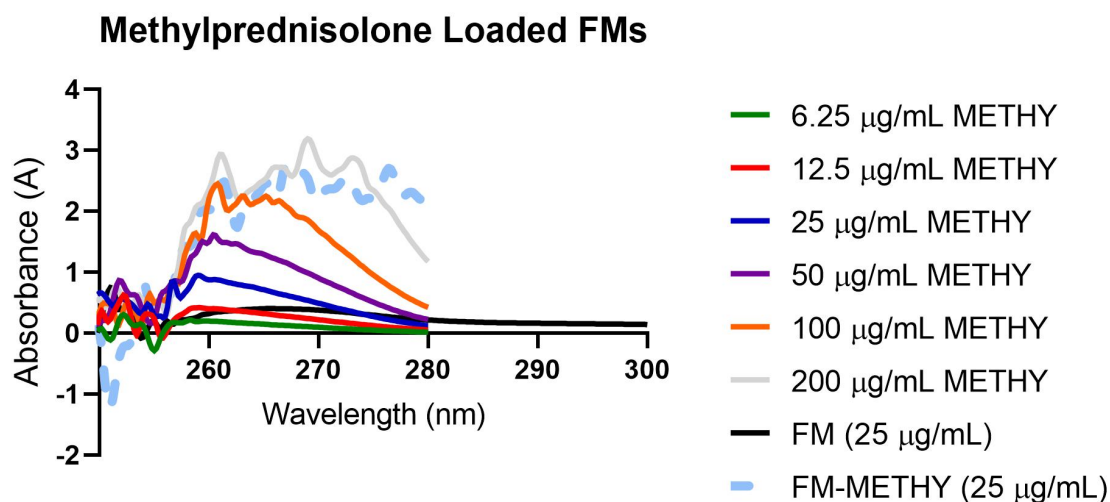
Figure A.3c: **Azathioprine or methylprednisolone load into FMs, continued.**
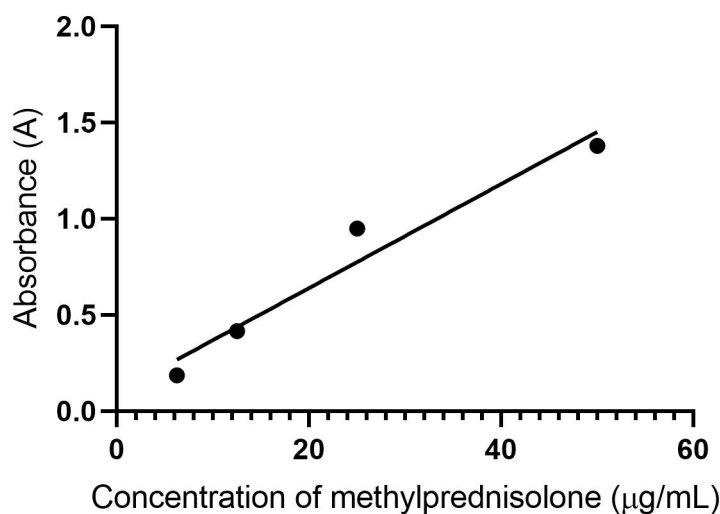
Figure A.3d: **Azathioprine or methylprednisolone load into FMs.** Serial dilutions of azathioprine (AZA) or methylprednisolone (METHY) in DMSO. Drug-loaded FMs (bold, dotted line) were normalized to blank FMs at 25 µg/mL total polymer. The loading capacity of FM-AZA was 396.17 µg drug per mg polymer and of FM-METHY was 95.64 µg drug per mg polymer, as determined by the standard curves found in **Figure A.3** (y = 0.052x + 0.042; R^2 = 0.99) and **Figure A.3** (y = 0.027x + 0.098; R^2 = 0.95).
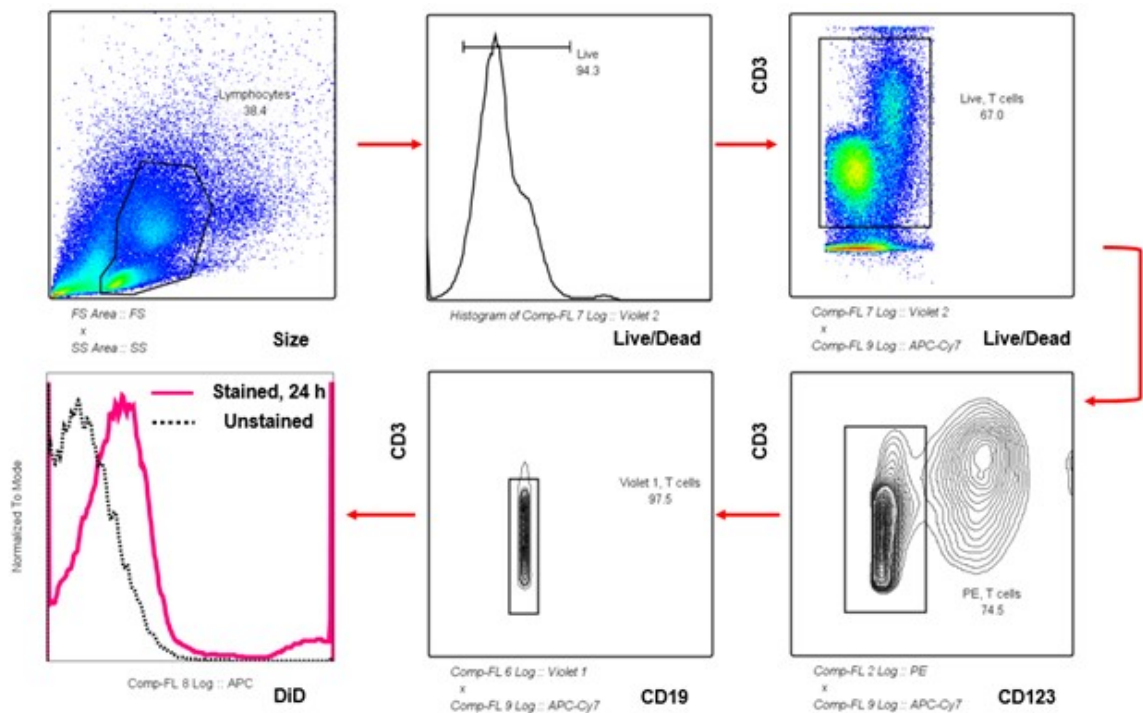
Figure A.4a: **Representative flow cytometry gating strategy for analysis of DiD-loaded FMs cultured with human PBMCs.**
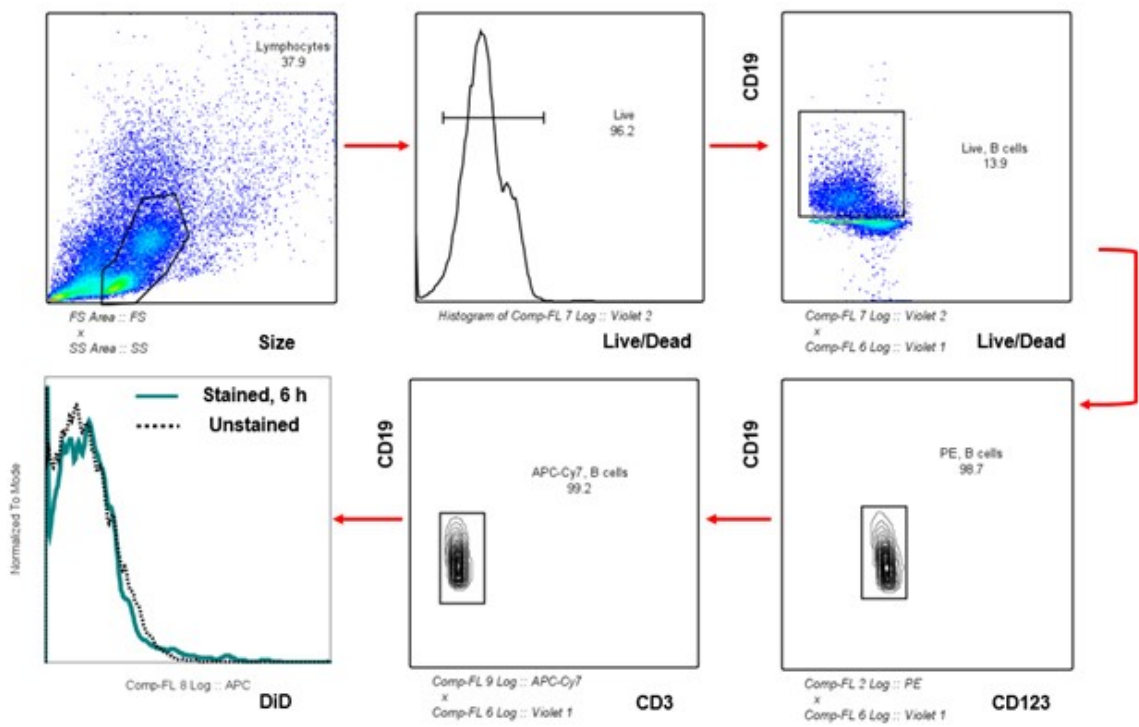
Figure A.4b: **Representative flow cytometry gating strategy for analysis of DiD-loaded FMs cultured with human PBMCs, continued.**
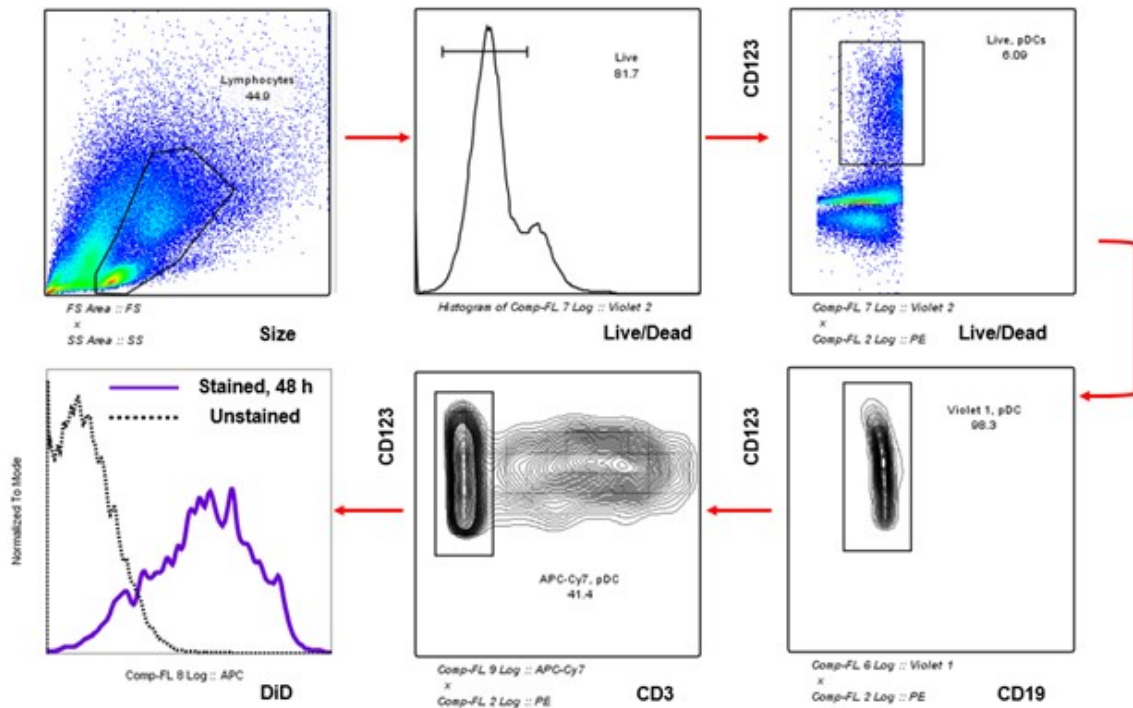
Figure A.4c: **Representative flow cytometry gating strategy for analysis of DiD-loaded FMs cultured with human PBMCs, continued.** Fresh human PBMCs cultured with 200 µg/mL DiD-loaded FMs in supplemented RPMI GlutaMAX medium plus 10% FBS and 20 ng/mL recombinant human IL-3 were stained with phenotypic cell surface markers: **Figure A.4a**) CD3+ T cells, **Figure A.4b**) CD19+ B cells, and **Figure A.4c**) CD123+ pDCs. DiD+ immune cells were determined as above and independent of other cell surface markers. Median fluorescence intensity of DiD was calculated for each cell type.
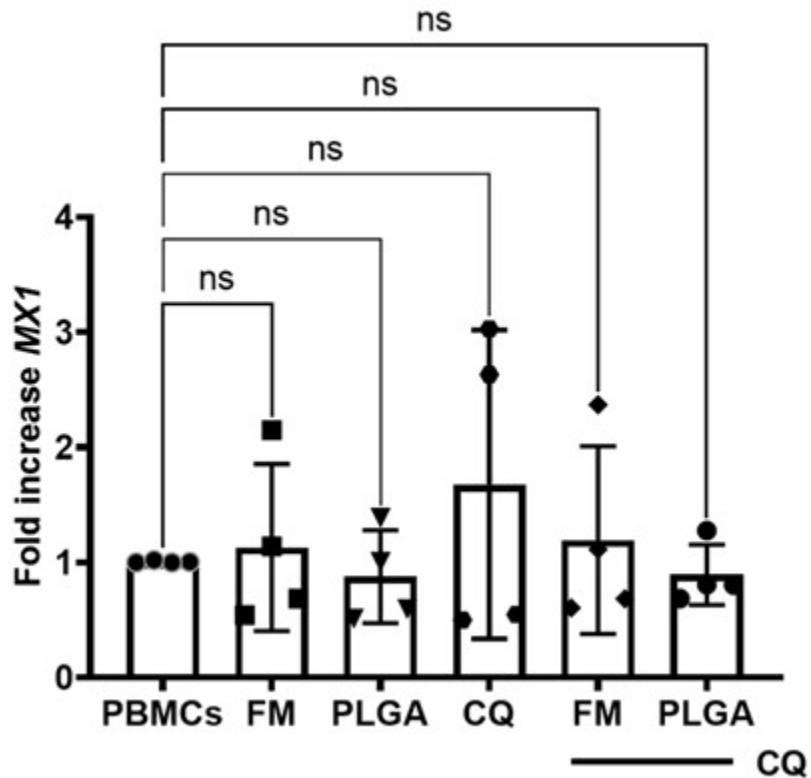
Figure A.5: **No significant difference between MX1 gene expression of empty nanocarriers, CQ alone, and empty nanocarriers with soluble CQ in human PBMCs.** Fresh, healthy human PBMCs were isolated and treated with empty FMs or PLGA nanocarriers with or without soluble CQ at 3.91 μM for 1 h. Total RNA was isolated and *MX1* expression quantified using TaqMan real-time RT-qPCR normalized to β-actin expression. Data are means and standard deviation for $n = 4$ independent donors. Statistical analysis: One-way ANOVA with Tukey's multiple comparisons test.

Bibliography

[1] Renaud Felten, Dan Lipsker, Jean Sibilia, François Chasset, and Laurent Ar-
naud. The history of lupus throughout the ages, 2020. ISSN 10976787.
URL `http://www.jaad.org/article/S0190962220307726/fulltexthttp:`
`//www.jaad.org/article/S0190962220307726/abstracthttps://www.`
`jaad.org/article/S0190-9622(20)30772-6/abstract`.

[2] S Al Sawah, R P Daly, S Foster, A Naegeli, K Benjamin, H Doll, G Bond,
O Moshkovich, and G Alarcn. Sat0423 understanding delay in diagnosis, access
to care and satisfaction with care in lupus: Findings from a cross-sectional online
survey in the united states. *Ann. Rheum. Dis.*, 74:812, 6 2015.

[3] Gabrielle McDonald, Nicholas Cabal, Augustin Vannier, Benjamin Umiker, Ray-
mund H Yin, Arturo V Orjalo Jr, Hans E Johansson, Jin-Hwan Han, and Thereza
Imanishi-Kari. Female bias in systemic lupus erythematosus is associated with the
differential expression of x-linked toll-like receptor 8. *Front. Immunol.*, 6:457, 9
2015.

[4] G Murphy and D Isenberg. Effect of gender on clinical presentation in systemic
lupus erythematosus. *Rheumatology (Oxford)*, 52:2108–2115, 2013. ISSN 1462-
0332. doi: 10.1093/rheumatology/ket160. URL `https://www.ncbi.nlm.nih.`
`gov/pubmed/23641038`.

[5] Virginia Rider, Nabih I Abdou, Bruce F Kimler, Nanyan Lu, Susan Brown,
and Brooke L Fridley. Gender bias in human systemic lupus erythe-
matosus: A problem of steroid receptor action? *Frontiers in im-
munology*, 9:611, 2018. ISSN 1664-3224. doi: 10.3389/fimmu.2018.
00611. URL `http://www.ncbi.nlm.nih.gov/pubmed/29643853http://www.`
`pubmedcentral.nih.gov/articlerender.fcgi?artid=PMC5882779`.

[6] Andrea Fava and Michelle Petri. Systemic lupus erythematosus: Diagnosis and
clinical management, 1 2019. ISSN 10959157.

[7] A Velo-García, S G Castro, and D A Isenberg. The diagnosis and management of the haematologic manifestations of lupus. *J Autoimmun*, 74:139–160, 2016. ISSN 1095-9157. doi: 10.1016/j.jaut.2016.07.001. URL `https://www.ncbi.nlm.nih.gov/pubmed/27461045`.

[8] N I Maria and A Davidson. Protecting the kidney in systemic lupus erythematosus: from diagnosis to therapy. *Nat Rev Rheumatol*, 16:255–267, 2020. ISSN 1759-4804. doi: 10.1038/s41584-020-0401-9. URL `https://www.ncbi.nlm.nih.gov/pubmed/32203285`.

[9] Shaye Kivity, Nancy Agmon-Levin, Joab Zandman-Goddard Gisele, Chapman, and Yehuda Shoenfeld. Neuropsychiatric lupus: a mosaic of clinical presentations. *BMC Med.*, 13:43, 3 2015.

[10] Jennifer L Medlin, Karen E Hansen, Sara S McCoy, and Christie M Bartels. Pulmonary manifestations in late versus early systemic lupus erythematosus: A systematic review and meta-analysis. *Semin. Arthritis Rheum.*, 48:198–204, 10 2018.

[11] E Dein, H Douglas, M Petri, G Law, and H Timlin. Pericarditis in lupus. *Cureus*, 11:e4166, 2019. ISSN 2168-8184. doi: 10.7759/cureus.4166. URL `https://www.ncbi.nlm.nih.gov/pubmed/31086751`.

[12] Y Bai, Y Tong, Y Liu, and H Hu. Self-dsdna in the pathogenesis of systemic lupus erythematosus. *Clinical and experimental immunology*, 191: 1–10, 2018. ISSN 1365-2249. doi: 10.1111/cei.13041. URL `http://www.ncbi.nlm.nih.gov/pubmed/28836661http://www.pubmedcentral.nih.gov/articlerender.fcgi?artid=PMC5721232`.

[13] Marilyn E. Allen, Violeta Rus, and Gregory L. Szeto. Leveraging heterogeneity in systemic lupus erythematosus for new therapies, 2020. ISSN 1471499X. URL `https://pubmed.ncbi.nlm.nih.gov/33046407/`.

[14] Anselm Mak, Mike W-L Cheung, Hui Jin Chiew, Roger Chun-Man Liu Yang, and Ho. Global trend of survival and damage of systemic lupus erythematosus: meta-analysis and meta-regression of observational studies from the 1950s to 2000s. *Semin. Arthritis Rheum.*, 41:830–839, 6 2012.

[15] R R Singh and E Y Yen. Sle mortality remains disproportionately high, despite improvements over the last decade. *Lupus*, 27:1577–1581, 9 2018.

[16] Eric Y Yen and Ram R Singh. Brief report: Lupus-an unrecognized leading cause of death in young females: A population-based study using nationwide death certificates, 2000-2015. *Arthritis Rheumatol*, 70:1251–1255, 8 2018.

[17] Double stranded dna (dsdna) igg elisa. URL `www.sigmaaldrich.com`.

[18] Erin E Carter, Susan G Barr, and Ann E Clarke. The global burden of sle: prevalence, health disparities and socioeconomic impact. *Nat. Rev. Rheumatol.*, 12:605–620, 10 2016.

[19] Rachel Meacock, Nicola Dale, and Mark J Harrison. The humanistic and economic burden of systemic lupus erythematosus : a systematic review. *Pharmacoeconomics*, 31:49–61, 1 2013.

[20] Pantelis Panopalis, Jinoos Yazdany, Joann Zell Gillis, Laura Julian, Laura Trupin, Aimee O Hersh, Lindsey A Criswell, Patricia Katz, and Edward Yelin. Health care costs and costs associated with changes in work productivity among persons with systemic lupus erythematosus. *Arthritis and rheumatism*, 59:1788–95, 12 2008. ISSN 0004-3591. doi: 10.1002/art. 24063. URL `http://www.ncbi.nlm.nih.gov/pubmed/19035422http://www.pubmedcentral.nih.gov/articlerender.fcgi?artid=PMC2875149`.

[21] N Ruperto, L M Hanrahan, G S Alarcón, H M Belmont, R L Brey, P Brunetta, J P Buyon, M I Costner, M E Cronin, M A Dooley, G Filocamo, D Fiorentino, P R Fortin, A G Franks, G Gilkeson, E Ginzler, C Gordon, J Grossman, B Hahn, D A Isenberg, K C Kalunian, M Petri, L Sammaritano, J Sánchez-Guerrero, R D Sontheimer, V Strand, M Urowitz, J M von Feldt, V P Werth, J T Merrill, and I.c. International Flare Consensus Initiative of America. International consensus for a definition of disease flare in lupus. *Lupus*, 20:453–462, 2011. ISSN 1477-0962. doi: 10.1177/0961203310388445. URL `https://www.ncbi.nlm.nih.gov/pubmed/21148601`.

[22] D Fernandez and K A Kirou. What causes lupus flares? *Curr Rheumatol Rep*, 18:14, 2016. ISSN 1534-6307. doi: 10.1007/s11926-016-0562-3. URL `https://www.ncbi.nlm.nih.gov/pubmed/26951252`.

[23] A Fanouriakis, M Kostopoulou, A Alunno, M Aringer, I Bajema, J N Boletis, R Cervera, A Doria, C Gordon, M Govoni, F Houssiau, D Jayne, M Kouloumas, A Kuhn, J L Larsen, K Lerstrøm, G Moroni, M Mosca, M Schneider, J S Smolen, E Svenungsson, V Tesar, A Tincani, A Troldborg, R van Vollenhoven, J Wenzel, G Bertsias, and D T Boumpas. 2019 update of the eular recommendations for the management of systemic lupus erythematosus. *Ann Rheum Dis*, 78:736–745, 2019. ISSN 1468-2060. doi: 10.1136/annrheumdis-2019-215089. URL `https://www.ncbi.nlm.nih.gov/pubmed/30926722`.

[24] G S Alarcón, G McGwin, A M Bertoli, B J Fessler, J Calvo-Alén, H M Bastian, L M Vilá, J D Reveille, and LUMINA Study Group. Effect of hydroxychloroquine on the survival of patients with systemic lupus erythematosus: data from lumina, a multiethnic us cohort (lumina l). *Ann Rheum Dis*, 66:1168–1172, 2007. ISSN 0003-4967. doi: 10.1136/ard.2006.068676. URL `https://www.ncbi.nlm.nih.gov/pubmed/17389655`.

[25] G J Pons-Estel, G S Alarcón, L A González, J Zhang, L M Vilá, J D Reveille, G McGwin, and Lumina Study Group. Possible protective effect of hydroxychloroquine on delaying the occurrence of integument damage in lupus: Lxxi, data from a multiethnic cohort. *Arthritis Care Res (Hoboken)*, 62:393–400, 2010. ISSN 2151-4658. doi: 10.1002/acr.20097. URL https://www.ncbi.nlm.nih.gov/pubmed/20391486.

[26] R Kaiser, C M Cleveland, and L A Criswell. Risk and protective factors for thrombosis in systemic lupus erythematosus: results from a large, multi-ethnic cohort. *Ann Rheum Dis*, 68:238–241, 2009. ISSN 1468-2060. doi: 10.1136/ard.2008.093013. URL https://www.ncbi.nlm.nih.gov/pubmed/18782792.

[27] Ronald B. Melles and Michael F. Marmor. The risk of toxic retinopathy in patients on long-term hydroxychloroquine therapy. *JAMA Ophthalmology*, 132:1453, 12 2014. ISSN 2168-6165. doi: 10.1001/jamaophthalmol.2014.3459. URL http://archopht.jamanetwork.com/article.aspx?doi=10.1001/jamaophthalmol.2014.3459.

[28] J W Kim, Y Y Kim, H Lee, S H Park, S K Kim, and J Y Choe. Risk of retinal toxicity in longterm users of hydroxychloroquine. *J Rheumatol*, 44:1674–1679, 2017. ISSN 0315-162X. doi: 10.3899/jrheum.170158. URL https://www.ncbi.nlm.nih.gov/pubmed/28864645.

[29] Chandra Mohan and Chaim Putterman. Genetics and pathogenesis of systemic lupus erythematosus and lupus nephritis. *Nature Reviews Nephrology*, 11:329–341, 6 2015. ISSN 1759-5061. doi: 10.1038/nrneph.2015.33. URL http://www.nature.com/articles/nrneph.2015.33.

[30] Salem Almaani, Alexa Meara, and Brad H Rovin. Update on lupus nephritis. *Clinical journal of the American Society of Nephrology : CJASN*, 12:825–835, 5 2017. ISSN 1555-905X. doi: 10.2215/CJN.05780616. URL http://www.ncbi.nlm.nih.gov/pubmed/27821390http://www.pubmedcentral.nih.gov/articlerender.fcgi?artid=PMC5477208.

[31] J J Weening, V D D'Agati, M M Schwartz, S V Seshan, C E Alpers, G B Appel, J E Balow, J A Bruijn, T Cook, F Ferrario, A B Fogo, E M Ginzler, L Hebert, G Hill, P Hill, J C Jennette, N C Kong, P Lesavre, M Lockshin, L M Looi, H Makino, L A Moura, M Nagata, International Society of Nephrology Working Group on the Classification of Lupus Nephritis, and Renal Pathology Society Working Group on the Classification of Lupus Nephritis. The classification of glomerulonephritis in systemic lupus erythematosus revisited. *Kidney Int*, 65: 521–530, 2004. ISSN 0085-2538. doi: 10.1111/j.1523-1755.2004.00443.x. URL https://www.ncbi.nlm.nih.gov/pubmed/14717922.

[32] C A Clark, K A Spitzer, and C A Laskin. Decrease in pregnancy loss rates in patients with systemic lupus erythematosus over a 40-year period. *J Rheumatol*, 32:1709–1712, 2005. ISSN 0315-162X. URL https://www.ncbi.nlm.nih.gov/pubmed/16142865.

[33] A Lateef and M Petri. Managing lupus patients during pregnancy. *Best Pract Res Clin Rheumatol*, 27:435–447, 2013. ISSN 1532-1770. doi: 10.1016/j.berh.2013.07.005. URL https://www.ncbi.nlm.nih.gov/pubmed/24238698.

[34] G Moroni, A Doria, E Giglio, C Tani, M Zen, F Strigini, B Zaina, A Tincani, F de Liso, C Matinato, C Grossi, M Gatto, P Castellana, M Limardo, P L Meroni, P Messa, P Ravani, and M Mosca. Fetal outcome and recommendations of pregnancies in lupus nephritis in the 21st century. a prospective multicenter study. *J Autoimmun*, 74:6–12, 2016. ISSN 1095-9157. doi: 10.1016/j.jaut.2016.07.010. URL https://www.ncbi.nlm.nih.gov/pubmed/27496151.

[35] R Fischer-Betz and C Specker. Pregnancy in systemic lupus erythematosus and antiphospholipid syndrome. *Best Pract Res Clin Rheumatol*, 31:397–414, 2017. ISSN 1532-1770. doi: 10.1016/j.berh.2017.09.011. URL https://www.ncbi.nlm.nih.gov/pubmed/29224680.

[36] E G McDonald, L Bissonette, S Ensworth, N Dayan, A E Clarke, S Keeling, S Bernatsky, and E Vinet. Monitoring of systemic lupus erythematosus pregnancies: A systematic literature review. *J Rheumatol*, 45:1477–1490, 2018. ISSN 0315-162X. doi: 10.3899/jrheum.171023. URL https://www.ncbi.nlm.nih.gov/pubmed/30008450.

[37] M Y Kim, M M Guerra, E Kaplowitz, C A Laskin, M Petri, D W Branch, M D Lockshin, L R Sammaritano, J T Merrill, T F Porter, A Sawitzke, A M Lynch, J P Buyon, and J E Salmon. Complement activation predicts adverse pregnancy outcome in patients with systemic lupus erythematosus and/or antiphospholipid antibodies. *Ann Rheum Dis*, 77:549–555, 2018. ISSN 1468-2060. doi: 10.1136/annrheumdis-2017-212224. URL https://www.ncbi.nlm.nih.gov/pubmed/29371202.

[38] J Flint, S Panchal, A Hurrell, M van de Venne, M Gayed, K Schreiber, S Arthanari, J Cunningham, L Flanders, L Moore, A Crossley, N Purushotham, A Desai, M Piper, M Nisar, M Khamashta, D Williams, C Gordon, I Giles, BSR, G.idelines BHPR Standards, and Audit Working Group. Bsr and bhpr guideline on prescribing drugs in pregnancy and breastfeeding-part ii: analgesics and other drugs used in rheumatology practice. *Rheumatology (Oxford)*, 55:1698–1702, 2016. ISSN 1462-0332. doi: 10.1093/rheumatology/kev405. URL https://www.ncbi.nlm.nih.gov/pubmed/26750125.

[39] N Costedoat-Chalumeau, Z Amoura, P Duhaut, D L Huong, D Sebbough, B Wechsler, D Vauthier, I Denjoy, J M Lupoglazoff, and J C Piette. Safety of hydroxychloroquine in pregnant patients with connective tissue diseases: a study of one hundred thirty-three cases compared with a control group. *Arthritis Rheum*, 48: 3207–3211, 2003. ISSN 0004-3591. doi: 10.1002/art.11304. URL `https://www.ncbi.nlm.nih.gov/pubmed/14613284`.

[40] G Klinger, Y Morad, C A Westall, C Laskin, K A Spitzer, G Koren, S Ito, and R J Buncic. Ocular toxicity and antenatal exposure to chloroquine or hydroxychloroquine for rheumatic diseases. *Lancet*, 358:813–814, 2001. ISSN 0140-6736. doi: 10.1016/S0140-6736(01)06004-4. URL `https://www.ncbi.nlm.nih.gov/pubmed/11564493`.

[41] M R Seo, J Chae, Y M Kim, H S Cha, S J Choi, S Oh, and C R Roh. Hydroxychloroquine treatment during pregnancy in lupus patients is associated with lower risk of preeclampsia. *Lupus*, 28:722–730, 2019. ISSN 1477-0962. doi: 10.1177/0961203319843343. URL `https://www.ncbi.nlm.nih.gov/pubmed/30971164`.

[42] M E Clowse, L Magder, F Witter, and M Petri. Hydroxychloroquine in lupus pregnancy. *Arthritis Rheum*, 54:3640–3647, 2006. ISSN 0004-3591. doi: 10.1002/art.22159. URL `https://www.ncbi.nlm.nih.gov/pubmed/17075810`.

[43] G Ruiz-Irastorza, M Ramos-Casals, P Brito-Zeron, and M A Khamashta. Clinical efficacy and side effects of antimalarials in systemic lupus erythematosus: a systematic review. *Annals of the rheumatic diseases*, 69:20–8, 1 2010. ISSN 1468-2060. doi: 10.1136/ard.2008.101766. URL `http://www.ncbi.nlm.nih.gov/pubmed/19103632`.

[44] Hyon K. Choi, John D. Seeger, and Karen M. Kuntz. A cost-effectiveness analysis of treatment options for patients with methotrexate-resistant rheumatoid arthritis. *Arthritis Rheumatism*, 43:2316–2327, 10 2000. ISSN 0004-3591. doi: 10.1002/1529-0131(200010)43:10⟨2316::AID-ANR20⟩3.0.CO; 2-6. URL `http://doi.wiley.com/10.1002/1529-0131%28200010%2943% 3A10%3C2316%3A%3AAID-ANR20%3E3.0.CO%3B2-6`.

[45] Ewa Haładyj, Mariusz Sikora, Anna Felis-Giemza, and Marzena Olesinska. Antimalarials - are they effective and safe in rheumatic diseases? *Reumatologia*, 56:164–173, 2018. ISSN 00346233. doi: 10.5114/reum.2018. 76904. URL `/pmc/articles/PMC6052376/?report=abstracthttps://www. ncbi.nlm.nih.gov/pmc/articles/PMC6052376/`.

[46] Senq-J Lee, Earl Silverman, and Joanne M. Bargman. The role of antimalarial agents in the treatment of sle and lupus nephritis. *Nature Reviews Nephrology*, 7:718–729, 12 2011. ISSN 1759-5061. doi: 10.1038/nrneph.2011.

150. URL `http://www.ncbi.nlm.nih.gov/pubmed/22009248http://www.nature.com/articles/nrneph.2011.150`.

[47] S E Tett, D J Cutler, R O Day, and K F Brown. Bioavailability of hydroxychloroquine tablets in healthy volunteers. *British journal of clinical pharmacology*, 27:771–9, 6 1989. ISSN 0306-5251. URL `http://www.ncbi.nlm.nih.gov/pubmed/2757893http://www.pubmedcentral.nih.gov/articlerender.fcgi?artid=PMC1379804`.

[48] D. J. Cutler, A. C. MacIntyre, and S. E. Tett. Pharmacokinetics and cellular uptake of 4-aminoquinoline antimalarials. *Agents and actions. Supplements*, 24: 142–157, 1988. ISSN 03790363. doi: 10.1007/978-3-0348-9160-8_13. URL `https://pubmed.ncbi.nlm.nih.gov/3263755/`.

[49] R. L. Schroeder and J. P. Gerber. Chloroquine and hydroxychloroquine binding to melanin: Some possible consequences for pathologies. *Toxicology Reports*, 1:963–968, 1 2014. ISSN 22147500. doi: 10.1016/j.toxrep.2014.10.019. URL `/pmc/articles/PMC5598414/?report=abstracthttps://www.ncbi.nlm.nih.gov/pmc/articles/PMC5598414/`.

[50] April Jorge, Cindy Ung, Lucy H. Young, Ronald B. Melles, and Hyon K. Choi. Hydroxychloroquine retinopathy — implications of research advances for rheumatology care. *Nature Reviews Rheumatology*, 14:693–703, 12 2018. ISSN 1759-4790. doi: 10.1038/s41584-018-0111-8. URL `http://www.nature.com/articles/s41584-018-0111-8`.

[51] Lucy H. Liu, Helene B. Fevrier, Robert Goldfien, Anke Hemmerling, and Lisa J. Herrinton. Understanding nonadherence with hydroxychloroquine therapy in systemic lupus erythematosus. *Journal of Rheumatology*, 46:1309–1315, 10 2019. ISSN 14992752. doi: 10.3899/jrheum.180946. URL `www.jrheum.org`.

[52] Nathalie Costedoat-Chalumeau, Zahir Amoura, Jean Sébastien Hulot, Hala Abou Hammoud, Guy Aymard, Patrice Cacoub, Camille Francès, Bertrand Wechsler, Du Le Thi Huong, Pascale Ghillani, Lucile Musset, Philippe Lechat, and Jean Charles Piette. Low blood concentration of hydroxychloroquine is a marker for and predictor of disease exacerbations in patients with systemic lupus erythematosus. *Arthritis and Rheumatism*, 54:3284–3290, 10 2006. ISSN 00043591. doi: 10.1002/art.22156. URL `https://pubmed.ncbi.nlm.nih.gov/17009263/`.

[53] Eva Schrezenmeier and Thomas Dörner. Mechanisms of action of hydroxychloroquine and chloroquine: implications for rheumatology. *Nat. Rev. Rheumatol.*, 16: 155–166, 3 2020.

[54] Mario Mauthe, Idil Orhon, Cecilia Rocchi, Xingdong Zhou, Morten Luhr, Kerst Jan Hijlkema, Robert P. Coppes, Nikolai Engedal, Muriel Mari, and Fulvio Reggiori.

Chloroquine inhibits autophagic flux by decreasing autophagosome-lysosome fusion. *Autophagy*, 14:1435–1455, 8 2018. ISSN 15548635. doi: 10.1080/15548627. 2018.1474314. URL `https://pubmed.ncbi.nlm.nih.gov/29940786/`.

[55] Andrea Frustaci, Emanuela Morgante, Daniela Antuzzi, Matteo Antonio Russo, and Cristina Chimenti. Inhibition of cardiomyocyte lysosomal activity in hydroxychloroquine cardiomyopathy. *International Journal of Cardiology*, 157:117–119, 5 2012. ISSN 18741754. doi: 10.1016/j.ijcard.2012.03.112. URL `https://pubmed.ncbi.nlm.nih.gov/22481048/`.

[56] Staffan P. Sundelin and Alexei Terman. Different effects of chloroquine and hydroxychloroquine on lysosomal function in cultured retinal pigment epithelial cells. *APMIS*, 110:481–489, 2002. ISSN 09034641. doi: 10.1034/j.1600-0463.2002.100606. x. URL `https://pubmed.ncbi.nlm.nih.gov/12193209/`.

[57] Sarah E. Ewald, Bettina L. Lee, Laura Lau, Katherine E. Wickliffe, Guo Ping Shi, Harold A. Chapman, and Gregory M. Barton. The ectodomain of toll-like receptor 9 is cleaved to generate a functional receptor. *Nature*, 456:658–662, 12 2008. ISSN 00280836. doi: 10.1038/ nature07405. URL `/pmc/articles/PMC2596276/?report=abstracthttps://www.ncbi.nlm.nih.gov/pmc/articles/PMC2596276/`.

[58] Alenka Kuznik, Mojca Bencina, Urban Svajger, Matjaz Jeras, Blaz Rozman, and Roman Jerala. Mechanism of endosomal tlr inhibition by antimalarial drugs and imidazoquinolines. *Journal of immunology (Baltimore, Md. : 1950)*, 186:4794–804, 4 2011. ISSN 1550-6606. doi: 10.4049/jimmunol.1000702. URL `http://www.ncbi.nlm.nih.gov/pubmed/21398612`.

[59] Hans Häcker, Harald Mischak, Thomas Miethke, Susanne Liptay, Roland Schmid, Tim Sparwasser, Klaus Heeg, Grayson B. Lipford, and Hermann Wagner. Cpg-dna-specific activation of antigen-presenting cells requires stress kinase activity and is preceded by non-specific endocytosis and endosomal maturation. *EMBO Journal*, 17:6230–6240, 11 1998. ISSN 02614189. doi: 10.1093/emboj/17. 21.6230. URL `/pmc/articles/PMC1170949/?report=abstracthttps://www.ncbi.nlm.nih.gov/pmc/articles/PMC1170949/`.

[60] Christina M. Lau, Courtney Broughton, Abigail S. Tabor, Shizuo Akira, Richard A. Flavell, Mark J. Mamula, Sean R. Christensen, Mark J. Shlomchik, Gregory A. Viglianti, Ian R. Rifkin, and Ann Marshak-Rothstein. Rna-associated autoantigens activate b cells by combined b cell antigen receptor/toll-like receptor 7 engagement. *Journal of Experimental Medicine*, 202:1171–1177, 11 2005. ISSN 00221007. doi: 10.1084/jem.20050630. URL `/pmc/articles/PMC2213226/?report=abstracthttps://www.ncbi.nlm.nih.gov/pmc/articles/PMC2213226/`.

[61] Jörg Vollmer, Sibylle Tluk, Claudia Schmitz, Svetlana Hamm, Marion Jurk, Alexandra Forsbach, Shizuo Akira, Kindra M. Kelly, Westley H. Reeves, Stefan Bauer, and Arthur M. Krieg. Immune stimulation mediated by autoantigen binding sites within small nuclear rnas involves toll-like receptors 7 and 8. *Journal of Experimental Medicine*, 202:1575–1585, 12 2005. ISSN 00221007. doi: 10.1084/jem.20051696. URL /pmc/articles/PMC2213330/?report=abstracthttps://www.ncbi.nlm.nih.gov/pmc/articles/PMC2213330/.

[62] Xu Zhang, Jiaxi Wu, Fenghe Du, Hui Xu, Lijun Sun, Zhe Chen, Chad A Brautigam, Xuewu Zhang, and Zhijian J Chen. The cytosolic dna sensor cgas forms an oligomeric complex with dna and undergoes switch-like conformational changes in the activation loop. *Cell reports*, 6:421–430, 2 2014. ISSN 2211-1247. doi: 10.1016/j.celrep.2014.01.003. URL https://pubmed.ncbi.nlm.nih.gov/24462292https://www.ncbi.nlm.nih.gov/pmc/articles/PMC3969844/.

[63] Mary K. Crow. Type i interferon in the pathogenesis of lupus. *The Journal of Immunology*, 192:5459–5468, 6 2014. ISSN 0022-1767. doi: 10.4049/jimmunol.1002795. URL http://www.ncbi.nlm.nih.gov/pubmed/24907379http://www.pubmedcentral.nih.gov/articlerender.fcgi?artid=PMC4083591http://www.jimmunol.org/lookup/doi/10.4049/jimmunol.1002795.

[64] François Chasset and Laurent Arnaud. Targeting interferons and their pathways in systemic lupus erythematosus. *Autoimmunity Reviews*, 17:44–52, 1 2018. ISSN 1568-9972. doi: 10.1016/J.AUTREV.2017.11.009. URL https://www.sciencedirect.com/science/article/pii/S1568997217302823?via%3Dihub.

[65] L Rönnblom and D Leonard. Interferon pathway in sle: one key to unlocking the mystery of the disease. *Lupus Sci Med*, 6:e000270, 2019. ISSN 2053-8790. doi: 10.1136/lupus-2018-000270. URL https://www.ncbi.nlm.nih.gov/pubmed/31497305.

[66] Bing Yan, Shuang Ye, Guangjie Chen, Miao Kuang, Nan Shen, and Shunle Chen. Dysfunctional cd4+,cd25+ regulatory t cells in untreated active systemic lupus erythematosus secondary to interferon-alpha-producing antigen-presenting cells. *Arthritis Rheum.*, 58:801–812, 3 2008.

[67] P Blanco, A K Palucka, M Gill, V Pascual, and J Banchereau. Induction of dendritic cell differentiation by ifn-alpha in systemic lupus erythematosus. *Science*, 294:1540–1543, 11 2001.

[68] Kerstin Kiefer, Michael A Oropallo, Michael P Cancro, and Ann Marshak-Rothstein. Role of type i interferons in the activation of autoreactive b cells. *Immunol. Cell Biol.*, 90:498–504, 5 2012.

[69] Yong-Jun Liu. Ipc: Professional type 1 interferon-producing cells and plasmacytoid dendritic cell precursors. *Annual Review of Immunology*, 23:275–306, 4 2005. ISSN 0732-0582. doi: 10.1146/annurev.immunol.23.021704.115633. URL `http://www.annualreviews.org/doi/10.1146/annurev.immunol.23.021704.115633`.

[70] Daniel J. Wallace, Mariana Linker-Israeli, Allan L. Metzger, and Vera J. Stecher. The relevance of antimalarial therapy with regard to thrombosis, hypercholesterolemia and cytokines in sle. *Lupus*, 2:13–15, 2 1993. ISSN 0961-2033. doi: 10.1177/0961203393002001041. URL `http://journals.sagepub.com/doi/10.1177/0961203393002001041`.

[71] D.J. Wallace, M. Linker-Israeli, S. Hyun, J.R. Klinenberg, and V. Stecher. The effect of hydroxychloroquine therapy on serum levels of immunoregulatory molecules in patients with systemic lupus erythematosus - pubmed. *J. Rheumatol.*, pages 375–376, 1994. URL `https://pubmed.ncbi.nlm.nih.gov/8182661/`.

[72] van den Borne BE, Dijkmans BA, de Rooij HH, le Cessie S, and Verweij CL. Chloroquine and hydroxychloroquine equally affect tumor necrosis factor-alpha, interleukin 6, and interferon-gamma production by peripheral blood mononuclear cells - pubmed. *J Rheumatol.*, pages 55–60, 1997. URL `https://pubmed.ncbi.nlm.nih.gov/9002011/`.

[73] R. Willis, A. M. Seif, G. McGwin, L. A. Martinez-Martinez, E. B. González, N. Dang, E. Papalardo, J. Liu, L. M. Vilá, J. D. Reveille, G. S. Alarcón, and S. S. Pierangeli. Effect of hydroxychloroquine treatment on pro-inflammatory cytokines and disease activity in sle patients: Data from lumina (lxxv), a multiethnic us cohort. *Lupus*, 21:830–835, 7 2012. ISSN 09612033. doi: 10.1177/0961203312437270. URL `https://pubmed.ncbi.nlm.nih.gov/22343096/`.

[74] Shu Fen Wu, Chia Bin Chang, Jui Mei Hsu, Ming Chi Lu, Ning Sheng Lai, Chin Li, and Chien Hsueh Tung. Hydroxychloroquine inhibits cd154 expression in cd4+ t lymphocytes of systemic lupus erythematosus through nfat, but not stat5, signaling. *Arthritis Research and Therapy*, 19, 8 2017. ISSN 14786362. doi: 10.1186/s13075-017-1393-y. URL `https://pubmed.ncbi.nlm.nih.gov/28793932/`.

[75] Barri J. Fessler, Graciela S. Alarcón, Gerald McGwin, Jeffrey Roseman, Holly M. Bastian, Alan W. Friedman, Bruce A. Baethge, Luis Vilá, and John D. Reveille. Systemic lupus erythematosus in three ethnic groups: Xvi. association of hydroxychloroquine use with reduced risk of damage accrual. *Arthritis and Rheumatism*, 52:1473–1480, 5 2005. ISSN 00043591. doi: 10.1002/art.21039. URL `https://pubmed.ncbi.nlm.nih.gov/15880829/`.

[76] Laurence Brunton, Bruce Chabner, and Bjorn Knollmann. *Goodman Gilman's The Pharmacological Basis of Therapeutics*. McGraw-Hill Medical, 12 edition, 2011.

[77] Mark W. Tibbitt, James E. Dahlman, and Robert Langer. Emerging frontiers in drug delivery, 1 2016. ISSN 15205126. URL `https://pubmed.ncbi.nlm.nih.gov/26741786/`.

[78] Ismail Kola and John Landis. Can the pharmaceutical industry reduce attrition rates? *Nature Reviews Drug Discovery*, 3:711–715, 2004. ISSN 14741776. doi: 10.1038/nrd1470. URL `https://pubmed.ncbi.nlm.nih.gov/15286737/`.

[79] Nazila Kamaly, Basit Yameen, Jun Wu, and Omid C. Farokhzad. Degradable controlled-release polymers and polymeric nanoparticles: Mechanisms of controlling drug release. *Chemical Reviews*, 116:2602–2663, 2016. ISSN 15206890. doi: 10.1021/acs.chemrev.5b00346. URL `/pmc/articles/PMC5509216/?report=abstracthttps://www.ncbi.nlm.nih.gov/pmc/articles/PMC5509216/`.

[80] Mostafa F. Al-Hakkani. Biogenic copper nanoparticles and their applications: A review. *SN Applied Sciences*, 2(3):505, 2020. ISSN 2523-3971. doi: 10.1007/s42452-020-2279-1. URL `https://doi.org/10.1007/s42452-020-2279-1`.

[81] Jayanta Kumar Patra, Gitishree Das, Leonardo Fernandes Fraceto, Estefania Vangelie Ramos Campos, Maria Del Pilar Rodriguez-Torres, Laura Susana Acosta-Torres, Luis Armando Diaz-Torres, Renato Grillo, Mallappa Kumara Swamy, Shivesh Sharma, Solomon Habtemariam, and Han Seung Shin. Nano based drug delivery systems: Recent developments and future prospects. *Journal of Nanobiotechnology*, 16, 9 2018. ISSN 14773155. doi: 10.1186/s12951-018-0392-8.

[82] Elvin Blanco, Haifa Shen, and Mauro Ferrari. Principles of nanoparticle design for overcoming biological barriers to drug delivery. *Nature biotechnology*, 33:941–51, 9 2015. ISSN 1546-1696. doi: 10.1038/nbt.3330. URL `http://www.ncbi.nlm.nih.gov/pubmed/26348965http://www.pubmedcentral.nih.gov/articlerender.fcgi?artid=PMC4978509`.

[83] J.M. Harris and Robert B. Chess. Effect of pegylation on pharmaceuticals. *Nature Reviews Drug Discovery*, 2:214–221, 3 2003. ISSN 14741776. doi: 10.1038/nrd1033. URL `https://pubmed.ncbi.nlm.nih.gov/12612647/`.

[84] P.L. Rodriguez, T. Harada, D.A. Christian, D.A. Pantano, R.K. Tsai, and D.E. Discher. Minimal "self" peptides that inhibit phagocytic clearance and enhance delivery of nanoparticles. *Science (New York, N.Y.)*, 339, 2013. ISSN 1095-9203. doi: 10.1126/SCIENCE.1229568. URL `https://pubmed.ncbi.nlm.nih.gov/23430657/`.

[85] Alessandro Parodi, Nicoletta Quattrocchi, Anne L. Van De Ven, Ciro Chiappini, Michael Evangelopoulos, Jonathan O. Martinez, Brandon S. Brown, Sm Z. Khaled, Iman K. Yazdi, Maria Vittoria Enzo, Lucas Isenhart, Mauro Ferrari, and Ennio Tasciotti. Synthetic nanoparticles functionalized with

biomimetic leukocyte membranes possess cell-like functions. *Nature Nanotechnology*, 8:61–68, 2013. ISSN 17483395. doi: 10.1038/nnano.2012. 212. URL /pmc/articles/PMC3751189/?report=abstracthttps://www.ncbi.nlm.nih.gov/pmc/articles/PMC3751189/.

[86] Che Ming J. Hu, Li Zhang, Santosh Aryal, Connie Cheung, Ronnie H. Fang, and Liangfang Zhang. Erythrocyte membrane-camouflaged polymeric nanoparticles as a biomimetic delivery platform. *Proceedings of the National Academy of Sciences of the United States of America*, 108:10980–10985, 7 2011. ISSN 00278424. doi: 10. 1073/pnas.1106634108. URL https://pubmed.ncbi.nlm.nih.gov/21690347/.

[87] Yechezkel Barenholz. Doxil® - the first fda-approved nano-drug: Lessons learned. *Journal of Controlled Release*, 160:117–134, 6 2012. ISSN 01683659. doi: 10.1016/ j.jconrel.2012.03.020. URL https://pubmed.ncbi.nlm.nih.gov/22484195/.

[88] Denise Hinton. Moderna covid-19 vaccine eua letter of authorization, 2020. URL https://www.fda.gov/media/144636/download.

[89] Denise Hinton. Pfizer covid-19 vaccine eua letter of authorization, 2020. URL https://www.fda.gov/media/144412/download.

[90] Robert M. Herndon, Richard A. Rudick, Frederick E. Munschauer, Michele K. Mass, Andres M. Salazar, Michael E. Coats, Robert Labutta, John R. Richert, Stanley L. Cohan, Claude Genain, Donald Goodkin, Martin Toal, and Katherine Riester. Eight-year immunogenicity and safety of interferon beta-1a-avonex® treatment in patients with multiple sclerosis. *Multiple Sclerosis*, 11:409–419, 8 2005. ISSN 13524585. doi: 10.1191/1352458505ms1209oa. URL https://pubmed.ncbi.nlm.nih.gov/16042223/.

[91] Niti Goel and Sue Stephens. Certolizumab pegol. *mAbs*, 2:137–147, 3 2010. ISSN 19420862. doi: 10.4161/mabs.2.2.11271. URL /pmc/articles/PMC2840232/?report=abstracthttps://www.ncbi.nlm.nih.gov/pmc/articles/PMC2840232/.

[92] Ken Yamaji, Young-Joon Kim, Hiroshi Tsuda, and Yoshinari Takasaki. Long-term clinical outcomes of synchronized therapy with plasmapheresis and intravenous cyclophosphamide pulse therapy in the treatment of steroid-resistant lupus nephritis. *Ther. Apher. Dial.*, 12:298–305, 8 2008.

[93] Maria Giovanna Danieli, Carla Palmieri, Aldo Salvi, Maria Cristina Refe, Anna Stella Strusi, and Giovanni Danieli. Synchronised therapy and high-dose cyclophosphamide in proliferative lupus nephritis. *J. Clin. Apher.*, 17:72–77, 2002.

[94] Eda K Holl, Kara L Shumansky, Luke B Borst, Angela D Burnette, Christopher J Sample, Elizabeth A Ramsburg, and Bruce A Sullenger. Scavenging nucleic acid debris to combat autoimmunity and infectious disease.

Proceedings of the National Academy of Sciences of the United States of America, 113:9728–33, 8 2016. ISSN 1091-6490. doi: 10.1073/pnas. 1607011113. URL `http://www.ncbi.nlm.nih.gov/pubmed/27528673http: //www.pubmedcentral.nih.gov/articlerender.fcgi?artid=PMC5024580`.

[95] E E Solomou, Y T Juang, M F Gourley, G M Kammer, and G C Tsokos. Molecular basis of deficient il-2 production in t cells from patients with systemic lupus erythematosus. *J. Immunol.*, 166:4216–4222, 3 2001.

[96] Jens Y Humrich, Henner Morbach, Reinmar Undeutsch, Philipp Enghard, Stefan Rosenberger, Olivia Weigert, Lutz Kloke, Juliane Heimann, Timo Gaber, Susan Brandenburg, Alexander Scheffold, Jochen Huehn, Andreas Radbruch, Gerd-Rüdiger Burmester, and Gabriela Riemekasten. Homeostatic imbalance of regulatory and effector t cells due to il-2 deprivation amplifies murine lupus. *Proc. Natl. Acad. Sci. U. S. A.*, 107:204–209, 1 2010.

[97] Linda A Lieberman and George C Tsokos. The il-2 defect in systemic lupus erythematosus disease has an expansive effect on host immunity. *Journal of biomedicine biotechnology*, 2010:740619, 2010. ISSN 1110-7251. doi: 10.1155/ 2010/740619. URL `http://www.ncbi.nlm.nih.gov/pubmed/20625413http: //www.pubmedcentral.nih.gov/articlerender.fcgi?artid=PMC2896881`.

[98] Jing He, Ruijun Zhang, Miao Shao, Xiaozhen Zhao, Miao Miao, Jiali Chen, Jiajia Liu, Xia Zhang Xiaoying, Zhang, Yuebo Jin, Yu Wang, Shilei Zhang, Lei Zhu, Alexander Jacob, Rulin Jia, Xujie You, Xue Li, Chun Li, Yunshan Zhou, Yue Yang, Yanying Ye Hua, Liu, Yin Su, Nan Shen, Jianping Alexander Jessy, Guo, Julian Ambrus, Xin Lin, Di Yu, Xiaolin Sun, and Zhanguo Li. Efficacy and safety of low-dose il-2 in the treatment of systemic lupus erythematosus: a randomised, double-blind, placebo-controlled trial. *Ann. Rheum. Dis.*, 79:141–149, 1 2020.

[99] David A. Horwitz, Sean Bickerton, Michael Koss, Tarek M. Fahmy, and Antonio La Cava. Suppression of murine lupus by cd4+ and cd8+ treg cells induced by t cell–targeted nanoparticles loaded with interleukin-2 and transforming growth factor β. *Arthritis and Rheumatology*, 71:632–640, 4 2019. ISSN 23265205. doi: 10.1002/art.40773. URL `https://pubmed.ncbi.nlm.nih.gov/30407752/`.

[100] Michael Look, W Mark Saltzman, Joe Craft, and Tarek M Fahmy. The nanomaterial-dependent modulation of dendritic cells and its potential influence on therapeutic immunosuppression in lupus. *Biomaterials*, 35:1089–1095, 2014. doi: 10.1016/j.biomaterials.2013.10.046. URL `https://ac. els-cdn.com/S0142961213012763/1-s2.0-S0142961213012763-main. pdf?_tid=ec294218-fd2b-11e7-b8c6-00000aacb35d&acdnat=1516375255_ f31501e20cfc314b445dc068870b63a4`.

[101] Hideki Shimizu, Yuichi Hori, Shinya Kaname, Koei Yamada, Nobuhiro Nishiyama, Satoru Matsumoto, Kanjiro Miyata, Makoto Oba, Akira Yamada, Toshiro Kataoka Kazunori, and Fujita. sirna-based therapy ameliorates glomerulonephritis. *J. Am. Soc. Nephrol.*, 21:622–633, 4 2010.

[102] Yasunori Iwata, Takashi Wada, Kengo Furuichi, Norihiko Sakai, Kouji Matsushima, Hitoshi Yokoyama, and Ken ichi Kobayashi. p38 mitogen-activated protein kinase contributes to autoimmune renal injury in mrl-faslpr mice. *Journal of the American Society of Nephrology*, 14:57–67, 1 2003. ISSN 10466673. doi: 10.1097/01.ASN. 0000037402.83851.5F. URL https://pubmed.ncbi.nlm.nih.gov/12506138/.

[103] Patrizia Scapini, Yongmei Hu, Ching-Liang Chu, Thi-Sau Migone, Anthony L Defranco, Clifford A Cassatella Marco A, and Lowell. Myeloid cells, baff, and ifn-gamma establish an inflammatory loop that exacerbates autoimmunity in lyn-deficient mice. *J. Exp. Med.*, 207:1757–1773, 8 2010.

[104] Weiqing Huang, Ioana Moisini, Ranjit Bethunaickan Ramalingam, Sahu, Meredith Akerman, Dan Eilat, Martin Lesser, and Anne Davidson. Baff/april inhibition decreases selection of naive but not antigen-induced autoreactive b cells in murine systemic lupus erythematosus. *J. Immunol.*, 187:6571–6580, 12 2011.

[105] Joanna R Groom, Carrie A Fletcher, Stacey N Walters, Shane T Grey, Sally V Watt, Mathew J Sweet, Mark J Smyth, Charles R Mackay, and Fabienne Mackay. Baff and myd88 signals promote a lupuslike disease independent of t cells. *J. Exp. Med.*, 204:1959–1971, 8 2007.

[106] William Stohl, Falk Hiepe, Kevin M Latinis, Mathew Thomas, Morton A Scheinberg, Ann Clarke, Cynthia Aranow, Frank R Wellborne, Carlos Abud-Mendoza, Douglas R Hough, Lilia Pineda, Thi-Sau Migone, Z John Zhong, William W Freimuth, W Winn Chatham, BLISS-52 Study Group, and BLISS-76 Study Group. Belimumab reduces autoantibodies, normalizes low complement levels, and reduces select b cell populations in patients with systemic lupus erythematosus. *Arthritis Rheum.*, 64:2328–2337, 7 2012.

[107] Sandra V Navarra, Renato M Guzmán, Alberto E Gallacher, Stephen Hall, Roger A Levy, Renato E Jimenez, Edmund K-M Li, Mathew Thomas, Ho-Youn Kim, Manuel G León, Coman Tanasescu, Eugeny Nasonov, Joung-Liang Lan, Lilia Pineda, Z John Zhong, William Freimuth, Michelle A Petri, and BLISS-52 Study Group. Efficacy and safety of belimumab in patients with active systemic lupus erythematosus: a randomised, placebo-controlled, phase 3 trial. *Lancet*, 377:721–731, 2 2011.

[108] Ashok K Dubey, Shailendra S Handu, Suparna Dubey, Prashant Sharma, K K Sharma, and Qazi M Ahmed. Belimumab: First targeted biological treatment for systemic lupus erythematosus. *J. Pharmacol. Pharmacother.*, 2:317–319, 10 2011.

[109] Mélanie Souyris, Claire Cenac, Pascal Azar, Danièle Daviaud, Astrid Canivet, Solange Grunenwald, Catherine Pienkowski, Julie Chaumeil, José E Mejía, and Jean-Charles Guéry. Tlr7 escapes x chromosome inactivation in immune cells. *Science immunology*, 3:eaap8855, 1 2018. ISSN 2470-9468. doi: 10.1126/sciimmunol. aap8855. URL http://www.ncbi.nlm.nih.gov/pubmed/29374079.

[110] Roberto Lande, Dipyaman Ganguly, Valeria Facchinetti, Loredana Frasca, Curdin Conrad, Josh Gregorio, Stephan Meller, Georgios Chamilos, Valeria Sebasigari Rosalie, Riccieri, Roland Bassett, Hideki Amuro, Shirou Fukuhara, Tomoki Ito, Yong-Jun Liu, and Michel Gilliet. Neutrophils activate plasmacytoid dendritic cells by releasing self-dna-peptide complexes in systemic lupus erythematosus. *Sci. Transl. Med.*, 3:73ra19, 3 2011.

[111] Luis E Muñoz, Kirsten Lauber, Martin Schiller, Angelo A Manfredi, and Martin Herrmann. The role of defective clearance of apoptotic cells in systemic autoimmunity. *Nat. Rev. Rheumatol.*, 6:280–289, 5 2010.

[112] Yan wei Wu, Wei Tang, and Jian ping Zuo. Toll-like receptors: potential targets for lupus treatment. *Acta pharmacologica Sinica*, 36: 1395–407, 12 2015. ISSN 1745-7254. doi: 10.1038/aps.2015.91. URL http://www.ncbi.nlm.nih.gov/pubmed/26592511http://www.pubmedcentral.nih.gov/articlerender.fcgi?artid=PMC4816237.

[113] Annemie Rehor, Jeffrey A. Hubbell, and Nicola Tirelli. Oxidation-sensitive polymeric nanoparticles. *Langmuir*, 21:411–417, 1 2005. ISSN 07437463. doi: 10.1021/la0478043. URL https://pubs.acs.org/sharingguidelines.

[114] Sean D. Allen, Yu Gang Liu, Sharan Bobbala, Lei Cai, Peter I. Hecker, Ryan Temel, and Evan A. Scott. Polymersomes scalably fabricated via flash nanoprecipitation are non-toxic in non-human primates and associate with leukocytes in the spleen and kidney following intravenous administration. *Nano Research*, 11, 2018. ISSN 19980000. doi: 10.1007/s12274-018-2069-x.

[115] Jonathan K. Armstrong, Georg Hempel, Susanne Koling, Linda S. Chan, Timothy Fisher, Herbert J. Meiselman, and George Garratty. Antibody against poly(ethylene glycol) adversely affects peg-asparaginase therapy in acute lymphoblastic leukemia patients. *Cancer*, 110:103–111, 7 2007. ISSN 0008543X. doi: 10.1002/cncr.22739. URL https://pubmed.ncbi.nlm.nih.gov/17516438/https://pubmed.ncbi.nlm.nih.gov/17516438/?dopt=Abstract.

[116] Michael S. Hershfield, Nancy J. Ganson, Susan J. Kelly, Edna L. Scarlett, Denise A. Jaggers, and John S. Sundy. Induced and pre-existing anti-polyethylene glycol antibody in a trial of every 3-week dosing of pegloticase for refractory gout, including in organ transplant recipients. *Arthritis Research and Therapy*, 16, 3 2014. ISSN

14786362. doi: 10.1186/ar4500. URL `https://pubmed.ncbi.nlm.nih.gov/`
`24602182/https://pubmed.ncbi.nlm.nih.gov/24602182/?dopt=Abstract.`

[117] Asher Chanan-Khan, J. Szebeni, S. Savay, L. Liebes, N. M. Rafique, C. R. Alving, and F. M. Muggia. Complement activation following first exposure to pegylated liposomal doxorubicin (doxil®): Possible role in hypersensitivity reactions. *Annals of Oncology*, 14:1430–1437, 9 2003. ISSN 09237534. doi: 10.1093/annonc/mdg374. URL `https://pubmed.ncbi.nlm.nih.gov/12954584/`.

[118] Johan J.F. Verhoef, John F. Carpenter, Thomas J. Anchordoquy, and Huub Schellekens. Potential induction of anti-peg antibodies and complement activation toward pegylated therapeutics, 11 2014. ISSN 18785832.

[119] Kenneth Murphy and Casey Weaver. *Janeway's Immunobiology*. W. W. Norton Company, 9 edition, 3 2016. ISBN 081534550X.

[120] Alessandro Napoli, Massimiliano Valentini, Nicola Tirelli, Martin Müller, and Jeffrey A Hubbell. Oxidation-responsive polymeric vesicles. 2004. doi: 10.1038/nmat1081. URL `www.nature.com/naturematerials`.

[121] Sijia Yi, Sean David Allen, Yu Gang Liu, Brian Zhou Ouyang, Xiaomo Li, Punn Augsornworawat, Edward Benjamin Thorp, and Evan Alexander Scott. Tailoring nanostructure morphology for enhanced targeting of dendritic cells in atherosclerosis. *ACS Nano*, 10:11290–11303, 12 2016. ISSN 1936086X. doi: 10.1021/acsnano.6b06451.

[122] H. Zhong, G. Chan, Y. Hu, H. Hu, and D. Ouyang. A comprehensive map of fda-approved pharmaceutical products. *Pharmaceutics*, 10(4), 2018. ISSN 1999-4923. doi: 10.3390/pharmaceutics10040263. URL `https://www.ncbi.nlm.nih.gov/pubmed/30563197`.

[123] S. Cerritelli, C. P. O'Neil, D. Velluto, A. Fontana, M. Adrian, J. Dubochet, and J. A. Hubbell. Aggregation behavior of poly(ethylene glycol-bl-propylene sulfide) di- and triblock copolymers in aqueous solution. *Langmuir*, 25(19):11328–35, 2009. ISSN 0743-7463. doi: 10.1021/la900649m. URL `https://www.ncbi.nlm.nih.gov/pubmed/19711914`.

[124] Giuseppe Battaglia* and Anthony J. Ryan. Pathways of polymeric vesicle formation. 2006. doi: 10.1021/JP060728N. URL `https://pubs.acs.org/doi/10.1021/jp060728n`.

[125] Jing Han, Zhengxi Zhu, Haitao Qian, Adam R. Wohl, Charles J. Beaman, Thomas R. Hoye, and Christopher W. Macosko. A simple confined impingement jets mixer for flash nanoprecipitation. *Journal of Pharmaceutical Sciences*, 101:4018–4023, 2012. ISSN 15206017. doi: 10.1002/jps.23259. URL `https://pubmed.ncbi.nlm.nih.gov/22777753/`.

[126] Rebecca L McCall and Rachael W Sirianni. Plga nanoparticles formed by single- or double-emulsion with vitamin e-tpgs. *Journal of visualized experiments : JoVE*, page 51015, 12 2013. ISSN 1940-087X. doi: 10.3791/51015. URL http://www.ncbi.nlm.nih.gov/pubmed/24429733http://www.pubmedcentral.nih.gov/articlerender.fcgi?artid=PMC4106449.

[127] Carlos E. Astete and Cristina M. Sabliov. Synthesis and characterization of plga nanoparticles. *Journal of Biomaterials Science, Polymer Edition*, 17:247–289, 2006. ISSN 15685624. doi: 10.1163/156856206775997322. URL https://pubmed.ncbi.nlm.nih.gov/16689015/.

[128] Nicholas B. Karabin, Sean Allen, Ha Kyung Kwon, Sharan Bobbala, Emre Firlar, Tolou Shokuhfar, Kenneth R. Shull, and Evan A. Scott. Sustained micellar delivery via inducible transitions in nanostructure morphology. *Nature Communications*, 9, 12 2018. ISSN 20411723. doi: 10.1038/s41467-018-03001-9.

[129] Holger Borchert, Elena V. Shevchenko, Aymeric Robert, Ivo Mekis, Andreas Kornowski, Gerhard Grübel, and Horst Weller. Determination of nanocrystal sizes: A comparison of tem, saxs, and xrd studies of highly monodisperse copt 3 particles. *Langmuir*, 21:1931–1936, 3 2005. ISSN 07437463. doi: 10.1021/la0477183. URL https://pubs.acs.org/sharingguidelines.

[130] Patrícia M. Carvalho, Mário R. Felício, Nuno C. Santos, Sónia Gonçalves, and Marco M. Domingues. Application of light scattering techniques to nanoparticle characterization and development, 6 2018. ISSN 22962646. URL www.frontiersin.org.

[131] Jessica Rodríguez-Fernández, Jorge Pérez-Juste, Luis M. Liz-Marzán, and Peter R. Lang. Dynamic light scattering of short au rods with low aspect ratios. *Journal of Physical Chemistry C*, 111:5020–5025, 4 2007. ISSN 19327447. doi: 10.1021/jp067049x. URL https://pubs.acs.org/doi/abs/10.1021/jp067049x.

[132] Sweta Modi and Bradley D. Anderson. Determination of drug release kinetics from nanoparticles: Overcoming pitfalls of the dynamic dialysis method. *Molecular Pharmaceutics*, 10:3076–3089, 8 2013. ISSN 15438384. doi: 10.1021/mp400154a. URL https://pubs.acs.org/sharingguidelines.

[133] Frank Alexis, Eric Pridgen, Linda K. Molnar, and Omid C. Farokhzad. Factors affecting the clearance and biodistribution of polymeric nanoparticles. *Molecular Pharmaceutics*, 5:505–515, 7 2008. ISSN 15438384. doi: 10.1021/mp800051m. URL https://pubmed.ncbi.nlm.nih.gov/18672949/.

[134] Kai Xiao, Yuanpei Li, Juntao Luo, Joyce S. Lee, Wenwu Xiao, Abby M. Gonik, Rinki G. Agarwal, and Kit S. Lam. The effect of surface charge on in vivo

biodistribution of peg-oligocholic acid based micellar nanoparticles. *Biomaterials*, 32:3435–3446, 5 2011. ISSN 01429612. doi: 10.1016/j.biomaterials.2011.01.021. URL `/pmc/articles/PMC3055170/?report=abstracthttps://www.ncbi.nlm.nih.gov/pmc/articles/PMC3055170/`.

[135] Yan Geng, Paul Dalhaimer, Shenshen Cai, Richard Tsai, Manorama Tewari, Tamara Minko, and Dennis E Discher. Shape effects of filaments versus spherical particles in flow and drug delivery. *Nature nanotechnology*, 2:249–55, 4 2007. ISSN 1748-3395. doi: 10.1038/nnano.2007.70. URL `http://www.ncbi.nlm.nih.gov/pubmed/18654271http://www.pubmedcentral.nih.gov/articlerender.fcgi?artid=PMC2740330`.

[136] J. A. Champion and S. Mitragotri. Shape induced inhibition of phagocytosis of polymer particles. *Pharm Res*, 26(1):244–9, 2009. ISSN 0724-8741. doi: 10.1007/s11095-008-9626-z. URL `https://www.ncbi.nlm.nih.gov/pubmed/18548338`.

[137] David J Dowling, Evan A Scott, Annette Scheid, Ilana Bergelson, Sweta Joshi, Carlo Pietrasanta, Spencer Brightman, Guzman Sanchez-Schmitz, Simon D Van Haren, Jana Ninkovi, Dina Kats, Cristiana Guiducci, Alexandre de Titta, Daniel K Bonner, Sachiko Hirosue, Melody A Swartz, Jeffrey A Hubbell, Ofer Levy, and à Boston. Toll-like receptor 8 agonist nanoparticles mimic immunomodulating effects of the live bcg vaccine and enhance neonatal innate and adaptive immune responses. 2017. doi: 10.1016/j.jaci.2016.12.985. URL `http://dx.doi.org/10.1016/j.jaci.2016.12.985`.

[138] Alex Pellerin, Karel Otero, Julie M Czerkowicz, Hannah M Kerns, Renée I Shapiro, Ann M Ranger, Kevin L Otipoby, Frederick R Taylor, Joanne L Cameron Thomas O, Viney, and Dania Rabah. Anti-bdca2 monoclonal antibody inhibits plasmacytoid dendritic cell activation through fc-dependent and fc-independent mechanisms. *EMBO Mol. Med.*, 7:464–476, 4 2015.

[139] W Cao, L Zhang, D B Rosen, L Bover, G Watanabe, M Bao, L L Lanier, and Y J Liu. Bdca2/fc epsilon ri gamma complex signals through a novel bcr-like pathway in human plasmacytoid dendritic cells. *PLoS Biol*, 5:e248, 2007. ISSN 1545-7885. doi: 10.1371/journal.pbio.0050248. URL `https://www.ncbi.nlm.nih.gov/pubmed/17850179`.

[140] Jürgen Röck, Erik Schneider, Andreas Grün Joachim R, Grützkau, Ralf Küppers, Jürgen Schmitz, and Gregor Winkels. Cd303 (bdca-2) signals in plasmacytoid dendritic cells via a bcr-like signalosome involving syk, slp65 and plcgamma2. *Eur. J. Immunol.*, 37:3564–3575, 12 2007.

[141] Richard A Furie, Eric F Morand, Ian N Bruce, Susan Manzi, Kenneth C Kalunian, Edward M Vital, Theresa Lawrence Ford, Ramesh Gupta, Falk Hiepe, Mittermayer

Santiago, Philip Z Brohawn, Anna Berglind, and Raj Tummala. Type i interferon inhibitor anifrolumab in active systemic lupus erythematosus (tulip-1): a randomised, controlled, phase 3 trial. *The Lancet Rheumatology*, 1:e208–e219, 12 2019.

[142] Marco Tucci, Cosima Quatraro, Lucia Lombardi, Cecilia Pellegrino, Franco Dammacco, and Franco Silvestris. Glomerular accumulation of plasmacytoid dendritic cells in active lupus nephritis: Role of interleukin-18. *Arthritis Rheumatism*, 58:251–262, 1 2008. ISSN 00043591. doi: 10.1002/art.23186. URL `http://doi.wiley.com/10.1002/art.23186`.

[143] W Vermi, S Lonardi, M Morassi, C Rossini, R Tardanico, M Venturini, R Sala, A Tincani, P L Poliani, P G Calzavara-Pinton, L Cerroni, A Santoro, and F Facchetti. Cutaneous distribution of plasmacytoid dendritic cells in lupus erythematosus. selective tropism at the site of epithelial apoptotic damage. *Immunobiology*, 214:877–886, 2009. ISSN 1878-3279. doi: 10.1016/j.imbio.2009.06.013. URL `https://www.ncbi.nlm.nih.gov/pubmed/19625100`.

[144] Erik C Dreaden, Lauren A Austin, Megan A Mackey, and Mostafa A El-Sayed. Size matters: gold nanoparticles in targeted cancer drug delivery. *Therapeutic delivery*, 3:457, 2012. URL `https://www.ncbi.nlm.nih.gov/pmc/articles/PMC3596176/`.

[145] H. M. Patel and S. M. Moghimi. Serum-mediated recognition of liposomes by phagocytic cells of the reticuloendothelial system - the concept of tissue specificity. *Adv Drug Deliv Rev*, 32(1-2):45–60, 1998. ISSN 1872-8294. doi: 10.1016/s0169-409x(97)00131-2. URL `https://www.ncbi.nlm.nih.gov/pubmed/10837635`.

[146] G. L. Szeto and E. B. Lavik. Materials design at the interface of nanoparticles and innate immunity. *J Mater Chem B*, 4(9):1610–1618, 2016. ISSN 2050-750X. doi: 10.1039/C5TB01825K. URL `https://www.ncbi.nlm.nih.gov/pubmed/27453783`.

[147] S. Tenzer, D. Docter, J. Kuharev, A. Musyanovych, V. Fetz, R. Hecht, F. Schlenk, D. Fischer, K. Kiouptsi, C. Reinhardt, K. Landfester, H. Schild, M. Maskos, S. K. Knauer, and R. H. Stauber. Rapid formation of plasma protein corona critically affects nanoparticle pathophysiology. *Nat Nanotechnol*, 8(10):772–81, 2013. ISSN 1748-3395. doi: 10.1038/nnano.2013.181. URL `https://www.ncbi.nlm.nih.gov/pubmed/24056901`.

[148] Gaurav Sahay, Daria Y Alakhova, and Alexander V Kabanov. Endocytosis of nanomedicines. *Journal of controlled release : official journal of the Controlled Release Society*, 145:182–95, 8 2010. ISSN 1873-4995. doi: 10.1016/j.jconrel.2010.01.036. URL `http://www.ncbi.nlm.nih.gov/pubmed/20226220http://www.pubmedcentral.nih.gov/articlerender.fcgi?artid=PMC2902597`.

[149] Julie A Champion and Samir Mitragotri. Role of target geometry in phagocy-
tosis. *Proceedings of the National Academy of Sciences of the United States
of America*, 103:4930–4, 3 2006. ISSN 0027-8424. doi: 10.1073/pnas.
0600997103. URL `http://www.ncbi.nlm.nih.gov/pubmed/16549762http:
//www.pubmedcentral.nih.gov/articlerender.fcgi?artid=PMC1458772`.

[150] E. C. Borden, G. C. Sen, G. Uze, R. H. Silverman, R. M. Ransohoff, G. R. Foster, and
G. R. Stark. Interferons at age 50: past, current and future impact on biomedicine.
Nat Rev Drug Discov, 6(12):975–90, 2007. ISSN 1474-1784. doi: 10.1038/nrd2422.
URL `https://www.ncbi.nlm.nih.gov/pubmed/18049472`.

[151] F. McNab, K. Mayer-Barber, A. Sher, A. Wack, and A. O'Garra. Type i interferons
in infectious disease. *Nat Rev Immunol*, 15(2):87–103, 2015. ISSN 1474-1741. doi:
10.1038/nri3787. URL `https://www.ncbi.nlm.nih.gov/pubmed/25614319`.

[152] K. B. Elkon and V. V. Stone. Type i interferon and systemic lupus erythematosus. *J
Interferon Cytokine Res*, 31(11):803–12, 2011. ISSN 1557-7465. doi: 10.1089/jir.
2011.0045. URL `https://www.ncbi.nlm.nih.gov/pubmed/21859344`.

[153] V. Oke, I. Gunnarsson, J. Dorschner, S. Eketjäll, A. Zickert, T. B. Niewold, and
E. Svenungsson. High levels of circulating interferons type i, type ii and type iii as-
sociate with distinct clinical features of active systemic lupus erythematosus. *Arthri-
tis Res Ther*, 21(1):107, 2019. ISSN 1478-6362. doi: 10.1186/s13075-019-1878-y.
URL `https://www.ncbi.nlm.nih.gov/pubmed/31036046`.

[154] Warren Greth, Gabriel J Robbie, Philip Brohawn, Micki Hultquist, and Bing Yao.
Targeting the interferon pathway with sifalimumab for the treatment of systemic
lupus erythematosus. *Immunotherapy*, 9:57–70, 1 2017.

[155] Avram Goldberg, Thomas Geppert, Elena Schiopu, Tracy Frech, Vivien Hsu,
Robert W Simms, Yihong Peng Stanford L, Yao, Nairouz Elgeioushi, Linda Chang,
Bing Wang, and Stephen Yoo. Dose-escalation of human anti-interferon-α recep-
tor monoclonal antibody medi-546 in subjects with systemic sclerosis: a phase 1,
multicenter, open label study. *Arthritis Res. Ther.*, 16:R57, 2 2014.

[156] Frederic A Houssiau, Aikaterini Thanou, Edgar Mazur Minodora, Ramiterre, Danny
Alexis Gomez Mora, Maria Misterska-Skora, Risto Alfredo Perich-Campos, Svet-
lana A Smakotina, Sergio Cerpa Cruz, Thérèse Louzir Bassem, Croughs, and
Michael Lucas Tee. Ifn-α kinoid in systemic lupus erythematosus: results from a
phase iib, randomised, placebo-controlled study. *Ann. Rheum. Dis.*, 79:347–355, 3
2020.

[157] Emily C Baechler, Franak M Batliwalla, George Karypis, Patrick M Gaffney,
Ward A Ortmann, Karl J Espe, Katherine B Shark, William J Grande, Karis M

Hughes, Vivek Kapur, Peter K Gregersen, and Timothy W Behrens. Interferon-inducible gene expression signature in peripheral blood cells of patients with severe lupus. *Proceedings of the National Academy of Sciences of the United States of America*, 100:2610–5, 3 2003. ISSN 0027-8424. doi: 10.1073/pnas. 0337679100. URL http://www.ncbi.nlm.nih.gov/pubmed/12604793http: //www.pubmedcentral.nih.gov/articlerender.fcgi?artid=PMC151388.

[158] Lynda Bennett, A Karolina Palucka, Edsel Arce, Victoria Cantrell, Josef Borvak, Jacques Banchereau, and Virginia Pascual. Interferon and granulopoiesis signatures in systemic lupus erythematosus blood. *The Journal of experimental medicine*, 197:711–23, 3 2003. ISSN 0022-1007. doi: 10.1084/jem. 20021553. URL http://www.ncbi.nlm.nih.gov/pubmed/12642603http:// www.pubmedcentral.nih.gov/articlerender.fcgi?artid=PMC2193846.

[159] John W Schoggins and Charles M Rice. Interferon-stimulated genes and their antiviral effector functions. *Current opinion in virology*, 1: 519–25, 12 2011. ISSN 1879-6265. doi: 10.1016/j.coviro.2011.10. 008. URL http://www.ncbi.nlm.nih.gov/pubmed/22328912http://www. pubmedcentral.nih.gov/articlerender.fcgi?artid=PMC3274382.

[160] O. Haller and G. Kochs. Human mxa protein: an interferon-induced dynamin-like gtpase with broad antiviral activity. *J Interferon Cytokine Res*, 31(1):79–87, 2011. ISSN 1557-7465. doi: 10.1089/jir.2010.0076. URL https://www.ncbi.nlm.nih. gov/pubmed/21166595.

[161] W. M. Lambers, K. de Leeuw, B. Doornbos-van der Meer, G. F. H. Diercks, H. Bootsma, and J. Westra. Interferon score is increased in incomplete systemic lupus erythematosus and correlates with myxovirus-resistance protein a in blood and skin. *Arthritis Res Ther*, 21(1):260, 2019. ISSN 1478-6362. doi: 10.1186/s13075-019-2034-4. URL https://www.ncbi.nlm.nih.gov/pubmed/ 31791398.

[162] M. K. Bach and J. R. Brashler. Isolation of subpopulations of lymphocytic cells by the use of isotonically balanced solutions of ficoll. i. development of methods and demonstration of the existence of a large but finite number of subpopulations. *Experimental Cell Research*, 61:387–396, 1970. ISSN 00144827. doi: 10.1016/ 0014-4827(70)90462-3. URL https://pubmed.ncbi.nlm.nih.gov/4918197/.

[163] Dejiang Zhou, Kyung Hee Kang, and Stephen A Spector. Production of interferon α by human immunodeficiency virus type 1 in human plasmacytoid dendritic cells is dependent on induction of autophagy. *The Journal of infectious diseases*, 205:1258–67, 4 2012. ISSN 1537-6613. doi: 10.1093/infdis/ jis187. URL http://www.ncbi.nlm.nih.gov/pubmed/22396599http://www. pubmedcentral.nih.gov/articlerender.fcgi?artid=PMC3308911.

[164] A Krug, S Rothenfusser, V Hornung, B Jahrsdörfer, S Blackwell, Z K Ballas, S Endres, A M Krieg, and G Hartmann. Identification of cpg oligonucleotide sequences with high induction of ifn-alpha/beta in plasmacytoid dendritic cells. *European journal of immunology*, 31:2154–63, 7 2001. ISSN 0014-2980. doi: 10.1002/1521-4141(200107)31:7⟨2154::AID-IMMU2154gt;3.0.CO;2-U. URL `http://www.ncbi.nlm.nih.gov/pubmed/11449369`.

[165] F. Heil, Hiroaki Hemmi, Hubertus Hochrein, Franziska Ampenberger, Carsten Kirschning, Shizuo Akira, Grayson Lipford, Hermann Wagner, and Stefan Bauer. Species-specific recognition of single-stranded rna via toll-like receptor 7 and 8. *Science*, 303:1526–1529, 3 2004. ISSN 0036-8075. doi: 10.1126/science. 1093620. URL `http://www.ncbi.nlm.nih.gov/pubmed/14976262http://www.sciencemag.org/cgi/doi/10.1126/science.1093620`.

[166] S. S. Diebold, Tsuneyasu Kaisho, Hiroaki Hemmi, Shizuo Akira, and Caetano Reis e Sousa. Innate antiviral responses by means of tlr7-mediated recognition of single-stranded rna. *Science*, 303:1529–1531, 3 2004. ISSN 0036-8075. doi: 10.1126/science.1093616. URL `http://www.ncbi.nlm.nih.gov/pubmed/14976261http://www.sciencemag.org/cgi/doi/10.1126/science.1093616`.

[167] E M Tan, P H Schur, R I Carr, and H G Kunkel. Deoxybonucleic acid (dna) and antibodies to dna in the serum of patients with systemic lupus erythematosus. *J Clin Invest*, 45:1732–1740, 1966. ISSN 0021-9738. doi: 10.1172/JCI105479. URL `https://www.ncbi.nlm.nih.gov/pubmed/4959277`.

[168] Yuka Shimizu, Shinsuke Yasuda, Taichi Kimura, Saori Nishio, Michihiro Kono, Kazumasa Ohmura, Sanae Shimamura, Michihito Kono, Yuichiro Fujieda, Masaru Kato, Kenji Oku, Toshiyuki Bohgaki, Yuichiro Fukasawa, Shinya Tanaka, and Tatsuya Atsumi. Interferon-inducible mx1 protein is highly expressed in renal tissues from treatment-naïve lupus nephritis, but not in those under immunosuppressive treatment. *Modern Rheumatology*, 28:661–669, 7 2018. ISSN 1439-7595. doi: 10.1080/14397595.2017.1404711. URL `https://www.tandfonline.com/doi/full/10.1080/14397595.2017.1404711`.

[169] K. Gibbert, J. F. Schlaak, D. Yang, and U. Dittmer. Ifn-α subtypes: Distinct biological activities in anti-viral therapy. *British Journal of Pharmacology*, 168:1048–1058, 3 2013. ISSN 00071188. doi: 10.1111/bph. 12010. URL `/pmc/articles/PMC3594665/?report=abstracthttps://www.ncbi.nlm.nih.gov/pmc/articles/PMC3594665/`.

[170] C. H. Jang, J. H. Choi, M. S. Byun, and D. M. Jue. Chloroquine inhibits production of tnf-alpha, il-1beta and il-6 from lipopolysaccharide-stimulated human

monocytes/macrophages by different modes. *Rheumatology (Oxford)*, 45(6):703–10, 2006. ISSN 1462-0324. doi: 10.1093/rheumatology/kei282. URL `https://www.ncbi.nlm.nih.gov/pubmed/16418198`.

[171] I Karres, J P Kremer, I Dietl, U Steckholzer, M Jochum, and W Ertel. Chloroquine inhibits proinflammatory cytokine release into human whole blood. *The American journal of physiology*, 274:R1058–64, 4 1998. ISSN 0002-9513. URL `http://www.ncbi.nlm.nih.gov/pubmed/9575969`.

[172] J. A. Martinson, C. J. Montoya, X. Usuga, R. Ronquillo, A. L. Landay, and S. N. Desai. Chloroquine modulates hiv-1-induced plasmacytoid dendritic cell alpha interferon: implication for t-cell activation. *Antimicrob Agents Chemother*, 54(2):871–81, 2010. ISSN 1098-6596. doi: 10.1128/AAC.01246-09. URL `https://www.ncbi.nlm.nih.gov/pubmed/19949061`.

[173] Xiaoyu Wang and Yumin Xia. Anti-double stranded dna antibodies: Origin, pathogenicity, and targeted therapies. *Front. Immunol.*, 10:1667, 7 2019.

[174] J. Tian, A. M. Avalos, S. Y. Mao, B. Chen, K. Senthil, H. Wu, P. Parroche, S. Drabic, D. Golenbock, C. Sirois, J. Hua, L. L. An, L. Audoly, G. La Rosa, A. Bierhaus, P. Naworth, A. Marshak-Rothstein, M. K. Crow, K. A. Fitzgerald, E. Latz, P. A. Kiener, and A. J. Coyle. Toll-like receptor 9-dependent activation by dna-containing immune complexes is mediated by hmgb1 and rage. *Nat Immunol*, 8(5):487–96, 2007. ISSN 1529-2908. doi: 10.1038/ni1457. URL `https://www.ncbi.nlm.nih.gov/pubmed/17417641`.

[175] C. E. Weckerle, B. S. Franek, J. A. Kelly, M. Kumabe, R. A. Mikolaitis, S. L. Green, T. O. Utset, M. Jolly, J. A. James, J. B. Harley, and T. B. Niewold. Network analysis of associations between serum interferon-α activity, autoantibodies, and clinical features in systemic lupus erythematosus. *Arthritis Rheum*, 63(4):1044–53, 2011. ISSN 1529-0131. doi: 10.1002/art.30187. URL `https://www.ncbi.nlm.nih.gov/pubmed/21162028`.

[176] S. M. Ziegler, C. Beisel, K. Sutter, M. Griesbeck, H. Hildebrandt, S. H. Hagen, U. Dittmer, and M. Altfeld. Human pdcs display sex-specific differences in type i interferon subtypes and interferon α/β receptor expression. *Eur J Immunol*, 47(2):251–256, 2017. ISSN 1521-4141. doi: 10.1002/eji.201646725. URL `https://www.ncbi.nlm.nih.gov/pubmed/27891600`. Ziegler, Susanne M Beisel, Claudia Sutter, Kathrin Griesbeck, Morgane Hildebrandt, Heike Hagen, Sven H Dittmer, Ulf Altfeld, Marcus 2016/11/29.

[177] A. Agrawal. Mechanisms and implications of age-associated impaired innate interferon secretion by dendritic cells: a mini-review. *Gerontology*, 59(5):421–6, 2013. ISSN 1423-0003. doi: 10.1159/000350536. URL `https://www.ncbi.nlm.nih.gov/pubmed/23615484`. Agrawal, Anshu 2013/4/26.

[178] G. S. Cooper, S. L. Makris, P. J. Nietert, and J. Jinot. Evidence of autoimmune-related effects of trichloroethylene exposure from studies in mice and humans. *Environ Health Perspect*, 117(5):696–702, 2009. ISSN 1552-9924. doi: 10.1289/ehp. 11782. URL https://www.ncbi.nlm.nih.gov/pubmed/19479009.

[179] D. E. Keil, M. M. Peden-Adams, S. Wallace, P. Ruiz, and G. S. Gilkeson. Assessment of trichloroethylene (tce) exposure in murine strains genetically-prone and non-prone to develop autoimmune disease. *J Environ Sci Health A Tox Hazard Subst Environ Eng*, 44(5):443–53, 2009. ISSN 1093-4529. doi: 10. 1080/10934520902719738. URL https://www.ncbi.nlm.nih.gov/pubmed/ 19241258.

[180] M. M. Peden-Adams, J. G. Eudaly, A. M. Lee, J. Miller, D. E. Keil, and G. S. Gilkeson. Lifetime exposure to trichloroethylene (tce) does not accelerate autoimmune disease in mrl +/+ mice. *J Environ Sci Health A Tox Hazard Subst Environ Eng*, 43(12):1402–9, 2008. ISSN 1093-4529. doi: 10.1080/10934520802232063. URL https://www.ncbi.nlm.nih.gov/pubmed/18780217.

[181] M Satoh and W H Reeves. Induction of lupus-associated autoantibodies in balb/c mice by intraperitoneal injection of pristane. *The Journal of experimental medicine*, 180:2341–6, 12 1994. ISSN 0022-1007. doi: 10.1084/jem.180. 6.2341. URL http://www.ncbi.nlm.nih.gov/pubmed/7964507http://www. pubmedcentral.nih.gov/articlerender.fcgi?artid=PMC2191761.

[182] J. Avigan and M. Blumer. On the origin of pristane in marine organisms. *J Lipid Res*, 9(3):350–2, 1968. ISSN 0022-2275. URL https://www.ncbi.nlm.nih. gov/pubmed/5646185.

[183] W. H. Reeves, P. Y. Lee, J. S. Weinstein, M. Satoh, and L. Lu. Induction of autoimmunity by pristane and other naturally occurring hydrocarbons. *Trends Immunol*, 30(9):455–64, 2009. ISSN 1471-4981. doi: 10.1016/j.it.2009.06.003. URL https://www.ncbi.nlm.nih.gov/pubmed/19699150.

[184] M Satoh, H B Richards, V M Shaheen, H Yoshida, M Shaw, J O Naim, P H Wooley, and W H Reeves. Widespread susceptibility among inbred mouse strains to the induction of lupus autoantibodies by pristane. *Clinical and experimental immunology*, 121:399–405, 8 2000. ISSN 0009-9104. doi: 10.1046/j.1365-2249. 2000.01276.x. URL http://www.ncbi.nlm.nih.gov/pubmed/10931159http: //www.pubmedcentral.nih.gov/articlerender.fcgi?artid=PMC1905709.

[185] M. Satoh, A. Kumar, Y. S. Kanwar, and W. H. Reeves. Anti-nuclear antibody production and immune-complex glomerulonephritis in balb/c mice treated with pristane. *Proc Natl Acad Sci U S A*, 92(24):10934–8, 1995. ISSN 0027-8424. doi: 10.1073/ pnas.92.24.10934. URL https://www.ncbi.nlm.nih.gov/pubmed/7479913.

[186] Daniel Perry, Allison Sang, Yiming Yin, Ying-Yi Zheng, and Laurence Morel. Murine models of systemic lupus erythematosus. *Journal of biomedicine biotechnology*, 2011:271694, 2011. ISSN 1110-7251. doi: 10.1155/2011/ 271694. URL http://www.ncbi.nlm.nih.gov/pubmed/21403825http://www. pubmedcentral.nih.gov/articlerender.fcgi?artid=PMC3042628.

[187] Mara Lennard Richard and Gary Gilkeson. Mouse models of lupus: what they tell us and what they don't. *Lupus science medicine*, 5: e000199, 2018. ISSN 2053-8790. doi: 10.1136/lupus-2016-000199. URL http://www.ncbi.nlm.nih.gov/pubmed/29387435http://www. pubmedcentral.nih.gov/articlerender.fcgi?artid=PMC5786947.

[188] Haoyang Zhuang, Christopher Szeto, Shuhong Han, Lijun Yang, and West-ley H Reeves. Animal models of interferon signature positive lupus. *Frontiers in immunology*, 6:291, 2015. ISSN 1664-3224. doi: 10.3389/fimmu.2015. 00291. URL http://www.ncbi.nlm.nih.gov/pubmed/26097482http://www. pubmedcentral.nih.gov/articlerender.fcgi?artid=PMC4456949.

[189] M. Ramanujam, P. Kahn, W. Huang, H. Tao, M. P. Madaio, S. M. Factor, and A. Davidson. Interferon-alpha treatment of female (nzw x bxsb)f(1) mice mimics some but not all features associated with the yaa mutation. *Arthritis Rheum*, 60(4):1096–101, 2009. ISSN 0004-3591. doi: 10.1002/art.24414. URL https: //www.ncbi.nlm.nih.gov/pubmed/19333924.

[190] A. Boneparth, W. Huang, R. Bethunaickan, M. Woods, R. Sahu, S. Arora, M. Ak-erman, M. Lesser, and A. Davidson. Tlr7 influences germinal center selection in murine sle. *PLoS One*, 10(3):e0119925, 2015. ISSN 1932-6203. doi: 10. 1371/journal.pone.0119925. URL https://www.ncbi.nlm.nih.gov/pubmed/ 25794167.

[191] Zheng Liu and Anne Davidson. Ifnα inducible models of murine sle. *Frontiers in immunology*, 4:306, 10 2013. ISSN 1664-3224. doi: 10.3389/fimmu.2013. 00306. URL http://www.ncbi.nlm.nih.gov/pubmed/24106491http://www. pubmedcentral.nih.gov/articlerender.fcgi?artid=PMC3788378.

[192] M. Macanovic, D. Sinicropi, S. Shak, S. Baughman, S. Thiru, and P. J. Lachmann. The treatment of systemic lupus erythematosus (sle) in nzb/w f1 hybrid mice; studies with recombinant murine dnase and with dexamethasone. *Clin Exp Immunol*, 106 (2):243–52, 1996. ISSN 0009-9104. doi: 10.1046/j.1365-2249.1996.d01-839.x. URL https://www.ncbi.nlm.nih.gov/pubmed/8918569.

[193] L. Ozmen, D. Roman, M. Fountoulakis, G. Schmid, B. Ryffel, and G. Garotta. Experimental therapy of systemic lupus erythematosus: the treatment of nzb/w

mice with mouse soluble interferon-gamma receptor inhibits the onset of glomeru-lonephritis. *Eur J Immunol*, 25(1):6–12, 1995. ISSN 0014-2980. doi: 10.1002/eji.1830250103. URL https://www.ncbi.nlm.nih.gov/pubmed/7843255.

[194] D. Kienhöfer, J. Hahn, J. Stoof, J. Z. Csepregi, C. Reinwald, V. Urbonaviciute, C. Johnsson, C. Mauerōder, M. J. Podolska, M. H. Biermann, M. Leppkes, T. Har-rer, M. Hultqvist, P. Olofsson, L. E. Munoz, A. Mocsai, M. Herrmann, G. Schett, R. Holmdahl, and M. H. Hoffmann. Experimental lupus is aggravated in mouse strains with impaired induction of neutrophil extracellular traps. *JCI Insight*, 2 (10), 2017. ISSN 2379-3708. doi: 10.1172/jci.insight.92920. URL https://www.ncbi.nlm.nih.gov/pubmed/28515366.

[195] Z. Liu, R. Bethunaickan, W. Huang, U. Lodhi, I. Solano, M. P. Madaio, and A. Davidson. Interferon-α accelerates murine systemic lupus erythematosus in a t cell-dependent manner. *Arthritis Rheum*, 63(1):219–29, 2011. ISSN 1529-0131. doi: 10.1002/art.30087. URL https://www.ncbi.nlm.nih.gov/pubmed/20954185.

[196] A. Mathian, A. Weinberg, M. Gallegos, J. Banchereau, and S. Koutouzov. Ifn-alpha induces early lethal lupus in preautoimmune (new zealand black x new zealand white) f1 but not in balb/c mice. *J Immunol*, 174(5):2499–506, 2005. ISSN 0022-1767. doi: 10.4049/jimmunol.174.5.2499. URL https://www.ncbi.nlm.nih.gov/pubmed/15728455.

[197] M. Yokogawa, M. Takaishi, K. Nakajima, R. Kamijima, C. Fujimoto, S. Kataoka, Y. Terada, and S. Sano. Epicutaneous application of toll-like receptor 7 agonists leads to systemic autoimmunity in wild-type mice: a new model of systemic lupus erythematosus. *Arthritis Rheumatol*, 66(3):694–706, 2014. ISSN 2326-5205. doi: 10.1002/art.38298. URL https://www.ncbi.nlm.nih.gov/pubmed/24574230.

[198] R. A. Eisenberg and C. S. Via. T cells, murine chronic graft-versus-host disease and autoimmunity. *J Autoimmun*, 39(3):240–7, 2012. ISSN 1095-9157. doi: 10.1016/j.jaut.2012.05.017. URL https://www.ncbi.nlm.nih.gov/pubmed/22704961. Eisenberg, Robert A Via, Charles S 2012/6/19.

[199] W. Li, A. A. Titov, and L. Morel. An update on lupus animal models. *Curr Opin Rheumatol*, 29(5):434–441, 2017. ISSN 1531-6963. doi: 10.1097/BOR.0000000000000412. URL https://www.ncbi.nlm.nih.gov/pubmed/28537986. Li, Wei Titov, Anton A Morel, Laurence 2017/5/26.

[200] B. S. Andrews, R. A. Eisenberg, A. N. Theofilopoulos, S. Izui, C. B. Wilson, P. J. McConahey, E. D. Murphy, J. B. Roths, and F. J. Dixon. Spontaneous murine lupus-like syndromes. clinical and immunopathological manifestations in several strains. *J Exp Med*, 148(5):1198–215, 1978. ISSN 0022-1007. doi: 10.1084/jem.148.5.1198. URL https://www.ncbi.nlm.nih.gov/pubmed/309911. Andrews, B S

Eisenberg, R A Theofilopoulos, A N Izui, S Wilson, C B McConahey, P J Murphy, E D Roths, J B Dixon, F J 1978/11/1.

[201] F. Conti, F. Ceccarelli, C. Perricone, L. Massaro, E. Marocchi, F. Miranda, F. R. Spinelli, S. Truglia, C. Alessandri, and G. Valesini. Systemic lupus erythematosus with and without anti-dsdna antibodies: Analysis from a large monocentric cohort. *Mediators Inflamm*, 2015:328078, 2015. ISSN 1466-1861. doi: 10.1155/2015/328078. URL https://www.ncbi.nlm.nih.gov/pubmed/26063969.

[202] Yihuang Lin, Yu Yan, Huifang Zhang, Yucai Chen, Yangyang He, Shoubao Wang, Lianhua Fang, Yang Lv, and Guanhua Du. Salvianolic acid a alleviates renal injury in systemic lupus erythematosus induced by pristane in balb/c mice. *Acta Pharmaceutica Sinica B*, 7:159–166, 3 2017. ISSN 2211-3835. doi: 10.1016/J.APSB.2016.07.001. URL https://www.sciencedirect.com/science/article/pii/S2211383516300879?via%3Dihub. Contains protocol for autoantibody ELISA (i.e. Anti-¡b¿Sm¡/b¿, ¡b¿dsDNA¡/b¿ and histone).

[203] L. D. Bowers. Kinetic serum creatinine assays i. the role of various factors in determining specificity. *Clin Chem*, 26(5):551–4, 1980. ISSN 0009-9147. URL https://www.ncbi.nlm.nih.gov/pubmed/7261300.

[204] C. Slot. Plasma creatinine determination. a new and specific jaffe reaction method. *Scand J Clin Lab Invest*, 17(4):381–7, 1965. ISSN 0036-5513. doi: 10.3109/00365516509077065. URL https://www.ncbi.nlm.nih.gov/pubmed/5838275.

[205] A. S. Levey, R. D. Perrone, and N. E. Madias. Serum creatinine and renal function. *Annu Rev Med*, 39:465–90, 1988. ISSN 0066-4219. doi: 10.1146/annurev.me.39.020188.002341. URL https://www.ncbi.nlm.nih.gov/pubmed/3285786.

[206] Anroop B Nair and Shery Jacob. A simple practice guide for dose conversion between animals and human. *Journal of basic and clinical pharmacy*, 7:27–31, 3 2016. ISSN 0976-0105. doi: 10.4103/0976-0105.177703. URL http://www.ncbi.nlm.nih.gov/pubmed/27057123http://www.pubmedcentral.nih.gov/articlerender.fcgi?artid=PMC4804402.

[207] P. Y. Lee, J. S. Weinstein, D. C. Nacionales, P. O. Scumpia, Y. Li, E. Butfiloski, N. van Rooijen, L. Moldawer, M. Satoh, and W. H. Reeves. A novel type i ifn-producing cell subset in murine lupus. *J Immunol*, 180(7):5101–8, 2008. ISSN 0022-1767. doi: 10.4049/jimmunol.180.7.5101. URL https://www.ncbi.nlm.nih.gov/pubmed/18354236.

[208] B. H. Rovin, Y. K. O. Teng, E. M. Ginzler, C. Arriens, D. J. Caster, J. Romero-Diaz, K. Gibson, J. Kaplan, L. Lisk, S. Navarra, S. V. Parikh, S. Randhawa, N. Solomons, and R. B. Huizinga. Efficacy and safety of voclosporin versus placebo

for lupus nephritis (aurora 1): a double-blind, randomised, multicentre, placebo-controlled, phase 3 trial. *Lancet*, 397(10289):2070–2080, 2021. ISSN 1474-547X. doi: 10.1016/S0140-6736(21)00578-X. URL `https://www.ncbi.nlm.nih.gov/pubmed/33971155`.

[209] Keqiang Chen, Ji Ming Wang, Ruoxi Yuan, Xiang Yi, Liangzhu Li, Wanghua Gong, Tianshu Yang, Liwu Li, and Shaobo Su. Tissue-resident dendritic cells and diseases involving dendritic cell malfunction. *International immunopharmacology*, 34:1–15, 5 2016. ISSN 1878-1705. doi: 10.1016/j.intimp.2016.02.007. URL `http://www.ncbi.nlm.nih.gov/pubmed/26906720http://www.pubmedcentral.nih.gov/articlerender.fcgi?artid=PMC4818737`.

[210] J. H. Kim, K. W. Kim, M. H. Kim, and Y. S. Yu. Intravenously administered gold nanoparticles pass through the blood-retinal barrier depending on the particle size, and induce no retinal toxicity. *Nanotechnology*, 20(50):505101, 2009. ISSN 1361-6528. doi: 10.1088/0957-4484/20/50/505101. URL `https://www.ncbi.nlm.nih.gov/pubmed/19923650`.

[211] S. Zhu, L. Gong, Y. Li, H. Xu, Z. Gu, and Y. Zhao. Safety assessment of nanomaterials to eyes: An important but neglected issue. *Adv Sci (Weinh)*, 6(16):1802289, 2019. ISSN 2198-3844. doi: 10.1002/advs.201802289. URL `https://www.ncbi.nlm.nih.gov/pubmed/31453052`.

[212] H. Gao, W. Shi, and L. B. Freund. Mechanics of receptor-mediated endocytosis. *Proc Natl Acad Sci U S A*, 102(27):9469–74, 2005. ISSN 0027-8424. doi: 10.1073/pnas.0503879102. URL `https://www.ncbi.nlm.nih.gov/pubmed/15972807`.

[213] M. Swiecki and M. Colonna. The multifaceted biology of plasmacytoid dendritic cells. *Nat Rev Immunol*, 15(8):471–85, 2015. ISSN 1474-1741. doi: 10.1038/nri3865. URL `https://www.ncbi.nlm.nih.gov/pubmed/26160613`.

[214] K. Al-Hourani, N. Ramamurthy, E. Marchi, R. M. Eichinger, L. N. Lee, P. Fabris, P. Klenerman, and H. Drakesmith. Innate triggering and antiviral effector functions of activin a. *bioRxiv*, page 2021.03.23.436626, 2021. doi: 10.1101/2021.03.23.436626. URL `http://biorxiv.org/content/early/2021/03/23/2021.03.23.436626.abstract`.

[215] Michael Look, Eric Stern, Qin A Wang, Leah D DiPlacido, Michael Kashgarian, Joe Craft, and Tarek M Fahmy. Nanogel-based delivery of mycophenolic acid ameliorates systemic lupus erythematosus in mice. *The Journal of clinical investigation*, 123:1741–9, 4 2013. ISSN 1558-8238. doi: 10.1172/JCI65907. URL `http://www.ncbi.nlm.nih.gov/pubmed/23454752http://www.pubmedcentral.nih.gov/articlerender.fcgi?artid=PMC3613921`.

[216] R. Ganugula, M. Arora, D. Zou, S. K. Agarwal, C. Mohan, and M. N. V.R Kumar. A highly potent lymphatic system-targeting nanoparticle cyclosporine prevents glomerulonephritis in mouse model of lupus. *Sci Adv*, 6(24):eabb3900, 2020. ISSN 2375-2548. doi: 10.1126/sciadv.abb3900. URL `https://www.ncbi.nlm.nih.gov/pubmed/32582860`.

[217] J. Hu, M. Wang, X. Xiao, B. Zhang, Q. Xie, X. Xu, S. Li, Z. Zheng, D. Wei, and X. Zhang. A novel long-acting azathioprine polyhydroxyalkanoate nanoparticle enhances treatment efficacy for systemic lupus erythematosus with reduced side effects. *Nanoscale*, 12(19):10799–10808, 2020. ISSN 2040-3372. doi: 10.1039/d0nr01308k. URL `https://www.ncbi.nlm.nih.gov/pubmed/32391836`.

[218] F. Yuan, R. K. Nelson, D. E. Tabor, Y. Zhang, M. P. Akhter, K. A. Gould, and D. Wang. Dexamethasone prodrug treatment prevents nephritis in lupus-prone (nzb × nzw)f1 mice without causing systemic side effects. *Arthritis Rheum*, 64(12):4029–39, 2012. ISSN 1529-0131. doi: 10.1002/art.34667. URL `https://www.ncbi.nlm.nih.gov/pubmed/22886616`.

[219] F. Goldblatt, S. Chambers, A. Rahman, and D. A. Isenberg. Serious infections in british patients with systemic lupus erythematosus: hospitalisations and mortality. *Lupus*, 18(8):682–9, 2009. ISSN 0961-2033. doi: 10.1177/0961203308101019. URL `https://www.ncbi.nlm.nih.gov/pubmed/19502263`.

[220] C. J. Edwards, T. Y. Lian, H. Badsha, C. L. Teh, N. Arden, and H. H. Chng. Hospitalization of individuals with systemic lupus erythematosus: characteristics and predictors of outcome. *Lupus*, 12(9):672–6, 2003. ISSN 0961-2033. doi: 10.1191/0961203303lu452oa. URL `https://www.ncbi.nlm.nih.gov/pubmed/14514129`.

[221] Eric F Morand, Richard Furie, Yoshiya Tanaka, Ian N Bruce, Anca D Askanase, Christophe Richez, Sang-Cheol Bae, Philip Z Brohawn, Lilia Pineda, Anna Berglind, Raj Tummala, and TULIP-2 Trial Investigators. Trial of anifrolumab in active systemic lupus erythematosus. *N. Engl. J. Med.*, 382:211–221, 1 2020.

[222] Renaud Felten, Florence Scher, Flora Sagez, François Chasset, and Laurent Arnaud. Spotlight on anifrolumab and its potential for the treatment of moderate-to-severe systemic lupus erythematosus: evidence to date. *Drug Des. Devel. Ther.*, 13:1535–1543, 5 2019.

[223] Jamal Mikdashi and Ola Nived. Measuring disease activity in adults with systemic lupus erythematosus: the challenges of administrative burden and responsiveness to patient concerns in clinical research. *Arthritis Res. Ther.*, 17:183, 7 2015.

[224] Sharan Bobbala, Sean David Allen, and Evan Alexander Scott. Flash nanoprecipitation permits versatile assembly and loading of polymeric bicontinuous cubic nanospheres. *Nanoscale*, 10:5078–5088, 3 2018. ISSN 20403372. doi: 10.1039/c7nr06779h.

[225] Nicholas B. Karabin, Michael P. Vincent, Sean D. Allen, Sharan Bobbala, Molly A. Frey, Sijia Yi, Yufan Yang, and Evan A. Scott. The combination of morphology and surface chemistry defines the biological identity of nanocarriers in human blood. *bioRxiv*, page 2020.09.02.280404, 2020. doi: 10.1101/2020.09.02. 280404. URL http://biorxiv.org/content/early/2020/09/03/2020.09. 02.280404.abstract.